Ultrafast Optical Control of Ring-Opening and Isomerization in 7-Dehydrocholesterol and Stilbene

by

Broc D. Smith

A dissertation submitted in partial fulfillment
of the requirements for the degree of
Doctor of Philosophy
(Chemistry)
in The University of Michigan
2015

Doctoral Committee:

Professor Roseanne J. Sension, Chair
Professor Raoul Kopelman
Associate Professor Kevin J. Kubarych
Associate Professor Jennifer P. Ogilvie

Dedication

To my parents

Acknowledgements

None of the things that I've accomplished over the past six years would have been possible without the incredible amount of encouragement and support that I've received from my family, friends, colleagues, and mentors. I feel incredibly lucky to have reached this point, and I couldn't have done it without you.

First, I would like to thank my advisor, Prof. Roseanne Sension. I initially got a taste of the Sension lab as an undergraduate participant in the UM Chemistry REU program. When I returned to UM as a graduate student, you were kind enough to allow me to join your lab for the long haul. I am indebted to you for your guidance and patience over the course of my graduate career. I am especially grateful for your support leading up to and during my return to Lock Haven University to teach this past academic year.

I'd also like to say thank you to Prof. Ken Spears, who was basically my second advisor. You've taught me more about lasers and how to fix them (and then break them and fix them again!) than anyone else. If it weren't for you I'd still be struggling to get the noise level of the laser to even half of what is required to take measurements.

Next I would like to say thank you to my committee. Thanks to Prof. Raoul Kopelman and Prof. Kevin Kubarych for being with me since the beginning and giving me plenty of ideas (about my work and otherwise) to think about over the years. It was also a pleasure to have had the opportunity to teach with both of you.

I would also like to give a huge thank you to Prof. Jennifer Ogilvie for being kind enough to step in at the last minute in order to fill the empty position on my committee. Although not officially a member of my committee at the time this document was submitted, I would certainly like to express my gratitude to Prof. Duncan Steel for serving as a committee member for the majority of my time as a graduate student.

To the guys who were part of the lab when I was an REU student: Aaron Rury, Jian Peng, Andy Stickrath, Cassey Tang, and Mike Orozco, thanks for being my introduction to the world of real scientific research. To the newer generation of the Sension lab: Brenden Arruda, Ted Wiley, Nick Miller, and Kaitlynn Arnholt, we've had a lot of interesting and fruitful conversations, as well as quite a few laughs over the years. It was awesome to work with all of you.

To the faculty at Lock Haven University, you not only gave me an excellent undergraduate education, but also gave me the opportunity to return to the university as your colleague. The year I spent teaching at LHU was an incredible experience. Thank you for helping me improve my abilities as a teacher and for everything else you've done for me in the 10(!) years that I've known you.

I've been fortunate enough to make many friends over the course of my life. To all of you I say thanks for being awesome. You know who you are.

Last, but most certainly not least, I'm grateful for the remarkable family that I am privileged to have. Mom and Dad, you've always been extraordinarily supportive of every dream that I've pursued throughout the course of my life. This one was no different. Travis, I couldn't have asked for a better little brother (and now thanks to you, I have a wonderful sister in Macenzie!). To my grandparents, Carol, Dick, Boog, and

Lidy, you were always there for me and I'm sorry that not all of you are here to see me finally reach the end of this journey. To all of my immediate and extended family, I love you guys. Thanks for making me the person I am today.

Table of Contents

List of Figures

Chapter 1

Introduction

1.1 Motivation

In its infancy, the science of modern chemistry dealt with observations of the structure and properties of the substances that make up the world around us and their reactivity with one another. As our knowledge about these chemical reactions has grown, so too has our desire to be able to control them in order to produce a desirable set of materials or properties. One class of reactions that is an ideal candidate for controllability is photoisomerization. Many light-driven isomerization reactions are reversible and fast, and some of the molecules that undergo these photoreactions find applications in photochromic materials,[1-2] optical data storage,[3-4] molecular switches or valves,[5-8] and molecular motors.[9-12] Molecules that photoisomerize and show changes in some physical property (e.g. one conformer exhibits a higher electrical conductance due to a change in conjugation) are ideal candidates for molecular switches. Diarylethene and fulgide derivatives are two of the most popular choices.[3-4] It has already been shown that using a photoswitch as a bridge between an energy donor and acceptor can allow for energy transfer to occur in only one conformation.[13-14] Molecules that involve a unidirectional rotation about some bond following photoexcitation are ideal candidates for the rotary motors that power molecular machines.[10, 12]

One obstacle that stands in the way of the efficient use of photoactive molecules as molecular switches or motors is the quantum yield of photoisomerization (Φ). Many of these molecules of interest exhibit quantum yields much less than one. While efforts have been made to modify the structures of the functional groups connected to the chromophore backbone in order to improve quantum yields, in many cases these changes improve the quantum yield of photoisomerization in one direction, but do not affect or may actually reduce it in the opposite direction. For example, diarylethenes, which undergo a typical photochemical ring-opening reaction, have a quantum yield very close to one for cyclization.[4] However, the ring-open form of these molecules can exist in two conformational isomers, only one of which may undergo the ring-closing cyclization. Since the two conformers exist in a near 1:1 ratio, this means that the effective quantum yield is ~0.5. Adding bulky substituent groups to the ring system in these molecules affects the equilibrium between the two conformers, increasing the number of molecules able to undergo cyclization. Thus, the quantum yield of cyclization can be increased. Unfortunately, the addition of these substituent groups also reduces the quantum yield of the ring-opening reaction in many of the molecules studied.[4]

There can also be cases where it is necessary for the substituent groups to be chosen based on some other property related to the molecule's chosen application even though the quantum yield may be sensitive to this substitution. The ability to modify the structure of a molecular switch or motor to obtain some desirable property without the worry that this structural change will negatively impact the quantum yield of photoisomerization is an important step in these fields of study. This is where the technique of optical control becomes key.

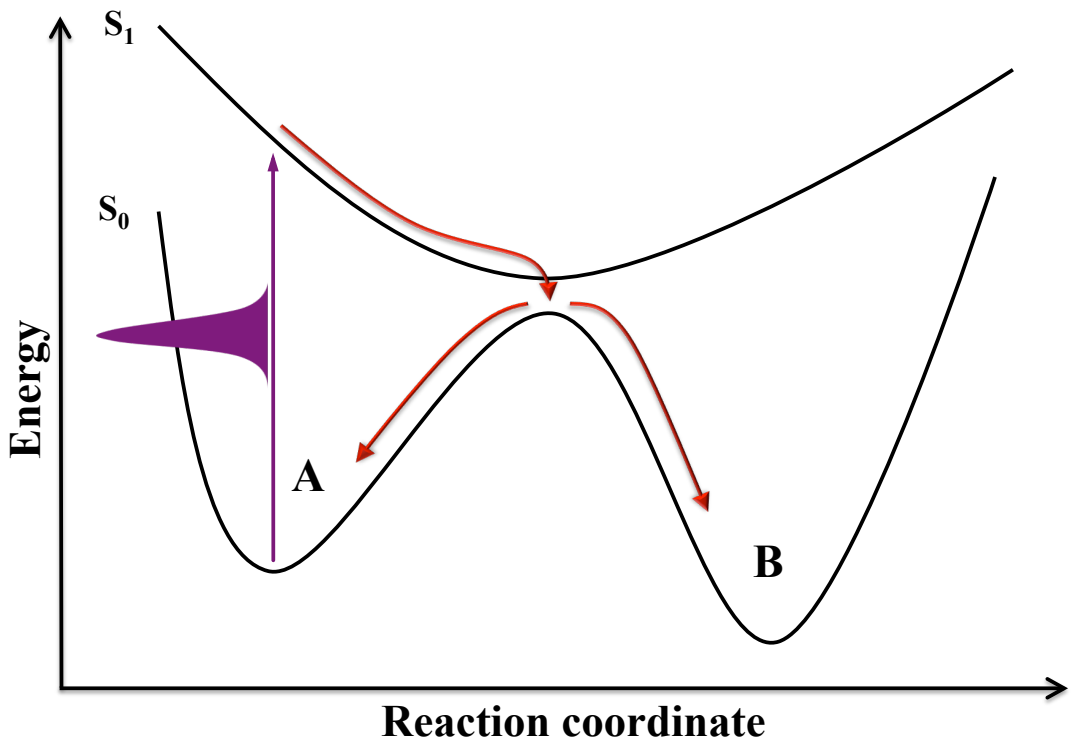

Figure 1.1 *Cartoon depicting a model two-product system for optical control. Following excitation of some reactant molecule, A, from the S_0 state, the excited wavepacket evolves on the S_1 state and eventually returns to the S_0 state via internal conversion. The quantum yield of the photoreaction determines the probability that the excited molecule reacts to form a product molecule, B.*

1.2 Optical Control

With the arrival of the laser in the late 1950's and early 1960's, it was thought that the control of chemical reactions using light would soon be a realistic possibility. One pursued course of action was selective bond breaking in various types of polyatomic molecules.[15] It was believed that if the frequency of a laser was tuned to match the frequency of a local mode in a molecule, this bond could be selectively broken with a high enough energy input. Unfortunately, due to the inherent anharmonic coupling between the normal modes in the molecule, the incident energy of the laser is rapidly

distributed throughout the entire molecule through intramolecular vibrational redistribution (IVR), making this approach impractical.[16-18]

While the IVR can be explained as a classical process due to the anharmonic coupling of vibrational modes, the molecular world is also quantum mechanical. These quantum processes are sensitive to the constructive and destructive interference of the wave functions in superposition states. Thus, if one could control the interference between these different quantum states, one could influence the outcome of a chemical reaction.[19] With the development of ultrashort laser pulses, the possibility of quantum control was once again within reach, and multiple quantum control schemes have been developed in the years since in order to take advantage of the available technology.[20]

Many techniques focus on control with the use of multiple lasers or laser pulses. Brumer and Shapiro showed theoretically that adjusting the relative phase and amplitude between two lasers centered at different frequencies could control photodissociation yields.[21] This was later confirmed experimentally.[22] Rice, Tannor, and Kosloff[23] proposed a pump-probe technique that adjusted the delay between two femtosecond pulses in order to control the propagation time of a wave packet on the electronic excited state surface of a molecule. This approach has also been confirmed experimentally.[24] Shi, Woody, and Rabitz,[25] proposed another method that uses a single, ultrashort pulse to control a reaction. They suggest that since chemical systems can be quite complicated, ultrashort pulses should be tailored for individual molecules in order to force the system down a particular reaction path. Although the first two methods have been shown to be experimentally achievable, the third option is often the ideal choice for control experiments as some studies have shown that changing only a single parameter is not

usually sufficient in controlling the outcome of a photochemical reaction.[26] However, a long standing hypothesis in coherent control theory is that single photon control, such as that suggested by Shi, Woody, and Rabitz, is not possible.[27]

1.2.1 Single pulse control

At its heart, the idea of single-pulse coherent control is to use a control field to prepare and interfere with a coherent state and utilize this interference to control the outcome of a particular quantum process. This type of control mechanism can be further broken down into strong vs. weak field control. In the weak field limit, the pulse intensities are much lower than the intensities that are required to observe high order nonlinear processes. Laser pulses with optical intensities large enough to see nonlinear processes are considered to be in the strong field limit. Coherent control in the strong field regime has been demonstrated in the literature.[28-34] Single photon control in the weak-field limit has long been challenged theoretically, but the results of some recent experiments demonstrate the possibility of weak-field control.[35-37] Spanner, Arango, and Brumer have shown that the impossibility of one photon control is usually only true in some isolated systems, and that, if a system is open (e.g., a molecule in a solvent environment), one photon control is indeed possible.[38] Their argument is outlined below.

One can write the complex electric field in the frequency domain of a laser pulse as:

$$\tilde{E}(\omega) = A(\omega)e^{i\varphi(\omega)} \tag{1.1}$$

where $A(\omega)$ is the spectral amplitude of the pulse and $\varphi(\omega)$ is the spectral phase of the pulse. When dealing with short pulses of light, it is easier to work in the frequency

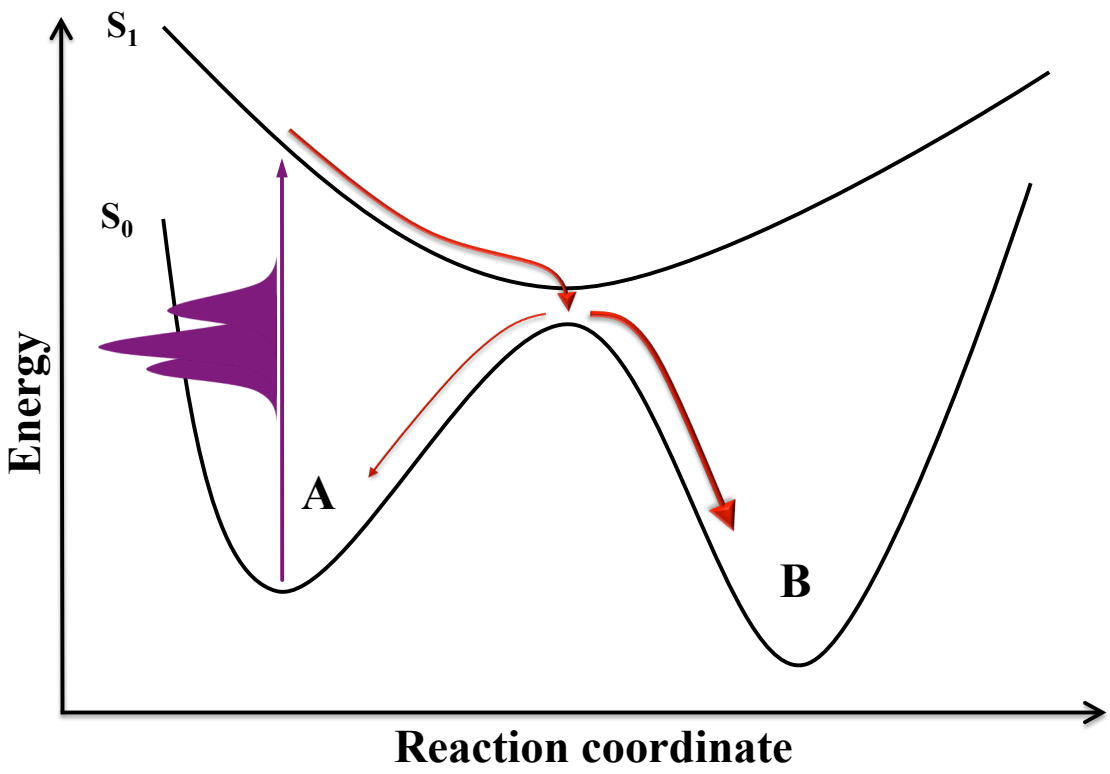

Figure 1.2 *Cartoon of a single pulse control scheme. In this example, the phase-shaped, ultrafast pump pulse increases the probability of the excited molecules forming the B product as they undergo internal conversion back to the ground state potential energy surface.*

domain rather than the time domain due to the broad range of frequencies present. The overall phase of the pulse can be written as a Taylor expansion about ω_0 (the center frequency of the laser pulse):

$$\varphi(\omega) = \varphi_0^{(0)} + \varphi_0^{(1)}(\omega - \omega_0) + \frac{1}{2}\varphi_0^{(2)}(\omega - \omega_0)^2 + \frac{1}{6}\varphi_0^{(3)}(\omega - \omega_0)^3 + \ldots + \frac{1}{n!}\varphi_0^{(n)}(\omega - \omega_0)^n \tag{1.2a}$$

$$\varphi_0^{(0)} = \varphi(\omega_0)$$
$$\varphi_0^{(n)} = \left(\frac{d^n\varphi}{d\omega^n}\right)_{\omega_0} \tag{1.2b}$$

Each one of the $\varphi_0^{(n)}$ terms affects the overall phase in a different way. The $\varphi_0^{(0)}$ term is

the absolute phase of the pulse, which is simply the phase delay between the center pulse frequency and the pulse envelope. The $\varphi_0^{(1)}$ term is the group delay, which is simply the overall time delay of the pulse with respect to some point in time. The higher order phase terms ($\varphi_0^{(2)}$ and above) deal with the chirp of the pulse, which involves the phase difference and relative time delay between the different spectral components of the pulse.

Assuming a system with Hamiltonian, $\hat{H}_0$, eigenenergies, $\{E_n\}$, and eigenstates, $\{|\varphi_n\rangle\}$, the phase of the excitation pulse has been shown to have an influence on the expectation value of some observable $\hat{O}$ of the system starting from some initial state $|\varphi_{n_0}\rangle$[38]:

$$\begin{aligned}\langle \hat{O}(t)\rangle &= \sum_n O_{nn}\left|\mu_{nn_0}\right|^2\left|A(\omega_{nn_0})\right|^2 \\ &+ \sum_{n\neq m}\left|O_{nm}\mu_{mn_0}\mu_{nn_0}A(\omega_{mn_0})A(\omega_{nn_0})\right| \times \cos\left[\omega_{nm}t + \theta_{nm} + \varphi_s(\omega_{mn_0}) - \varphi_s(\omega_{nn_0})\right]\end{aligned} \tag{1.3}$$

where $O_{nm} = \langle \phi_n|\hat{O}|\phi_m\rangle$, $\mu_{nm} = \langle \phi_n|\hat{\mu}|\phi_m\rangle$ (transition dipole matrix elements), $\omega_{nm} = (E_n - E_m)/\hbar$, and θ_{nm} is the phase of the O_{nm} matrix element. In cases where $O_{nm} = 0$ $\left(\left[\hat{H}_0,\hat{O}\right] = 0\right)$, the expectation value of $\hat{O}$ is time and phase independent since the second term in Equation 3 disappears. When $O_{nm} \neq 0$ $\left(\left[\hat{H}_0,\hat{O}\right] \neq 0\right)$, the expectation value of $\hat{O}$ is dependent on both time and phase. The latter case is almost always true in an open system.[38] Since the expectation value of a particular observable can be considered a measure of the outcome of a reaction, and the expectation value of some observable may be dependent on the pulse phase, this means that the phase of the pulse could theoretically control the outcome of a reaction.

1.2.2 Multi-pulse control

Like the single pulse scheme, the first step in a coherent multi-pulse control scheme is to prepare a coherent wave packet on the excited state. Rather than using the phase of the excitation pulse to create interference, this excited population is allowed to evolve naturally in time without the presence of an electromagnetic field. Once a particular amount of time has passed, another laser pulse interacts with the system, coupling the current excited state to some other state with which it is resonant. The appeal of this technique is that the use of a second optical transition may allow one to bypass a critical point in the trajectory of the molecule on the excited state potential energy surface that can negatively affect the desired quantum yield of the photoproduct. The ability to adjust the delay between the two pulses in order to modify the propagation time on the excited state potential energy surface may prove to be important, especially if the molecule being studied has a long-lived excited state.

Depending on the structure of the molecule's excited state manifold, the second ultrafast pulse may couple the initially excited state to either to the ground state or to a higher excited state. This technique is referred to as either pump-dump (ground state) or pump-repump (higher excited state). Both variations have already been shown as viable methods of molecular control.[39-41] Some methods using only a single, strongly chirped pulse can be viewed as single pulse analogs that perform the same process as the two pulse pump-dump or pump-repump mechanisms.[42]

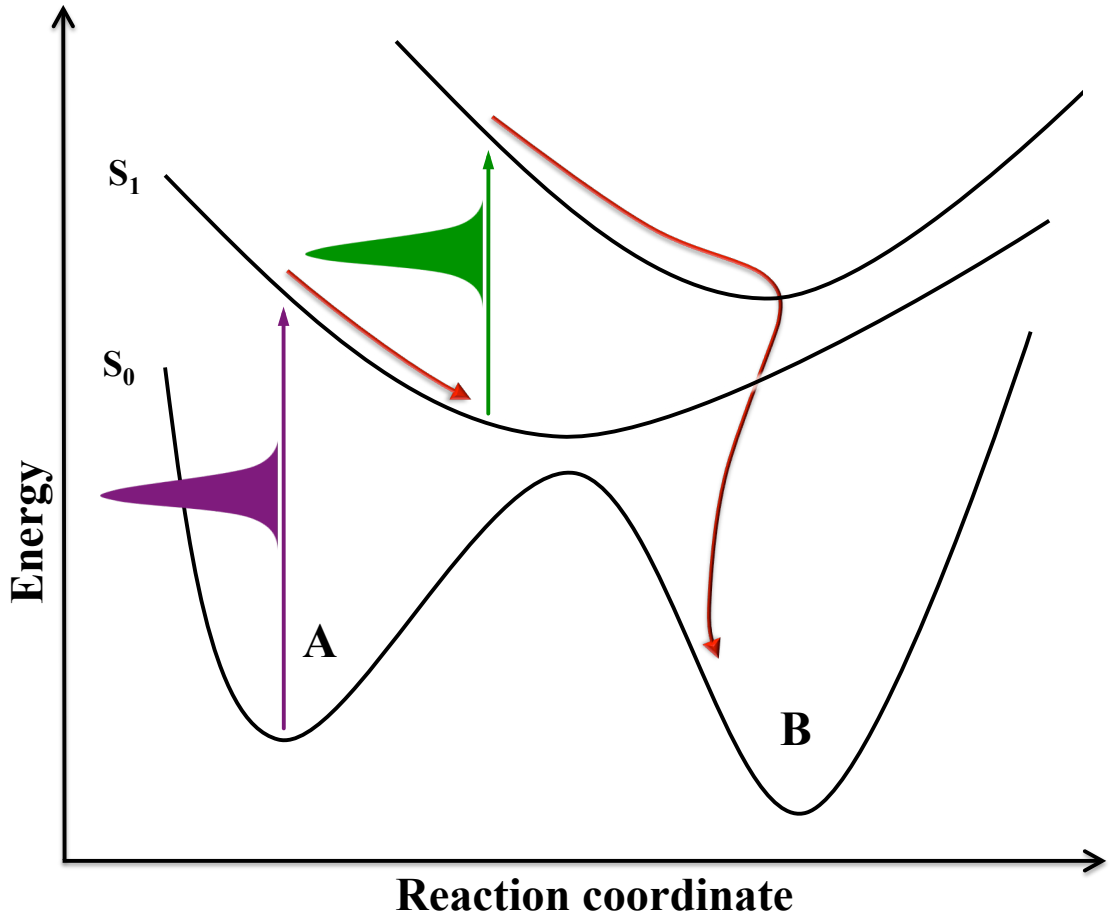

Figure 1.3 *Cartoon of a two pulse control scheme. A pump pulse first populates the excited state surface S_1. After a time delay a second pump pulse re-excites the molecule to the S_2 excited state surface. From here, the re-excited molecule follows a different relaxation pathway than if simply excited from S_0 to S_1 in order to form the B product.*

1.3 Molecular systems of interest

In this work, we use UV/Visible ultrafast laser pulses in an attempt to control the cis-trans photoisomerization and ring-opening reactions of small model systems for molecular switches and motors. Molecules studied here include 7-dehydrocholesterol, cis-stilbene, and trans-stilbene. These species are described below.

1.3.1 7-Dehydrocholesterol

An abundance of studies using ultrafast spectroscopy[43-50] and theoretical quantum chemistry techniques[51-52] have been performed on 1,3-cyclohexadiene (CHD) and related molecules. The cyclohexadiene chromophore is a conjugated diene that undergoes a single photon electrocyclic ring-opening reaction to form a conjugated triene. Diarylethene and fulgide derivatives, which contain the CHD chromophore, are two of the leading candidates for applications in molecular switches due to the intrinsic reversibility of this photochemical reaction.[3-4, 53] The CHD chromophore is also the photoactive component of the precursor to vitamin D_3, 7-dehydrocholesterol (Provitamin D_3, DHC). Provitamin D_3 itself has been the subject of theoretical studies on its electrical conductance before and after irradiation while embedded between two electrodes.[54]

Following UV excitation ($S_1 \leftarrow S_0$), DHC undergoes a ring-opening reaction to form cZc-Previtamin D_3 (Figure 1.4) with a quantum yield of 0.26.[55] This ring-open structure then undergoes a [1,7] sigmatropic hydride shift to form cholecalciferol (vitamin D_3).[56] The photochemical ring-opening occurs in a conrotatory fashion according to the Woodward-Hoffman rules. In contrast to the ring-opening photoreaction, which occurs on an ultrafast timescale of picoseconds,[57-63] the thermal hydride shift occurs on the order of hours to days.[64] Previtamin D_3 is a strong absorber in the UV and can also form various photochemical by-products. The excitation wavelength influences the yields of the various products in the photochemical pathway of vitamin D_3.[65-70]

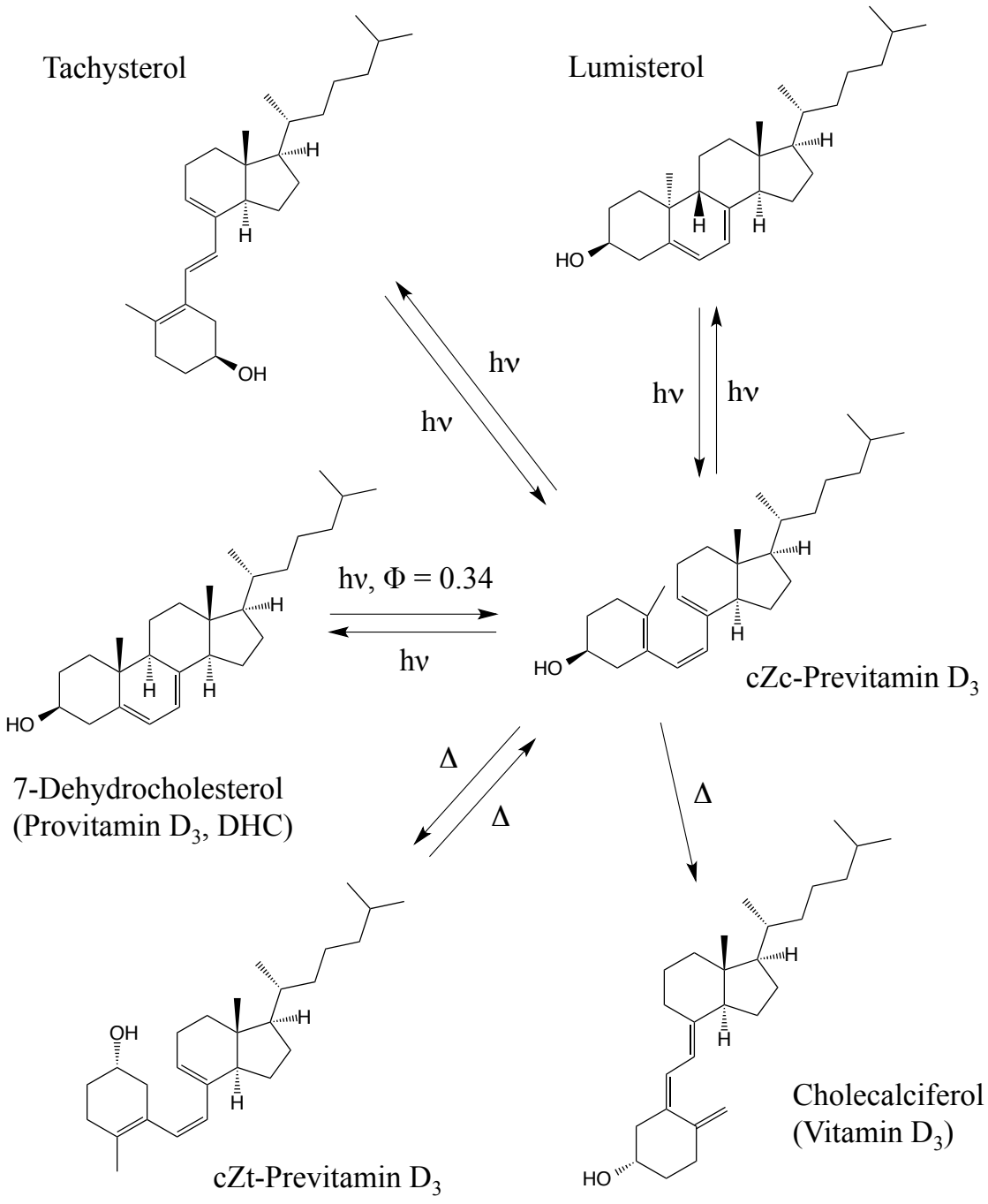

Figure 1.4 *Diagram of the photochemical and thermal reaction pathways between 7-dehydrocholesterol, vitamin D_3 and by-products with quantum yield of the DHC ring-opening. The Z in cZc and cZt refers to the stereochemistry of the second of the three conjugated alkene groups, while c and t refer to the cis or trans orientation of the first and third alkene groups.*

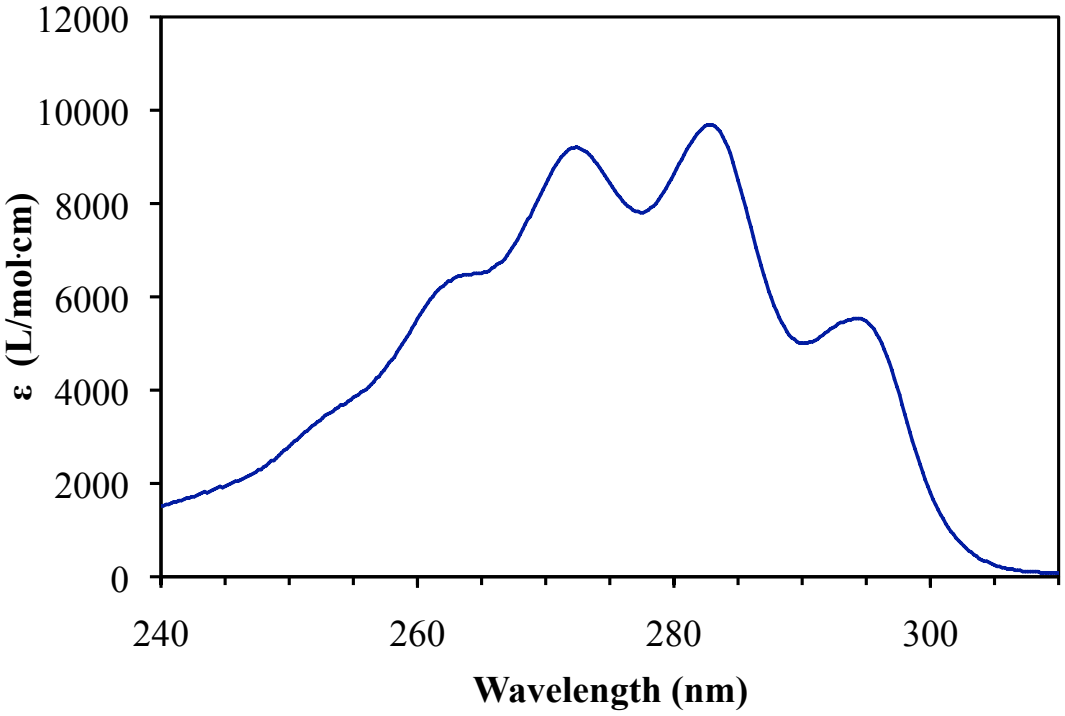

Figure 1.5 *Steady state absorption spectrum of 7-dehydrocholesterol.*

Early ultrafast transient absorption studies on DHC by Anderson et al. identified a strong excited state absorption (ESA, $S_n \leftarrow S_1$) in the visible region of the spectrum.[60, 71] More extensive studies by Tang et al. showed that the ESA is characterized by a strong peak at about 485 nm as well as a long tail extending to 770 nm.[58] The ESA appears to be composed of electronic transitions to two different S_n states. Tang et al. also demonstrated that the decay of the excited state absorption is biexponential with time constants of ~0.4–0.65 ps and ~1.0–1.8 ps depending on the solvent. It was proposed that the biexponential nature of the decay is due to a parallel decay process from the Franck Condon region to two non-symmetry equivalent intermediates as the ring begins to distort. In CHD, such a process would yield two degenerate intermediates due to the

symmetry of the molecule, resulting in a single exponential decay. In this dissertation, the influence of excitation energy on the excited state of DHC and attempts at coherent control of the ring-opening reaction will be explored.

1.3.2 Stilbene

Stilbene has long been regarded as an important model for photoisomerization reactions and has been studied extensively[72] using both steady-state[73-77] and ultrafast experimental techniques.[78-93] In addition, many theoretical studies have also been carried out.[94-101] Part of the reason for this interest in stilbene is its ability to reversibly interconvert between its cis and trans isomers, and the ability of cis-stilbene to undergo an electrocyclic ring-closure to form 4a,4b-dihydrophenanthrene, or DHP (Figure 1.6). All of these photochemical processes occur on an ultrafast timescale, though some happen much faster than others. Due to the reversibility of these isomerization reactions, stilbene is useful as a paradigm system for the field of molecular motors and switches. Many molecular systems developed for motor and switch studies are based upon a stilbene backbone or undergo similar cis-trans isomerization. Feringa et al. have shown that some of these molecules exhibit a unidirectional rotation, making them ideal candidates for molecular motor studies.[9-12, 102]

Though differing by a simple 180° rotation around the central double bond, cis and trans-stilbene have vastly different ground and excited state properties. Following UV excitation of cis-stilbene, the excited molecules (c*) may cross a small barrier (<1.5 kcal/mol) on the excited state potential surface on a time scale of ~1 ps depending on solvent before returning to the ground state through a conical intersection.[81-82, 85, 103-105]

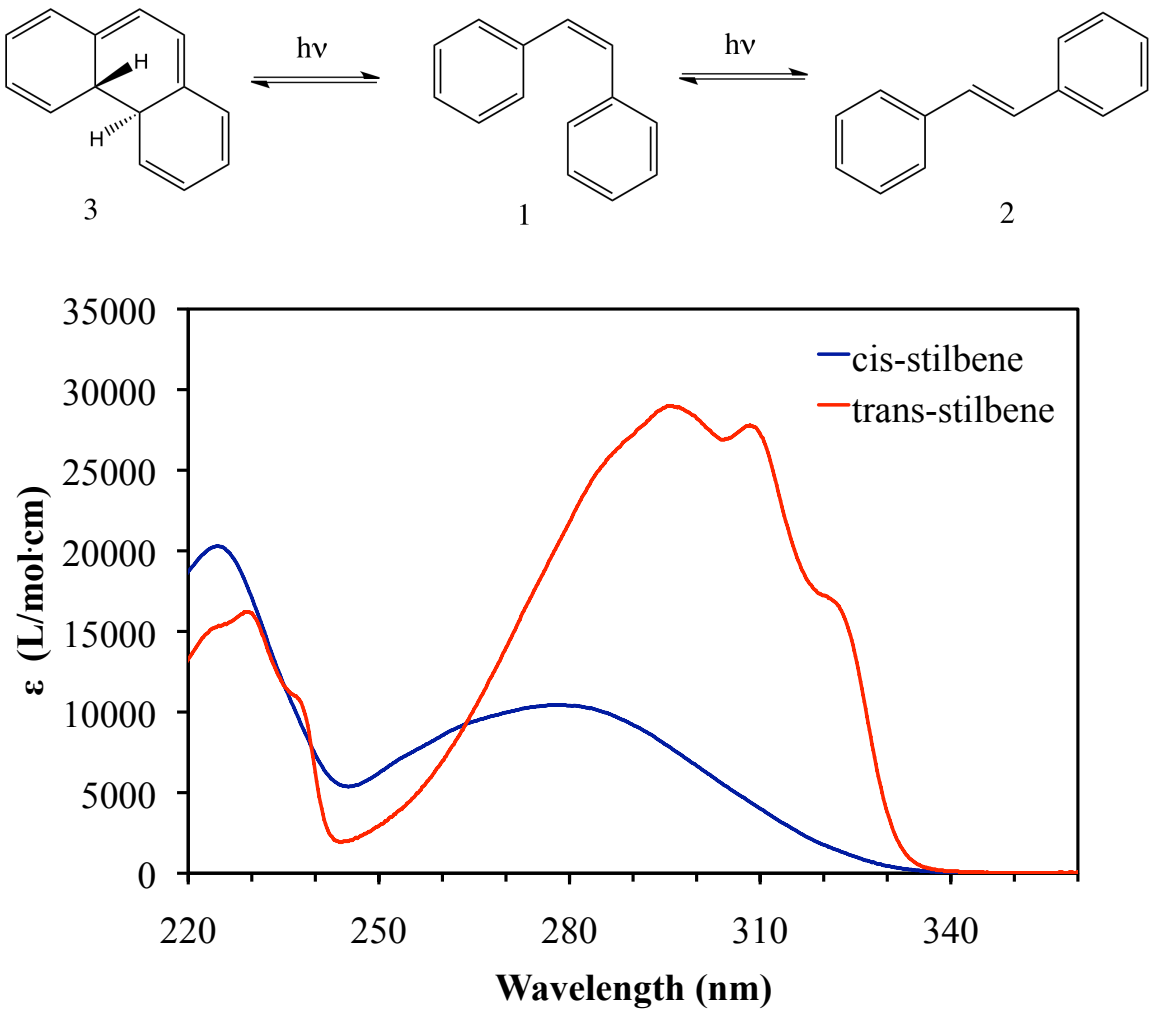

Figure 1.6 *(Top) Photoisomerization scheme of stilbene. Cis-stilbene (1) can isomerize to trans-stilbene (2) or DHP (3) upon excitation by a UV photon. Trans-stilbene and DHP may revert back to cis-stilbene upon UV or visible excitation, respectively. (Bottom) Steady state absorption spectra of cis-stilbene and trans-stilbene in 2-butanol. Though not included here, DHP exhibits a very broad spectrum in the visible that peaks near 450 nm.*

The motion corresponding to the reaction coordinate is a torsional rotation about the central C=C bond, and at the minimum of the excited state surface the dihedral angle of the two phenyl rings is 90°. This intermediate state is the so-called phantom state due to the difficulty in its detection.[73] From the phantom state, the molecule returns to the ground state and can either twist back to the cis-stilbene starting product or twist the

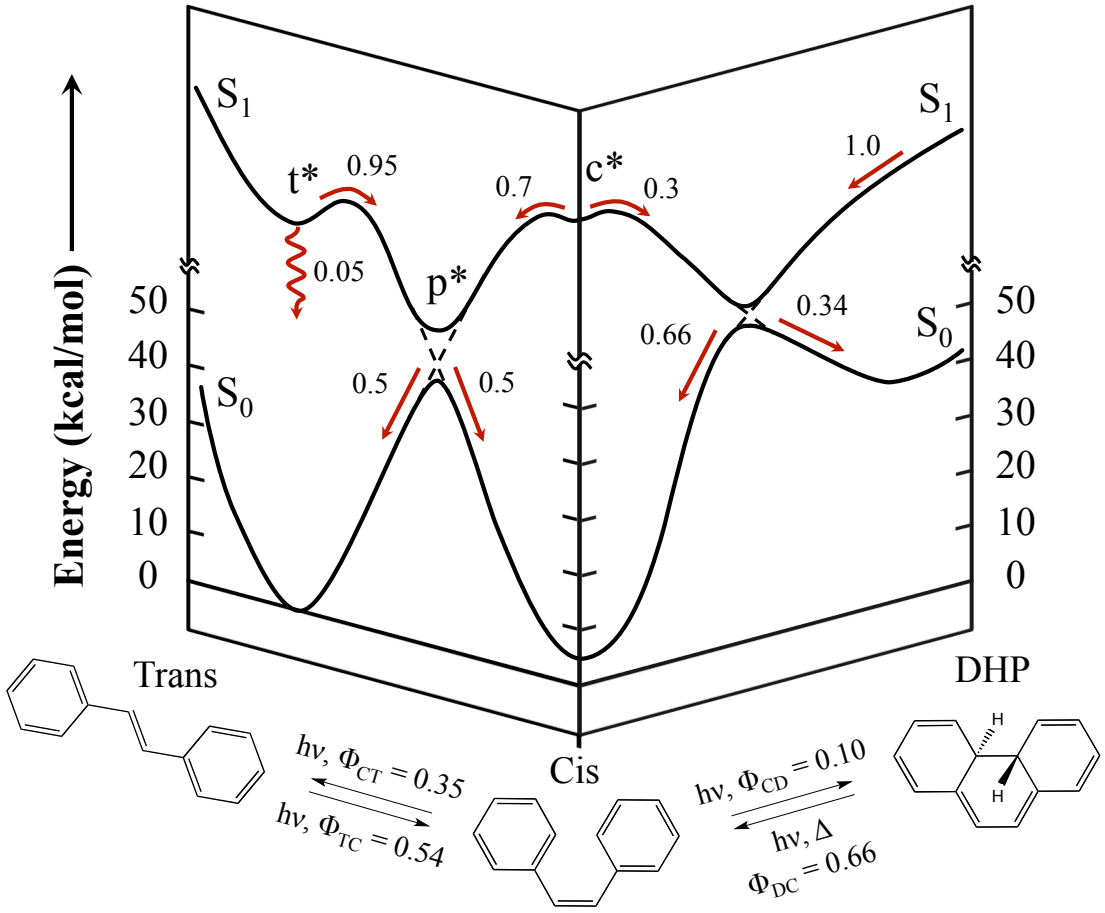

Figure 1.7 *Cartoon of the ground and excited state potential energy surfaces in stilbene and DHP with branching ratios and quantum yields for the different photochemical reactions. Adapted from a figure by Sension et al.*[85]

opposite direction to form trans-stilbene. The cis/trans-stilbene branching ratio from the phantom state is approximately 1:1.[106] The electrocyclic ring-closure reaction to form DHP occurs on about the same time scale as the competing twist on the excited state surface. The barrier over which the excited molecules must cross is ~2 kcal/mol.[105] After relaxing back to the ground state along this pathway, the branching ratio for formation of cis-stilbene/DHP is approximately 2:1.[85] The split on the excited state between the C=C twist and the ring-closure (involving a different type of twisting motion) is about 70/30.[85]

Upon excitation of trans-stilbene, the intrinsic barrier over which the initially excited molecules (t*) must cross on the excited state surface is much larger than that for cis-stilbene (~3.5 kcal/mol),[107-109] such that the trans-to-cis isomerization occurs on a time scale of ~30 ps in methanol to ~200 ps in hexadecane.[79, 109] Once again, the cis/trans-stilbene branching ratio at the phantom state is about 1:1. The t* state also exhibits a high amount of fluorescence with a quantum yield of ~0.05 at room temperature.[110] In this work, the pump-repump technique will be utilized in an attempt to modify the quantum yield of isomerization for cis and trans-stilbene.

1.4 Outline of Dissertation

This dissertation is concerned with the exploration of the control of photochemical reactions of small molecular systems in the solution phase through the use of shaped laser pulse and dual excitation pulse techniques. Broadband, UV/Visible transient absorption is utilized throughout the experiments described here in order to monitor the excited state and photoproduct spectra.

Chapter 2 describes the experimental apparatuses and methods used to perform the experiments detailed in later chapters. This includes the laser system used to generate the femtosecond pulses required for experiment and the techniques used to shape these pulses for some experiments. Chapter 3 describes transient absorption experiments on 7-dehydrocholesterol using a tunable excitation pulse. These experiments were performed to determine if excitation frequency had an effect on the excited state dynamics of 7-dehydrocholesterol. Chapter 4 describes attempts at coherent control using modulated excitation pulses with varying values of the second order spectral phase

term (linear chirp). The systems of interest for these experiments were 7-dehydrocholesterol and cis-stilbene. Chapter 5 describes a series of pump-repump transient absorption experiments, where a second pump pulse can excite the molecules that have already been excited by an initial pump pulse to an even higher energy state. These experiments were performed using repump pulses tuned to overlap the visible excited state absorption spectra of 7-dehydrocholesterol, cis-stilbene, and trans-stilbene. Chapter 6 summarizes the work described throughout the dissertation and characterizes future plans for control of these paradigm systems.

1.5 References

1. M. Irie; S. Kobatake; M. Horichi. *Science,* **2001,** *291*, 1769-1772.
2. S. Kobatake; S. Takami; H. Muto; T. Ishikawa; M. Irie. *Nature,* **2007,** *446*, 778-781.
3. Y. Yokoyama. *Chem. Rev.,* **2000,** *100*, 1717-1739.
4. M. Irie. *Chem. Rev.,* **2000,** *100*, 1685-1716.
5. Y. Yokoyama; T. Gushiken; T. Ubukata, Fulgides and Related Compounds. In *Molecular Switches*, Wiley-VCH Verlag GmbH & Co. KGaA: 2011; pp 81-95.
6. W. R. Browne; B. L. Feringa, Light Switching of Molecules on Surfaces. In *Annu. Rev. Phys. Chem.*, 2009; Vol. 60, pp 407-428.
7. B. L. Feringa; N. Koumura; R. A. Van Delden; M. K. J. Ter Wiel. *Appl. Phys. A Mater. Sci. Process.,* **2002,** *75*, 301-308.
8. A. Kocer; M. Walko; W. Meijberg; B. L. Feringa. *Science,* **2005,** *309*, 755-758.
9. W. R. Browne; B. L. Feringa. *Nat. Nanotechnol.,* **2006,** *1*, 25-35.
10. N. Koumura; R. W. J. Zijlstra; R. A. van Delden; N. Harada; B. L. Feringa. *Nature,* **1999,** *401*, 152-155.
11. R. A. van Delden; M. K. J. ter Wiel; M. M. Pollard; J. Vicario; N. Koumura; B. L. Feringa. *Nature,* **2005,** *437*, 1337-1340.

12. N. Koumura; E. M. Geertsema; M. B. van Gelder; A. Meetsma; B. L. Feringa. *J. Am. Chem. Soc.,* **2002,** *124*, 5037-5051.

13. J. M. Endtner; F. Effenberger; A. Hartschuh; H. Port. *J. Am. Chem. Soc.,* **2000,** *122*, 3037-3046.

14. I. B. Ramsteiner; A. Hartschuh; H. Port. *Chem. Phys. Lett.,* **2001,** *343*, 83-90.

15. D. F. Dever; E. Grunwald. *J. Am. Chem. Soc.,* **1976,** *98*, 5055-5062.

16. N. Bloembergen; A. H. Zewail. *J. Phys. Chem.,* **1984,** *88*, 5459-5465.

17. A. S. Sudbo; P. A. Schulz; E. R. Grant; Y. R. Shen; Y. T. Lee. *J. Chem. Phys.,* **1979,** *70*, 912-929.

18. J. M. Jasinski; J. K. Frisoli; C. B. Moore. *Faraday Discuss.,* **1983,** *75*, 289-299.

19. W. S. Warren; H. Rabitz; M. Dahleh. *Science,* **1993,** *259*, 1581-1589.

20. C. Brif; R. Chakrabarti; H. Rabitz. *New J. Phys.,* **2010,** *12*, 68.

21. M. Shapiro; P. Brumer. *Chem. Phys. Lett.,* **1988,** *149*, 451-454.

22. C. Chen; Y.-Y. Yin; D. S. Elliott. *Phys. Rev. Lett.,* **1990,** *64*, 507-510.

23. S. A. Rice; D. J. Tannor; R. Kosloff. *J. Chem. Soc., Faraday Trans. 2,* **1986,** *82*, 2423-2444.

24. E. D. Potter; J. L. Herek; S. Pedersen; Q. Liu; A. H. Zewail. *Nature,* **1992,** *355*, 66-68.

25. S. Shi; A. Woody; H. Rabitz. *J. Chem. Phys.,* **1988,** *88*, 6870-6883.

26. G. Vogt; G. Krampert; P. Niklaus; P. Nuemberger; G. Gerber. *Phys. Rev. Lett.,* **2005,** *94*, 068305.

27. P. Brumer; M. Shapiro. *J. Chem. Phys.,* **1989,** *139*, 221-228.

28. V. I. Prokhorenko; A. Halpin; P. J. M. Johnson; R. J. D. Miller; L. S. Brown. *J. Chem. Phys.,* **2011,** *134*, 085105.

29. G. Cerullo; C. J. Bardeen; Q. Wang; C. V. Shank. *Chem. Phys. Lett.,* **1996,** *262*, 362-368.

30. C. J. Bardeen; V. V. Yakovlev; J. A. Squier; K. R. Wilson. *J. Am. Chem. Soc.,* **1998,** *120*, 13023-13027.

31. D. Meshulach; Y. Silberberg. *Nature,* **1998,** *396*, 239-242.

32. K. A. Walowicz; I. Pastirk; V. V. Lozovoy; M. Dantus. *J. Phys. Chem. A,* **2002,** *106*, 9369-9373.

33. V. V. Lozovoy; I. Pastirk; K. A. Walowicz; M. Dantus. *J. Chem. Phys.,* **2003,** *118*, 3187-3196.

34. K. Mori; Y. Ishibashi; H. Matsuda; S. Ito; Y. Nagasawa; H. Nakagawa; K. Uchida; S. Yokojima; S. Nakamura; M. Irie; H. Miyasaka. *J. Am. Chem. Soc.,* **2011,** *133*, 2621-2625.

35. V. I. Prokhorenko; A. M. Nagy; R. J. D. Miller. *J. Chem. Phys.,* **2005,** *122*, 184502.

36. V. I. Prokhorenko; A. M. Nagy; S. A. Waschuk; L. S. Brown; R. R. Birge; R. J. D. Miller. *Science,* **2006,** *313*, 1257-1261.

37. P. v. d. Walle; M. T. W. Milder; L. Kuipers; J. L. Herek. *Proc. Natl. Acad. Sci.,* **2009,** *106*, 7714-7717.

38. M. Spanner; C. A. Arango; P. Brumer. *J. Chem. Phys.,* **2010,** *133*, 151101.

39. H. Miyasaka; M. Murakami; A. Itaya; D. Guillaumont; S. Nakamura; M. Irie. *J. Am. Chem. Soc.,* **2001,** *123*, 753-754.

40. C. L. Ward; C. G. Elles. *J. Phys. Chem. Lett.,* **2012,** *3*, 2995-3000.

41. C. L. Ward; C. G. Elles. *J. Phys. Chem. A,* **2014,** *118*, 10011-10019.

42. E. C. Carroll; A. C. Florean; P. H. Bucksbaum; K. G. Spears; R. J. Sension. *Chem. Phys.,* **2008,** *350*, 75-86.

43. N. A. Anderson; S. H. Pullen; L. A. Walker; J. J. Shiang; R. J. Sension. *J. Phys. Chem. A,* **1998,** *102*, 10588-10598.

44. S. A. Pullen; N. A. Anderson; L. A. Walker; R. J. Sension. *J. Chem. Phys.,* **1998,** *108*, 556-563.

45. D. A. Harris; M. B. Orozco; R. J. Sension. *J. Phys. Chem. A,* **2006,** *110*, 9325-9333.

46. E. C. Carroll; B. J. Pearson; A. C. Florean; P. H. Bucksbaum; R. J. Sension. *J. Chem. Phys.,* **2006,** *124*, 114506.

47. E. C. Carroll; J. L. White; A. C. Florean; P. H. Bucksbaum; R. J. Sension. *J. Phys. Chem. A,* **2008,** *112*, 6811-6822.

48. K. Kosma; S. A. Trushin; W. Fuß; W. E. Schmid. *Phys. Chem. Chem. Phys.,* **2009,** *11*, 172-181.

49. S. Lochbrunner; W. Fuss; K. L. Kompa; W. E. Schmid. *Chem. Phys. Lett.,* **1997,** *274*, 491-498.

50. S. Lochbrunner; W. Fuss; W. E. Schmid; K. L. Kompa. *J. Phys. Chem. A,* **1998,** *102*, 9334-9344.

51. M. Garavelli; C. S. Page; P. Celani; M. Olivucci; W. E. Schmid; S. A. Trushin; W. Fuß. *J. Phys. Chem. A,* **2001,** *105*, 4458-4469.

52. J. B. Schönborn; J. Sielk; B. Hartke. *J. Phys. Chem. A,* **2010,** *114*, 4036-4044.

53. D. Geppert; L. Seyfarth; R. de Vivie-Riedle. *Appl. Phys. B,* **2004,** *79*, 987-992.

54. N. L. Rangel; K. S. Williams; J. M. Seminario. *J. Phys. Chem. A,* **2009,** *113*, 6740-6744.

55. E. Havinga. *Experientia,* **1973,** *29*, 1181-1193.

56. W. H. Okamura; H. Y. Elnagar; M. Ruther; S. Dobreff. *J. Org. Chem.,* **1993,** *58*, 600-610.

57. B. C. Arruda; B. Smith; K. G. Spears; R. J. Sension. *Faraday Discuss.,* **2013,** *163*, 159-171.

58. K.-C. Tang; A. Rury; M. B. Orozco; J. Egendorf; K. G. Spears; R. J. Sension. *J. Chem. Phys.,* **2011,** *134*, 104503.

59. K.-C. Tang; R. J. Sension. *Faraday Discuss.,* **2011,** *153*, 117-129.

60. N. A. Anderson; J. J. Shiang; R. J. Sension. *J. Phys. Chem. A,* **1999,** *103*, 10730-10736.

61. W. Fuss; T. Höfer; P. Hering; K. L. Kompa; S. Lochbrunner; T. Schikarski; W. E. Schmid. *J. Phys. Chem.,* **1996,** *100*, 921-927.

62. J. Meyer-Ilse; D. Akimov; B. Dietzek. *J. Phys. Chem. Lett.,* **2012,** *3*, 182-185.

63. N. Gottfried; W. Kaiser; M. Braun; W. Fuß; K. L. Kompa. *Chem. Phys. Lett.,* **1984,** *110*, 335-339.

64. A. R. Webb; M. F. Holick. *Ann. Rev. Nutr.,* **1988,** *8*, 375-399.

65. E. Havinga; R. J. d. Kock; M. P. Rappoldt. *Tetrahedron,* **1960,** *11*, 276-284.

66. M. Braun; W. Fuß; K. L. Kompa; J. Wolfrum. *J. Photochem. Photobiol. A,* **1991,** *61*, 15-26.

67. W. Fuß; S. Lochbrunner. *J. Photochem. Photobiol. A,* **1997**, 159-164.

68. W. G. Dauben; B. Zhou; J. Y. L. Lam. *J. Org. Chem.,* **1997,** *62*, 9005-9008.

69. O. Dmitrenko; J. H. Frederick; W. Reischl. *J. Photochem. Photobiol. A,* **2001,** *139*, 125-131.

70. I. P. Terenetskaya. *Theor. Exp. Chem.,* **2008,** *44*, 286-291.

71. N. A. Anderson; R. J. Sension, Solvent Dependence of Excited State Lifetimes in 7-Dehydrocholesterol and Simple Polyenes. In *Liquid Dynamics*, American Chemical Society: 2002; Vol. 820, pp 148-158.

72. D. H. Waldeck. *Chem. Rev.,* **1991,** *91*, 415-436.

73. J. Saltiel. *J. Am. Chem. Soc.,* **1967,** *89*, 1036-1037.

74. D. J. S. Birch; J. B. Birks. *Chem. Phys. Lett.,* **1976,** *38*, 432-436.

75. J. Saltiel; A. S. Waller; D. F. Sears. *J. Photochem. Photobiol. A,* **1992,** *65*, 29-40.

76. J. Saltiel; A. S. Waller; D. F. Sears; C. Z. Garrett. *J. Phys. Chem.,* **1993,** *97*, 2516-2522.

77. T. Nakamura; S. Takeuchi; N. Suzuki; T. Tahara. *Chem. Phys. Lett.,* **2008,** *465*, 212-215.

78. S. K. Kim; G. R. Fleming. *J. Phys. Chem.,* **1988,** *92*, 2168-2172.

79. S. K. Kim; S. H. Courtney; G. R. Fleming. *Chem. Phys. Lett.,* **1989,** *159*, 543-548.

80. R. J. Sension; S. T. Repinec; R. M. Hochstrasser. *J. Chem. Phys.,* **1990,** *93*, 9185-9188.

81. D. C. Todd; J. M. Jean; S. J. Rosenthal; A. J. Ruggiero; D. Yang; G. R. Fleming. *J. Chem. Phys.,* **1990,** *93*, 8658-8668.

82. S. T. Repinec; R. J. Sension; A. Z. Szarka; R. M. Hochstrasser. *J. Phys. Chem.,* **1991,** *95*, 10380-10385.

83. R. J. Sension; S. T. Repinec; R. M. Hochstrasser. *J. Phys. Chem.,* **1991,** *95*, 2946-2948.

84. R. J. Sension; A. Z. Szarka; R. M. Hochstrasser. *J. Chem. Phys.,* **1992,** *97*, 5239-5242.

85. R. J. Sension; S. T. Repinec; A. Z. Szarka; R. M. Hochstrasser. *J. Chem. Phys.,* **1993,** *98*, 6291-6315.

86. A. Meyer; J. Schroeder; J. Troe. *J. Phys. Chem. A,* **1999,** *103*, 10528-10539.

87. W. Fuss; C. Kosmidis; W. E. Schmid; S. A. Trushin. *Chem. Phys. Lett.,* **2004,** *385*, 423-430.

88. W. Fuß; C. Kosmidis; W. E. Schmid; S. A. Trushin. *Angew. Chem. Int. Ed.,* **2004,** *43*, 4178-4182.

89. S. Takeuchi; S. Ruhman; T. Tsuneda; M. Chiba; T. Taketsugu; T. Tahara. *Science,* **2008,** *322*, 1073-1077.

90. S. A. Kovalenko; A. L. Dobryakov; I. Ioffe; N. P. Ernsting. *Chem. Phys. Lett.,* **2010,** *493*, 255-258.

91. A. L. Dobryakov; I. Ioffe; A. A. Granovsky; N. P. Ernsting; S. A. Kovalenko. *J. Chem. Phys.,* **2012,** *137*.

92. T. Nakamura; S. Takeuchi; T. Taketsugu; T. Tahara. *Phys. Chem. Chem. Phys.,* **2012,** *14*, 6225-6232.

93. S. A. Kovalenko; A. L. Dobryakov; E. Pollak; N. P. Ernsting. *J. Chem. Phys.,* **2013,** *139*.

94. V. Molina; M. Merchan; B. O. Roos. *J. Phys. Chem. A,* **1997,** *101*, 3478-3487.

95. V. Molina; M. Merchan; B. O. Roos. *Spectrochim. Acta Mol. Biomol. Spectrosc.,* **1999,** *55*, 433-446.

96. L. Gagliardi; G. Orlandi; V. Molina; P. A. Malmqvist; B. Roos. *J. Phys. Chem. A,* **2002,** *106*, 7355-7361.

97. C. Jiang; R. Xie; F. Li; R. E. Allen. *Chem. Phys. Lett.,* **2009,** *474*, 263-267.

98. J. Bao; P. M. Weber. *J. Phys. Chem. Lett.,* **2010,** *1*, 224-227.

99. N. Minezawa; M. S. Gordon. *J. Phys. Chem. A,* **2011,** *115*, 7901-7911.

100. R. K. Chaudhuri; K. F. Freed; S. Chattopadhyay; U. S. Mahapatra. *J. Phys. Chem. A,* **2013,** *117*, 9424-9434.

101. I. N. Ioffe; A. A. Granovsky. *J. Chem. Theory Comput.,* **2013,** *9*, 4973-4990.

102. J. Conyard; K. Addison; I. A. Heisler; A. Cnossen; W. R. Browne; B. L. Feringa; S. R. Meech. *Nat Chem,* **2012,** *4*, 547-551.

103. S. Abrash; S. Repinec; R. M. Hochstrasser. *J. Chem. Phys.,* **1990,** *93*, 1041-1053.

104. D. C. Todd; G. R. Fleming. *J. Chem. Phys.,* **1993,** *98*, 269-279.

105. L. Nikowa; D. Schwarzer; J. Troe; J. Schroeder. *J. Chem. Phys.,* **1992,** *97*, 4827-4835.

106. V. Sundström; T. Gillbro. *Chem. Phys. Lett.,* **1984,** *109*, 538-543.

107. S. H. Courtney; G. R. Fleming. *J. Chem. Phys.,* **1985,** *83*, 215-222.

108. G. Rothenberger; D. K. Negus; R. M. Hochstrasser. *J. Chem. Phys.,* **1983,** *79*, 5360-5367.

109. J. Saltiel; Y. P. Sun. *J. Phys. Chem.,* **1989,** *93*, 6246-6250.

110. M. Sumitani; N. Nakashima; K. Yoshihara; S. Nagakura. *Chem. Phys. Lett.,* **1977,** *51*, 183-185.

Chapter 2

Experimental Setup and Techniques

All of the experiments described within this dissertation require the use of ultrashort laser pulses in order to achieve the time resolution required to observe the excited state lifetimes of the molecules involved or to achieve the goal of controlling the processes these molecules undergo. This chapter includes descriptions of the ultrafast transient absorption spectroscopy technique as well as the instruments used for the experiment.

2.1 Ultrafast transient absorption spectroscopy

The core technique utilized for the experiments described in this dissertation is ultrafast, broadband transient absorption spectroscopy (TA) in the UV-Visible region. Transient absorption allows one to gain information about the nature of the excited state dynamics and/or photoproducts of a molecule of interest. First, a pump pulse interacts with the steady state population of molecules, optically exciting some percentage of this population to a higher electronic potential energy surface. Following excitation, a probe pulse interacts with the excited molecules, allowing for observation of the optical properties of the non-equilibrium excited state population. There is an adjustable time delay between the pump and the probe pulses that, when changed, allows one to collect

snapshots of the excited state absorption at specific times following excitation, allowing one to obtain information about the excited state populations.

The Beer-Lambert law defines the absorbance of some absorbing species as:

$$A = \varepsilon c \ell \tag{2.1a}$$

where ε is the molar extinction coefficient of the species, c is the concentration of the species, and ℓ is the path length of the sample. The total absorbance of a sample consisting of n absorbing species is simply the sum of the absorbance signals from each species:

$$A = \sum_{i=1}^{n} A_i = \sum_{i=1}^{n} \varepsilon_i c_i \ell \tag{2.1b}$$

This is an important consequence for ultrafast experiments since the pump pulse does not excite the majority of molecules. Because of this fact, if one were to attempt to collect an excited state absorption spectrum by simply measuring the absorbance of the sample following excitation, the result would look very similar to the ground state absorption spectrum.

In order to gather information about the excited state molecules (or if given enough time delay between laser pulses, the vibrationally excited ground state reactant or photoproduct molecules), one must define a difference spectrum that measures the change in the absorbance of the sample with and without the presence of the pump pulse (pump on/off):

$$\Delta A = A_{on} - A_{off} \tag{2.2}$$

The absorbance of the sample can be written in terms of transmittance:

$$A = -\log(T) = -\log\left(\frac{I}{I_0}\right) \tag{2.3}$$

where I is the intensity of the probe beam after interacting with the sample and I_0 is the initial probe intensity before the sample. Combining (2.2) and (2.3) yields:

$$\Delta A = -\log\left(\frac{I_{on}}{I_0}\right) + \log\left(\frac{I_{off}}{I_0}\right) = -\log\left(\frac{I_{on}}{I_{off}}\right) \tag{2.4}$$

Since it is assumed that the probe pulse does not significantly change between laser shots, the I_0 terms in the equation cancel, making it unnecessary to collect a reference spectrum. Therefore, the difference between the ground and excited state absorption spectra can be measured simply by comparing the intensities of the probe pulses after they interact with the sample. Using the transient absorption technique, it is possible to elucidate the reaction dynamics of a chemical system based on the observation of several types of processes and signals. Four commonly observed signals are ground state bleach, excited state absorption, stimulated emission the excited state, and ground state photoproduct absorption.

Following excitation, the molecules that have been excited from the ground state into some higher electronic state may be transparent to frequencies of light that would normally interact with and be absorbed by the ground state molecules. In the transient spectrum, this transparency results in higher probe intensity after the sample, which gives a net loss of absorption ($\Delta A < 0$). This is known as ground state bleach. In addition, the excited molecules may or may not exhibit their own separate absorption spectra. In many cases these absorption bands lie in a different spectral region than the ground state molecules, although the two bands could overlap. In these cases of excited state

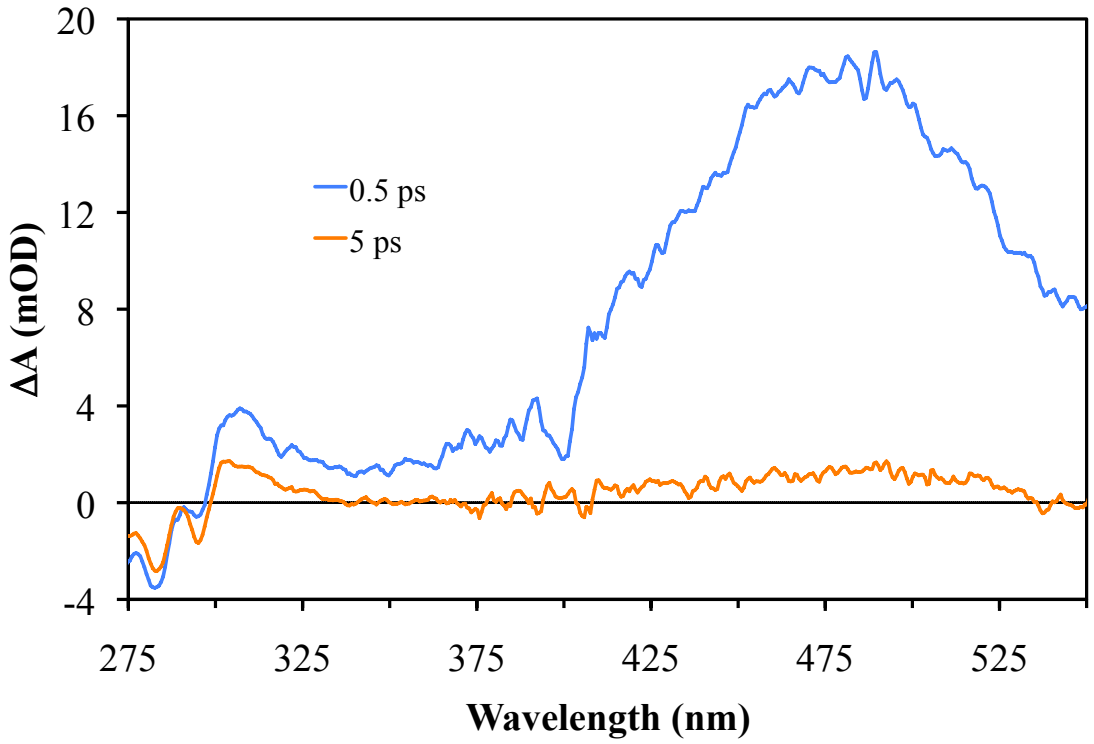

Figure 2.1 *Transient absorption spectrum of 7-dehydrocholesterol at ~0.5 and 5 ps exhibiting ground state bleach between 270-295 nm in both spectra, vibrationally excited photoproduct from 295-340 nm in the 5 ps spectrum, and excited state absorption between 375-550 nm in both spectra.*

absorption, the excited molecules absorb frequencies of light that previously showed no interaction with the ground state molecules, resulting in lower probe intensity after the sample and a net gain of absorption ($\Delta A > 0$). As the excited state population decays, photoproducts with distinct absorption spectra may result. These photoproducts will show the same type of increase in absorption as the excited state absorption signal.

In addition to the above phenomena, molecules may also display a stimulated emission process in the transient spectrum. When the probe pulse interacts with the excited state molecules, any probe frequencies overlapping with the molecules' emission spectra may stimulate the emission of a photon that propagates collinearly with the laser

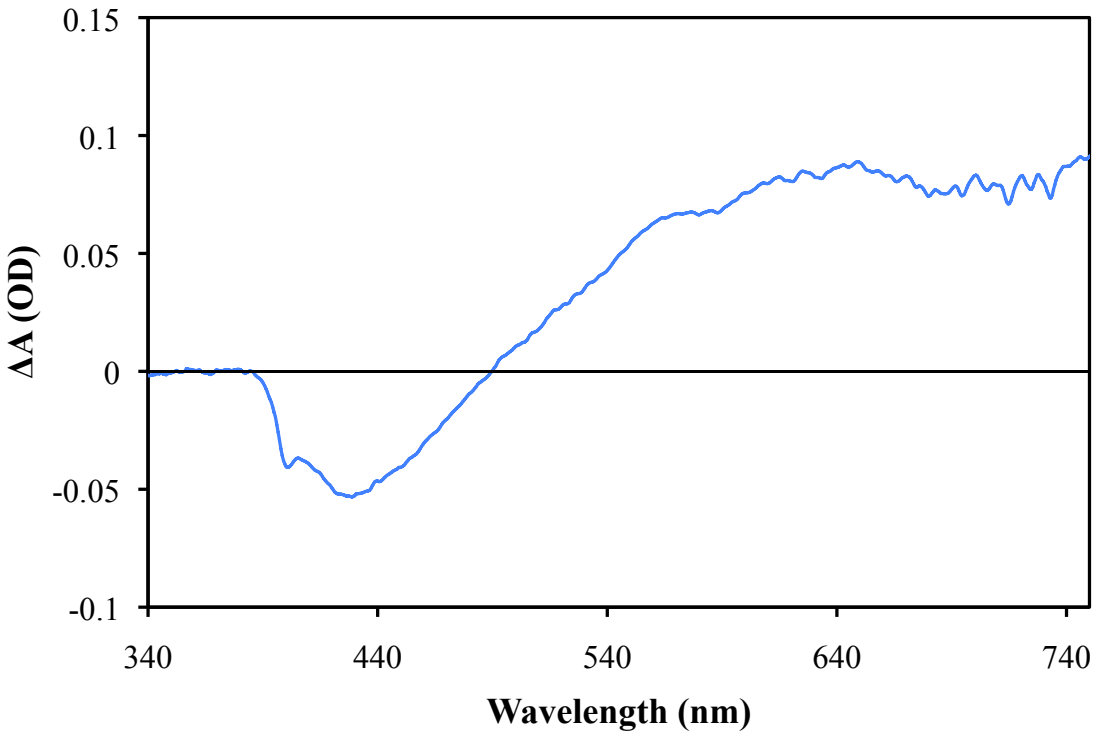

Figure 2.2 *Transient absorption spectrum of stilbene-3 laser dye at ~3 ps exhibiting an excited state absorption between 490 and 740 nm and a stimulated emission signal between 390 and 490 nm. Residual pump beam scattering into the spectrometer can be seen around 400 nm.*

pulse. This results in higher probe intensity after the sample and a net loss of absorption ($\Delta A < 0$).

2.2 Laser systems and instruments

2.2.1 Ti:Sapphire Oscillator

The time-bandwidth product describes the intrinsic link between the spectral bandwidth ($\Delta\nu$, FWHM of power spectrum) and the pulse duration (Δt, FWHM of pulse intensity) of a laser pulse. For example, a laser pulse with a Gaussian shape exhibits a time-bandwidth product described by the following inequality:[1]

$$\Delta\nu\Delta t \geq \frac{2\ln 2}{\pi} = 0.441 \tag{2.5}$$

Thus, for a given value of one quantity there is a minimum possible value for the other. A laser pulse with the shortest possible pulse duration for a given spectral bandwidth is known as the transform-limited pulse. Equation (2.5) makes it clear that in order to observe events that occur on very short time scales it is necessary to create laser pulses with very large spectral bandwidth. This phenomenon can be explained by considering the constructive and destructive interference between the many frequencies that make up the laser pulse.

Titanium-doped sapphire ($Ti:Al_2O_3$) is an excellent material for the generation of broadband, ultrafast laser pulses since it has an incredibly broad gain spectrum centered around 800 nm with a full width at half maximum of ~250 nm.[2] This corresponds to a gain bandwidth of ~100 THz. With a 1.65 m laser cavity, the frequency difference between adjacent longitudinal modes can be calculated to be 91 MHz. This means that the number of stable modes within the gain spectrum of Ti:sapphire is ~1.1 x 10^6. Such a high number of stable modes results in a broadband output spectrum, thus providing the means to generate ultrashort pulses.

The Ti:Sapphire oscillator used for these experiments is assembled from a Kapteyn-Murnane Laboratories kit and is similar in design to the oscillator described by Backus et al.[3] The laser used as a pump source for the Ti:Sapphire crystal is a Spectra Physics Millennia V (532 nm). The oscillator pulses are centered between 800-810 nm with a full width at half maximum (FWHM) of ~30 nm and have pulse widths on the order of 50 fs. The cavity length is 1.65 m, giving a temporal pulse separation of ~11 ns (the amount of time it takes for the light to complete one round trip in the laser cavity).

The oscillator is passively modelocked using the self-modulation of the light in the cavity by the optical Kerr effect, which is known as Kerr-lens modelocking. The Kerr effect is a change in the refractive index of a material due to the presence of an applied electric field, and in the case of the optical Kerr effect, this applied field is the electric field of the electromagnetic wave itself. The intensity dependent refractive index can be written as:[1]

$$n(I) = n_0 + n_2 I \tag{2.6}$$

where n_0 is the linear refractive index of the material, n_2 is the second order nonlinear refractive index of the material, and I is the intensity of the electromagnetic wave. Since the intensity profile of the laser varies spatially, the medium through which it is propagating will exhibit a spatial refractive index gradient that mimics the intensity profile of the beam. Due to this effect, the material acts as a lens, which causes the beam to undergo self-focusing.

A laser under continuous wave operation will focus itself differently than a laser in pulsed operation due to the higher peak intensity exhibited by the pulses, resulting in a different beam waist size and divergence outside of the gain medium. It is then possible to make the laser operate in a pulsed mode by making the cavity unstable for continuous wave operation. Once pulsed operation has begun, it is self-sustaining. In the case of our Ti:Sapphire oscillator, the beam profile slightly clips on the edge of one of the prisms in a prism pair that is used to correct for the dispersion introduced by the gain medium. A slight perturbation to this prism is enough to stabilize pulsed operation and modelock the oscillator.

2.2.2 Chirped pulse amplification

While the oscillator outputs pulses centered between 800-810 nm with pulse widths on the order of ~50 fs, each pulse only consists of ~5 nJ of energy, which is not enough energy to perform the types of nonlinear optical processes required to generate the optical frequencies and shaped pulses needed for experiments. This is overcome through the use of chirped pulse amplification to increase the pulse energy to a useable range. This method of pulse amplification first uses an optically dispersive element to stretch the seed pulse in time. Next, a separate optical pump source excites a gain medium through which the stretched seed pulse propagates. If the seed pulse is temporally and spatially overlapped with the pump pulse it will induce stimulated emission from the excited gain medium, resulting in amplification. Once the seed pulse is amplified it is then recompressed to a (near-)transform limited pulse duration. As Ti:Sapphire is used to generate the initial oscillator pulses, it is also used as the gain medium to amplify those pulses. The stretching of the pulse in time is important in this method, because if the pulse were injected into the amplification stage directly after exiting the oscillator, the peak intensity of the focused, amplified pulse inside the gain medium would exceed the damage threshold of the material.

Before the oscillator seed pulses are amplified, the pulse repetition rate must be reduced. The reason for this is two-fold. First, the high energy, visible lasers that are used to pump the gain medium generate pulses through the use of Q-switching, which limits their pulse repetition rate. Therefore, the repetition rate of the oscillator pulses must be reduced to match that of the amplifier pump laser. Second, the repetition rate of the oscillator is much too high for the experiments on some systems, as the 11 ns delay

between consecutive pulses can be on the same order of time as the photochemical processes being studied. This would lead to a situation where the sample cannot recover to the ground state before the next pulse in the pulse train arrives. Even if the excited molecules have enough time to relax back to the ground state, the sample cannot be flowed fast enough to refresh the volume between pulses. This can result in macroscopic heating due to thermal build up in the sample. Reducing the repetition rate of the oscillator pulses is done by selecting single pulses out of the pulse train at a frequency of 1 kHz using a Pockels cell paired with a polarizing cube. The Pockels cell crystal acts as a $\lambda/2$ waveplate when an external electric field is applied, which rotates the polarization of any light propagating through the crystal. A pulsed electrical signal allows for the polarization rotation of a single pulse (the response time is ~10 ns), and the polarizing cube reflects the non-rotated pulses while transmitting the rotated pulse.

Since multiple amplifiers were used for the different experiments described in this dissertation, these instruments are described separately. However, both instruments share the same stretcher, which consists of a single diffraction grating design that is aligned to introduce positive group delay dispersion to the pulse, thus chirping the pulse and increasing its temporal width to ~50 ps. While the amplifiers use different designs, the compressors for both systems are of a similar dual diffraction grating design. The compressors are aligned to complement the stretcher in order to introduce enough negative group delay dispersion to correct for the positive dispersion from the stretcher and that from the Ti:Sapphire crystals in the amplifiers.

The amplifier used for the chirped pulse experiments described in chapter 4 is a multipass design similar to the stage one amplifier described by Zhou et al.[4] with a

Ti:Sapphire crystal cut at Brewster's angle. Its design is such that the seed pulse from the oscillator is injected into a ring of mirrors and is directed into the same position in the crystal eight individual times. After the eighth pass, a pick off mirror sends the pulse to the compressor to be shortened. In order to amplify the seed pulses, a pump beam is focused into the Ti:Sapphire crystal so that it is spatially and temporally overlapped with the seed beam. The pump laser used for this amplifier is a flash lamp pumped, Q-switched Quantronix 527 Nd:YLF (527 nm) with a frequency doubled output pulse of 8.5-9.0 mJ, 200 ns at 527 nm. The stretched and amplified pulses that exit the amplifier are 0.75-0.90 mJ in pulse energy. Following compression, these pulses are reduced to ~60% of their pre-compression energies and have a pulse duration of ~80 fs.

The experiments described in chapters 3 and 5 used two amplifiers in series to generate the pulses needed for experiment. The preamplifier is a regenerative amplifier (regen) with a folded cavity design similar to that described by Squier et al.[5] Unlike multipass amplifiers in which the number of passes through the crystal is determined by the geometry of the optics, regenerative amplifiers control the number of passes through the use of electronics. First, a stretched, polarized seed pulse is injected into the regen cavity with a thin film polarizer set at Brewster's angle. A Pockels cell then flips the polarization of the pulse so that it is trapped inside of the cavity. The seed pulse is allowed to oscillate within the cavity, experiencing amplification with each pass through the pumped crystal, until the Pockels cell is used to flip its polarization. The pulse is then ejected from the cavity by the same thin film polarizer used for injection, and sent to a multipass post-amplifier with a 3-pass design similar to that of the multipass preamplifier described by Backus et al.[3]

The Ti:sapphire crystals in both amplifiers are pumped using a Spectra Physics Evolution-30 (527 nm). The 19 mJ, 200 ns pulses from this laser are split in order to pump both the regen and 3-pass amplifiers. Pump pulses sent to the regen have energy of 6.8 mJ. The amplified, stretched pulses out of the regen have pulse energy between 0.70-0.90 mJ. Pump pulses to the 3-pass amplifier have energy of 10.8 mJ. Amplified, stretched pulses exiting the 3-pass amplifier have energy of 1.2-1.5 mJ. Following compression the intense, ultrafast pulses have energy of 0.7-0.8 mJ and a pulse duration of ~80-90 fs.

2.2.3 Transient absorption apparatuses

UV pump pulses for all experiments were generated through either third harmonic generation using the fundamental pulses or by frequency doubling the output of a noncollinear optical parametric amplifier (NOPA) that produces visible pulses. NOPA output pulses were used as is for the repump pulses utilized in the experiments described in chapter 5. Probe pulses for all experiments were broadband white light continuum pulses generated by focusing either fundamental frequency or frequency doubled laser pulses into a 5 mm CaF_2 window. This window was kept in motion at all times in order to prevent optical damage. The continuum generated using the frequency doubled pulses extends further into the UV compared to those generated with fundamental pulses. All experiments used a spectrometer with a CCD array in order to detect the probe pulse intensity at many wavelengths, though different models were used between the two TA instruments. Probe pulses were coupled into the spectrometer by focusing into a fiber optic cable.

Mechanical delay stages are used in order to measure the spectra of the sample at different time delays between the pump and probe. A corner cube is mounted atop the motor that moves up and down the length of the stage. The pump or probe be can be sent to and reflected back from this optic, allowing for an adjustment of the path length of that particular beam as the stage moves, thus producing an adjustable delay between this beam and the other, stationary one. These delay stages are computer controlled and are able to take very fine steps (6.67 fs/step or 16 fs/step depending on the stage). For the pump-repump experiments in chapter 5, a second delay stage is used in order to create an adjustable delay between pump and repump pulses.

All samples used in experiment were continuously flowed in order to prevent photodegradation of the sample. This was done using either a quartz flow cell (0.5 or 1 mm path length) or a gravity-driven wire-guided flow instrument of similar design to the one described by Tauber et al.[6] In both cases, a peristaltic pump was used in order to maintain the flow of solution.

The ground state signal for a transient absorption measurement is generated without the presence of the pump pulse, and the excited state (plus residual ground state) signal is generated using a pump pulse at some time delay before the probe pulse arrives. One simple way to generate transient absorption difference spectra would be to place a beam block the path of the pump beam in order to collect the ground state signal at each time delay before unblocking the pump to collect the excited state signal. However, this method is not ideal as it is incredibly time consuming. Instead, we use an optical chopper in the pump beam path to block half of the pump pulses (pump off) and allow the rest to pass through to the sample (pump on). This allows the experimental software to collect

both the excited state and ground state signals consecutively at each time delay.

Due to limitations in the speed of the electronics and software used for data collection, it is not possible to collect alternating pump on and pump off by chopping at 500 Hz (one half of the 1kHz pulse repetition rate). Instead, lower frequencies must be used. For example, at 166 Hz six laser pulses arrive at the chopper within one chopper cycle. The first three will be blocked while the last three will not, giving alternating pump on and pump off sequences of three pulses each. The spectrometer is triggered at twice the chopping frequency in order to collect pump on and pump off measurements separately, and its integration time is set such that it only collects the first two pulses in each sequence. This is done in order to give the other electronics involved with the data collection software enough time to complete their respective tasks without risking overlap into the next three pulse sequence.

It is necessary for the software to be able to distinguish whether a particular spectrum is associated with a pump on or pump off sequence. In the past this was done by collecting the leftover pump pulses following sample excitation and directing them onto a photodiode. The photodiode output could then be measured to determine whether or not pump pulses were present for a particular collected spectrum. For our experiments, we utilize the square wave TTL signal output of the chopper to distinguish between pump on and pump off. The computer's data acquisition board monitors this TTL signal to determine whether a specific spectrum was collected with pump pulses present.

The equipment and techniques detailed within this chapter provide the tools needed to perform all of the experiments described throughout this dissertation. The

experiments described in chapters 3 and 5 use a different transient absorption apparatus than the experiments described in chapter 4. In addition, there are many significant changes to this equipment between experiments. Therefore, the details regarding pulse energy, wavelength, and other parameters, as well as the instruments specific to certain experiments, will be described in detail within their respective chapters.

2.3 References

1. A. M. Weiner, *Ultrafast Optics*. Wiley: 2009.
2. P. F. Moulton. *J. Opt. Soc. Am. B,* **1986,** *3*, 125-133.
3. S. Backus; C. G. Durfee; M. M. Murnane; H. C. Kapteyn. *Rev. Sci. Instrum.,* **1998,** *69*, 1207-1223.
4. J. Zhou; I. P. Christov; G. Taft; C.-P. Huang; M. M. Murnane; H. C. Kapteyn. *Opt. Lett.,* **1994,** *19*, 1149-1151.
5. J. Squier; F. Salin; G. Mourou; D. Harter. *Opt. Lett.,* **1991,** *16*, 324-326.
6. M. J. Tauber; R. A. Mathies. *Rev. Sci. Instrum.,* **2003,** *74*, 4958-4960.

Chapter 3

Transient Absorption of 7-Dehydrocholesterol with Tunable Ultraviolet Excitation

Many ultrafast pump-probe studies on DHC have utilized a UV pump pulse centered at or near 266 nm (the third harmonic of a Ti:sapphire laser centered at 800 nm or the fourth harmonic of an Nd:YAG laser).[1-6] This excitation wavelength falls on the blue edge of the $S_1 \leftarrow S_0$ transition and imparts excess vibrational energy to the molecule as it is resonant with the 0-3 vibronic transition (Figure 3.1). The peaks in the absorption spectrum are separated by ~1350 cm^{-1}, which corresponds to a vibrational mode associated with C=C stretching in the excited state. It is certainly possible that the excess vibrational energy placed into the carbon backbone modes in the excited molecule could have a significant effect on the dynamics of the ring-opening reaction.

Jacobs, Gielen, and Havinga showed that the quantum yield of the DHC ring-opening reaction (φ=0.34) did not change between excitation at 254 nm and 302.5 nm.[7] However, they reported that the quantum yield of the reverse reaction, the ring-closure from cZc-Previtamin D_3 back to DHC, did in fact show a difference between these two excitation wavelengths (as did the quantum yields for the other isomerization reactions possible for cZc-Pre). Further investigation by Dauben et al. of quantum yields of ring-closure and cis-trans isomerization of cZc-Previtamin D_3 at various other excitation

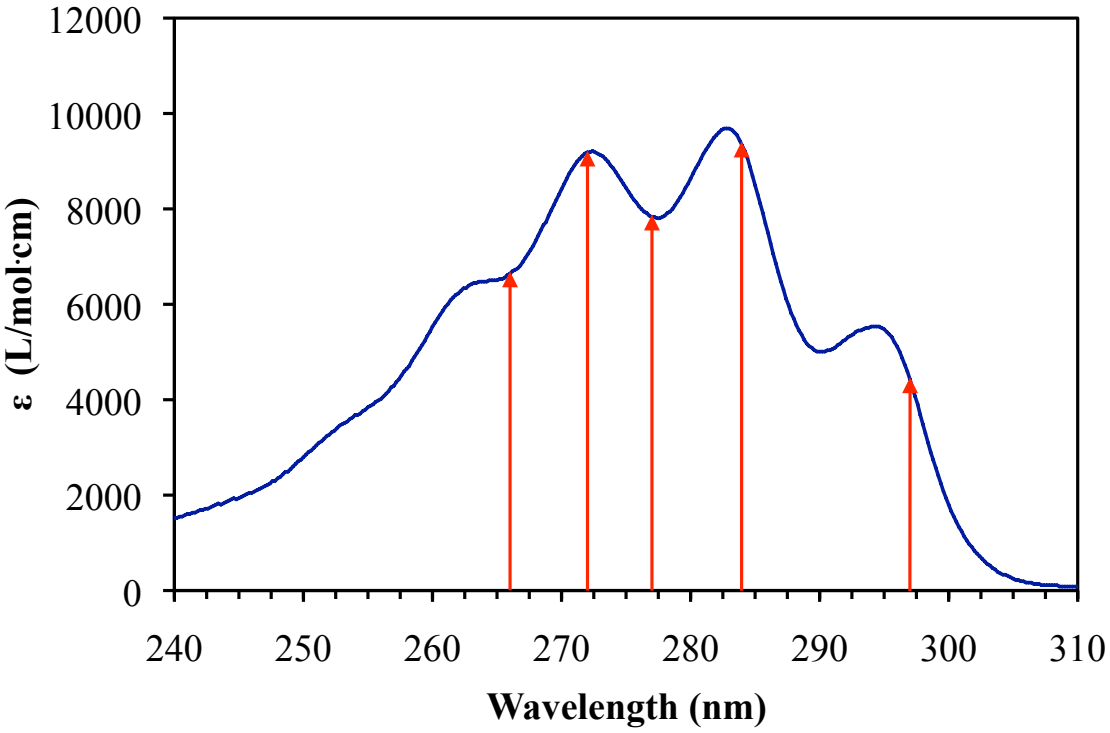

Figure 3.1 *DHC steady state absorbance spectrum in 2-butanol with arrows corresponding to the excitation wavelengths used in this experiment (266, 272, 277, 284, 297 nm).*

wavelengths revealed that the change in quantum yield occurred sharply near 302 nm.[8] It was suggested by Fuss and Lochbrunner that the wavelength dependence on these quantum yields arises from the competition between the ring-closing and double-bond isomerization.[9] Due to a barrier experienced by the latter process, the isomerization rate is dependent on photon energy.

In contrast to ring-closing, the ring-opening of DHC experiences no competing isomerization reaction, and the quantum yield is unaffected by excitation energy. However, this process does experience an intrinsic barrier of ~2 kJ/mol (167 cm^{-1}) as well as an extrinsic, solvent dependent barrier in the excited state along the reaction coordinate. In 2-butanol for example, the effective activation barriers for the fast and

slow components of the biexponential decay of the excited state are 8.3 and 9.9 kJ/mol (~700 cm^{-1} and ~830 cm^{-1}), respectively.[4] The size of the effective barriers is about half of one quantum of energy in the vibrational mode that is visible in the DHC steady state absorption spectrum (~1350 cm^{-1}). Therefore it is reasonable to assume that any amount of excess vibrational energy could play a significant role in the kinetics of the ring-opening reaction. In order to test this, transient absorption measurements exciting DHC at a range of wavelengths between 297 nm and 266 nm were performed.

3.1 Experimental details

Descriptions of the Ti:sapphire oscillator and the amplifier systems used to generate the intense, ultrafast pulses centered near 800 nm can be found in chapter 2. Following amplification and compression, pulses were split into pump and probe arms. Pump pulses were generated using a NOPA tunable between ~530-625 nm and then doubled using a Type I BBO crystal, resulting in UV pulses ranging between ~270-300 nm. 266 nm pump pulses were generated through third harmonic generation of the fundamental laser beam. Typical pulse energies at the sample were between ~220-300 nJ. Probe pulses were generated by focusing the fundamental laser pulses into a 5 mm CaF_2 plate. The plate was kept in motion in order to prevent optical damage. The spectrum of these pulses spanned the wavelength range between 350 nm and 650 nm (Figure 3.2). Residual 800 nm light was filtered out with either a BG-23 or KG3 Schott glass filter depending on the experiment.

Pump pulses were switched on and off at the sample by a Terahertz Technologies Digirad C-980 optical chopper set to a chopping frequency of 100 Hz (5 on, 5 off). The

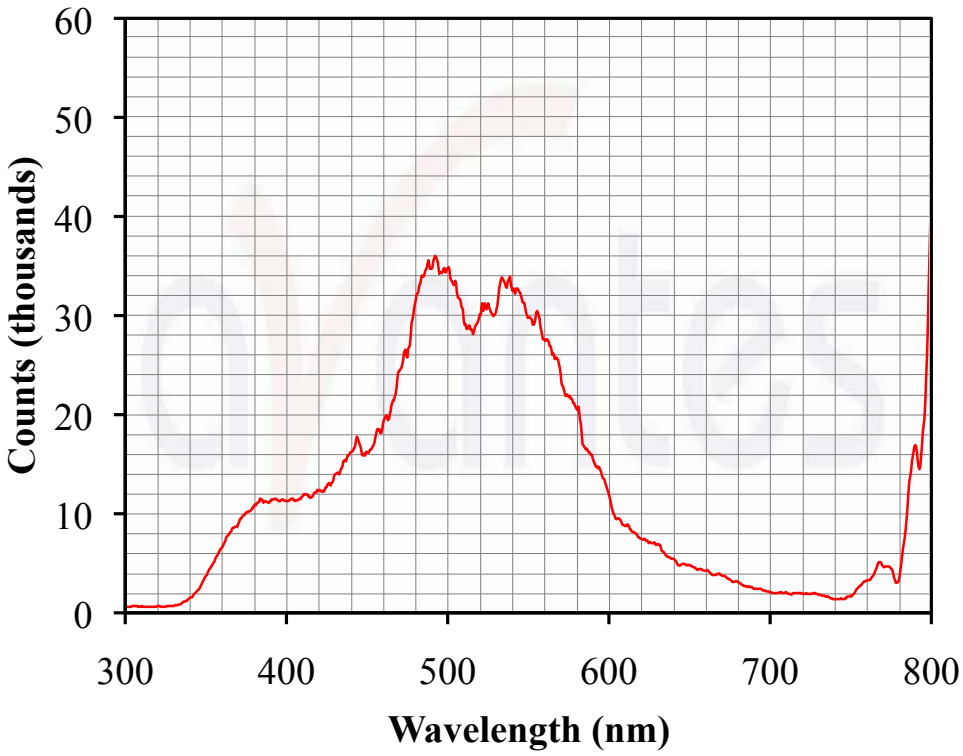

Figure 3.2 *Broadband white light continuum from CaF_2 used as probe pulses for these experiments.*

pump-probe delay was adjusted using a mechanical delay stage driven by a Parker Hannifin Compumotor LX-L20 indexer/microstepping drive. The angle between pump and probe beams at the sample was ~9 degrees. Pump pulses were focused into the sample with a fused silica lens (FL = 175 mm), and probe pulses were focused into the sample with a UV enhanced aluminum spherical mirror. After probing the sample, the white light pulses were focused into a 200 μm UV-Vis coated fiber from Avantes and coupled into a single-channel spectrometer (Avantes Avaspec, 2048-USB2-UA). For all measurements, the pump and probe polarizations were kept at magic angle (54.7°) in order to minimize contributions to the signal due to rotational diffusion. After the completion of each data set, the pre-zero baseline was subtracted from the data, and the

chirp of the white light continuum was corrected by fitting the coherent spike at t=0 ps with a 3rd order polynomial.

7-dehydrocholesterol (98%) was acquired from Sigma-Aldrich and used without further purification. A gravity driven wire-guided flow setup was used in order to reduce the amount of cross phase modulation between pump and probe. The thickness of the solvent sheet was adjusted by changing the flow rate of sample solution. The flatness of the sheet was determined by monitoring the focusing properties of the white light into the fiber and spectrometer after passing through the sheet. All ultrafast measurements discussed here were performed in 2-butanol. The concentration of the samples was ~0.8 mM. Samples were continually flowed during the experiments in order to prevent degradation.

3.2 Experimental results

Transient absorption (TA) spectra of DHC in 2-butanol were collected using 5 different excitation wavelengths: 266, 272, 277, 284, and 297 nm (Figure 3.1) for probe wavelengths from 350 nm to 650 nm and time delays out to 30 ps. This range allows for characterization of both the decay dynamics and the spectral structure of the excited state absorption. All scans exhibited a spike at t=0 ps that was due to the cross correlation of the pump and probe pulses when they are temporally and spatially overlapped. The size of this signal was reduced in the DHC scans due to the absorption of the pump by the chromophore.

The excited state spectra, integrated from 1-2.5 ps, are shown in Figure 3.3. Since signal size in each data set varied (mainly due to differences in pump energy), each

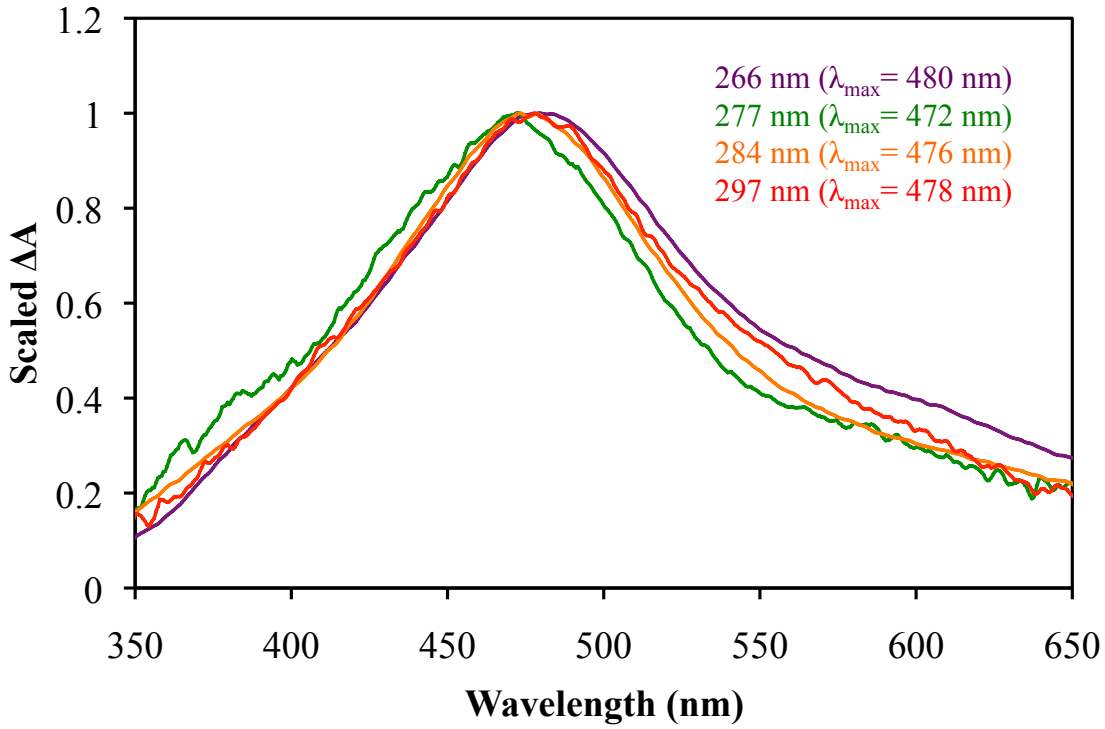

Figure 3.3 *Scaled excited state absorption (ESA) spectra of DHC in 2-butanol for four of the five different excitation wavelengths. Peak ESA positions are listed alongside the excitation wavelengths.*

spectrum is scaled to a maximum intensity of 1. The strong, visible excited state absorption (ESA) seen here is typical of DHC. The peak value of the ESA depends slightly on excitation wavelength, but the overall band shape is similar for all excitation wavelengths, although some data sets appear to have a slightly smaller shoulder on the red side of the ESA.

The kinetic analysis of each data set was performed by integrating over the excited state absorption peak from 450-500 nm (with the exception of the 272 data, which was integrated from 480-500 nm due to poor white light on the blue side of the ESA spectrum). The integrated intensity was fit using a simplex algorithm. Long time signals due to multiphoton fragmentation or ionization of the solvent were subtracted from each

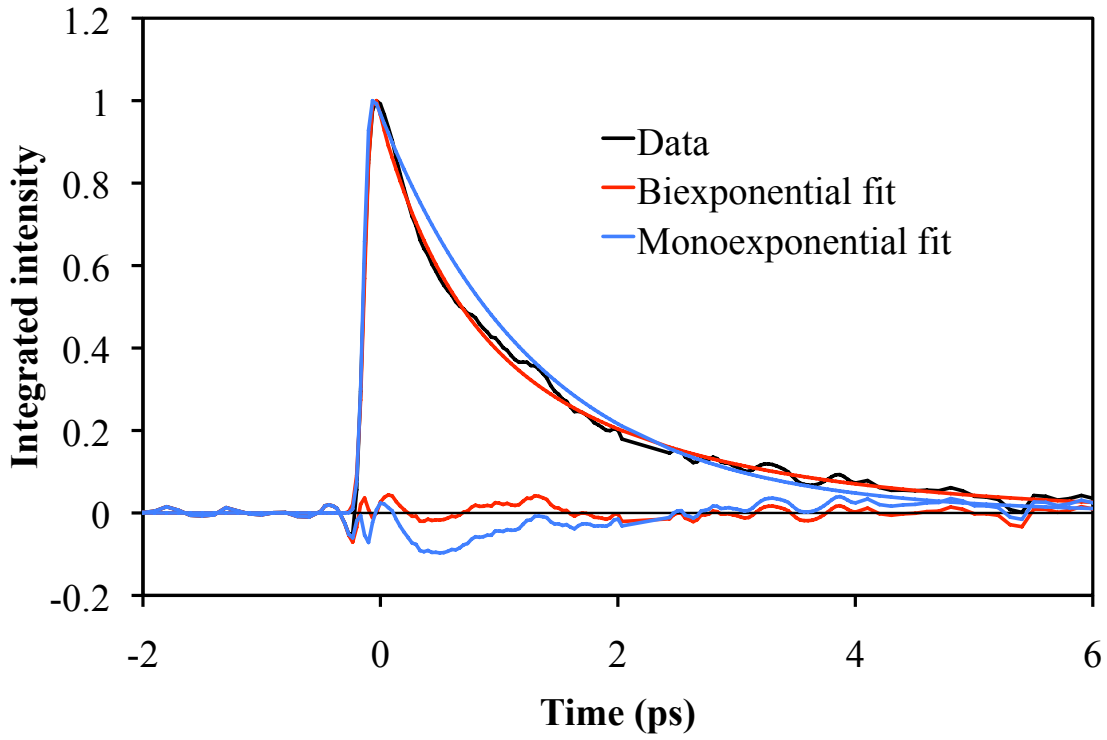

Figure 3.4 *Comparison of monoexponential and biexponential fits to kinetic trace of DHC excited state absorption integrated from 450-500 nm (297 nm excitation). Residuals are shown along with the fits.*

data set by first fitting only that piece and then subtracting this fit from the raw kinetic traces. Like the previously reported results, all data collected here required at least two exponential decay components.[4-5] Comparison of biexponential and monoexponential fits to the data can be seen in Figure 3.4. Examples of fits to each data set can be seen in Figure 3.5, and the time constants and relative amplitudes of the two decay components in the DHC ESA for each excitation wavelength are listed in Table 3.1. A plot comparing the time constants of the resultant fits with those previously reported by Tang et al. with 266 nm excitation in 2-butanol (0.56 ± 0.06 ps and 1.81 ± 0.15 ps)[4] is shown in Figure 3.6. While the 277 nm data appears to experience a slightly faster decay relative to the other data sets, within the reported error the time constants for each excitation wavelength are in agreement with the previously reported results.

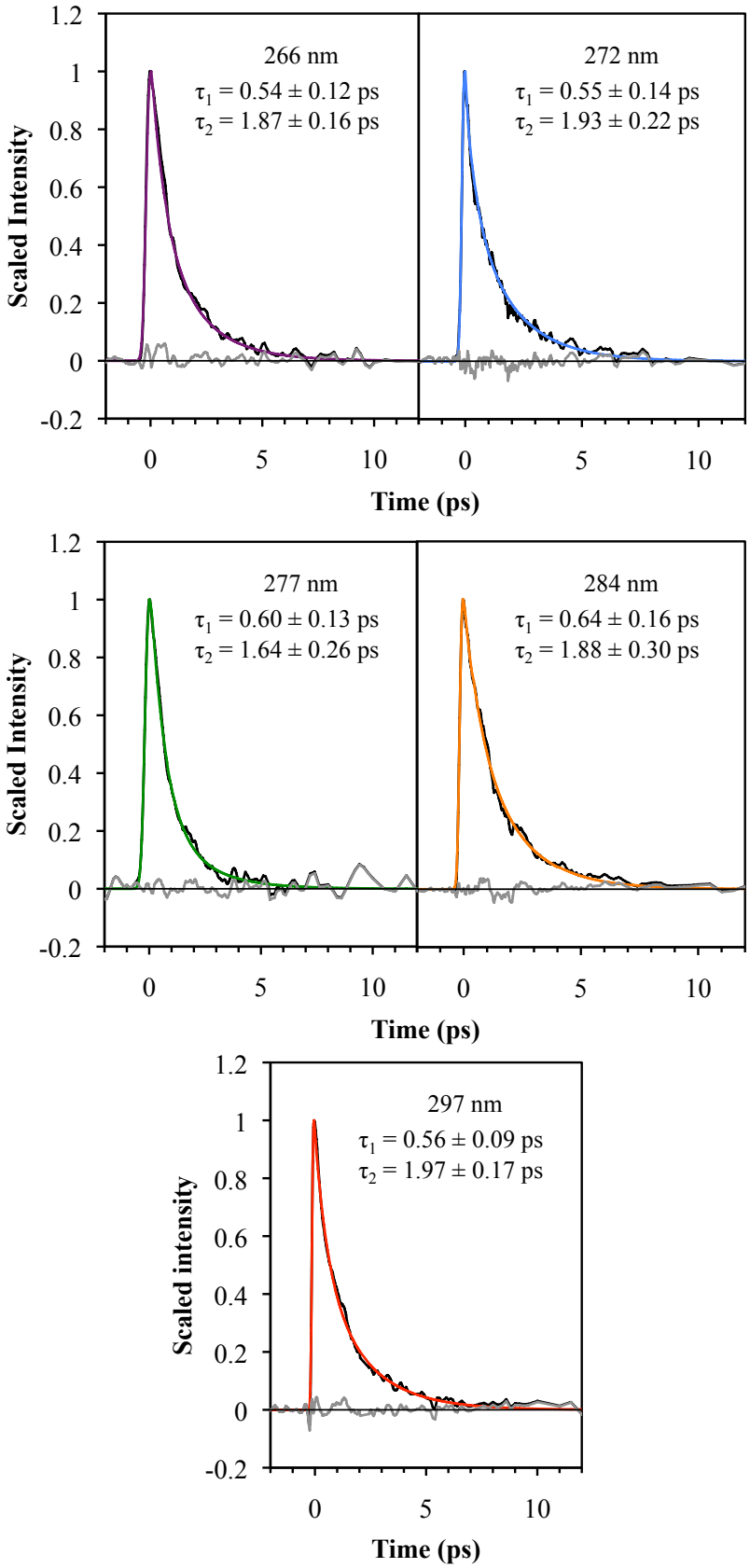

Figure 3.5 *Fits and residuals of ESA decay for the various excitation wavelengths.*

Table 3.1 *Time constants and fraction of total amplitude for each decay component obtained from multiple fits of integrated spectral data. Error bars reported here are the calculated standard errors of the mean from each fit. However, as explained in the text, these values are the minimum estimate for the errors, which are actually expected to be much larger.*

Excitation wavelength (nm)	$\frac{A_1}{A_1 + A_2}$	**τ_1 (ps)**	$\frac{A_2}{A_1 + A_2}$	**τ_2 (ps)**
266	*0.59*	*0.54 ± 0.12*	*0.41*	*1.87 ± 0.16*
272	*0.46*	*0.55 ± 0.14*	*0.54*	*1.93 ± 0.22*
277	*0.69*	*0.60 ± 0.13*	*0.31*	*1.64 ± 0.26*
284	*0.44*	*0.64 ± 0.16*	*0.56*	*1.88 ± 0.30*
297	*0.48*	*0.56 ± 0.09*	*0.52*	*1.97 ± 0.17*

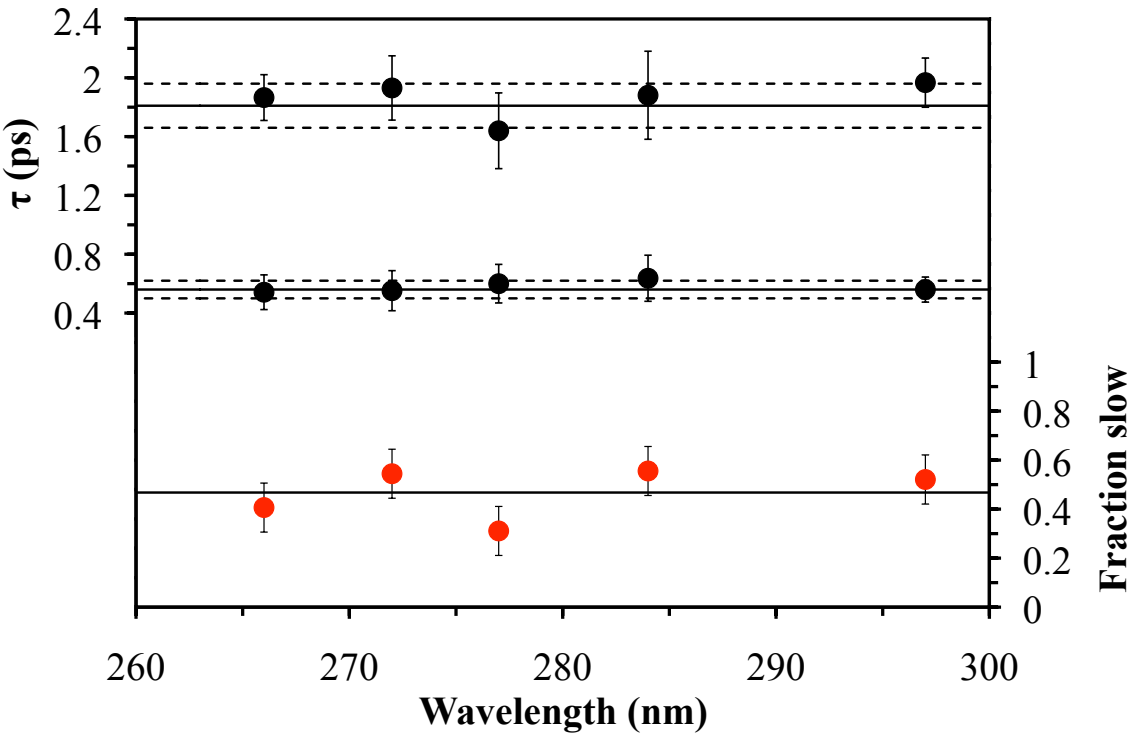

Figure 3.6 *(Top) Time constants of biexponential fits to the integrated spectra plotted alongside the previously reported values for decay following 266 nm excitation and their error bars (solid and dashed horizontal lines, respectively).*[4] *(Bottom) Fraction of the slow decay component relative to the total amplitude of the two fitting components. The solid, horizontal line is the average value of the five data points.*

. The relative amplitudes of the two components for each excitation wavelength are also shown in Figure 3.6 as the fraction of the total amplitude belonging to the slow component. The amplitudes of the fast and slow decay components have previously been shown to depend on the chirp of the excitation pulse.[5] Since chirp was not directly monitored in the current experiments (and almost certainly changed between each data set due to changes in the laser), it is unknown whether any differences in the fraction of the total amplitude of the slow component are a result of the chirp of the excitation pulse or the frequency of the pulse itself. However, these numbers show that, in general, the relative contributions of the fast and slow components are not significantly changed upon varying the excitation frequency.

Two-dimensional plots of the reduced χ^2 of each fit as a function of the two decay components were made in an attempt to gain a better understanding of the errors in the fits. An example of these plots can be seen in Figure 3.7. Considering the result shown in this figure, the errors in the fits are actually larger than those reported in Table 3.1. The very large reduced χ^2 value (>1) reported for the 266 data in this plot demonstrates that a biexponential fit is not a good model for these data. This is due to an underestimation of the intrinsic noise in the data and a systematic error that is related to the delay stage. This error is present in all scans (but is more noticeable in certain scans) and introduces artifacts into the data. Attempts to fit this artifact in addition to the exponential decay of the data were unsuccessful. It should also be noted that attempts were made to globally fit the transient data between 400-650 nm for each excitation wavelength, but the overall noise in the data and the systematic error mentioned above made global fitting exceedingly difficult.

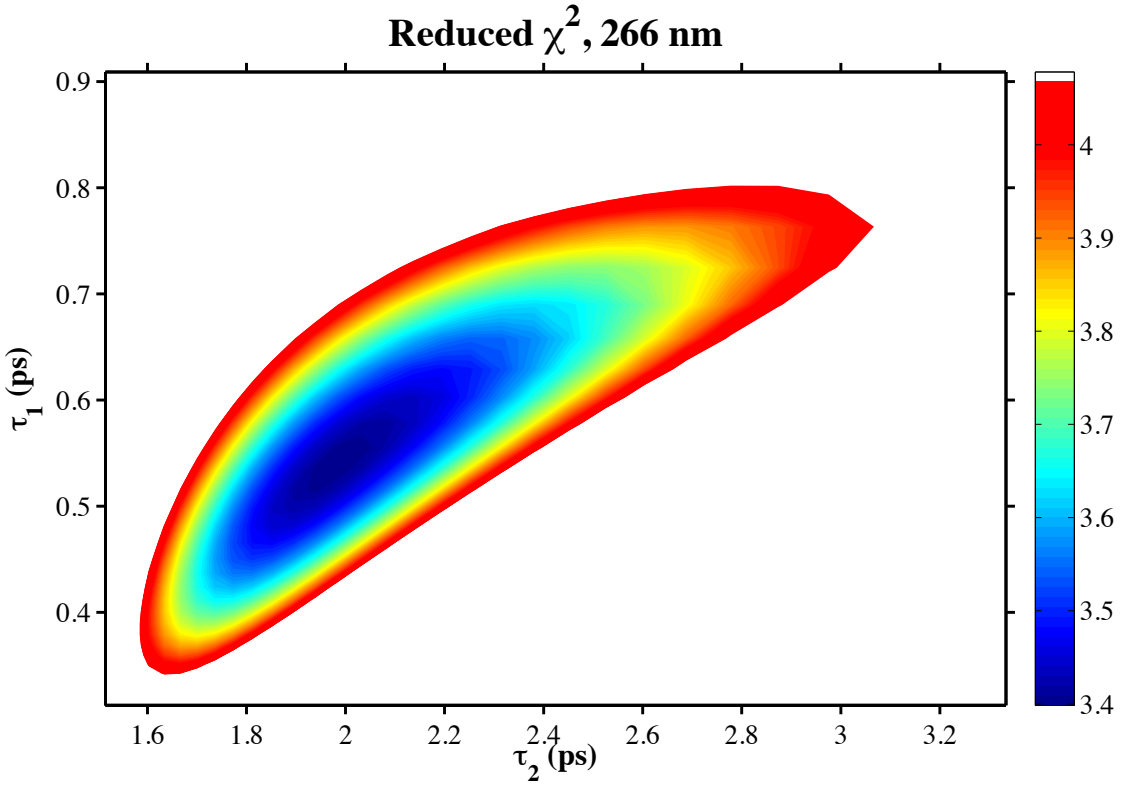

Figure 3.7 *Plot of the reduced χ^2 as a function of the two time constants used in fitting the data. The upper limit of the heat map is defined as a 20% increase in the minimum value of the reduced χ^2.*

3.3 Discussion

As the $S_1 \leftarrow S_0$ excitation frequency is increased, resulting in an increase in the vibrational energy of the excited molecule, one could expect that the $S_n \leftarrow S_1$ transition energy would decrease, resulting in a redshift of the excited state absorption (see Figure 3.8). This is not what was observed here. The position of the excited state absorption peak (and thus the $S_n \leftarrow S_1$ transition energy) does not follow a monotonic trend with respect to the excitation frequency. Rather, the excited state absorption peak wavelength

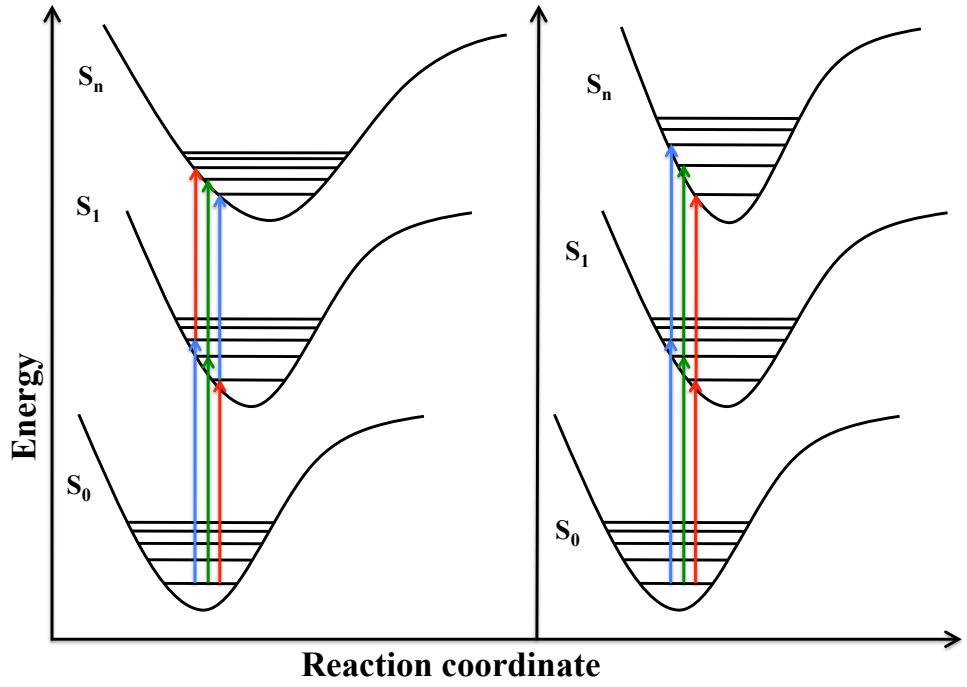

Figure 3.8 *Cartoon of potential energy surfaces which shows that as $S_1 \leftarrow S_0$ energy increases: $S_n \leftarrow S_1$ energy decreases when S_1 is steeper than S_n (left) and $S_n \leftarrow S_1$ energy increases when S_n is steeper than S_1 (right). Notice that in addition to the reversal of the trend, the case with the steeper S_n surface shows a larger change in energy between $S_n \leftarrow S_1$ transitions.*

decreases (and thus energy of the transition increases) with respect to the excitation wavelength in the following trend: 266, 284, 297, 277 nm (Figure 3.3).

One explanation for this unexpected trend is a difference in the vibronic transitions of the $S_n \leftarrow S_1$ transition. A blueshift of this excited state absorption could result when exciting to higher energies in the S_1 state simply due to the shape of the S_n potential surface (e.g. if the S_n potential energy surface were steeper along the reaction coordinate than the S_1 state, see Figure 3.8). The very broad excited state absorption in DHC supports this hypothesis. According to the spectroscopic reflection principle, the spectrum of an electronic transition broadens as the steepness of the upper state potential energy surface increases.[10]

One may also expect to see a change in the shape of the excited state absorption spectrum as the amount of vibrational energy in the excited molecule increases. With more vibrational energy, the excited molecule should experience a broadening of the excited state absorption spectrum due to the excited S_1 state having access to a larger number of vibrational modes in the S_n state(s). Similarly to the case of the peak position, this trend is not observed when considering the amount of excess energy imparted to the molecule by each excitation wavelength, but since the ESA spectrum is already very broad, it would be difficult to detect any additional broadening.

It is possible that the excess vibrational energy imparted to the molecule upon excitation could play a role in the relaxation of the excited state by providing enough energy to overcome the excited state barrier, but the current data shows no clear dependence of the decay rate on excitation wavelength. Two possible explanations for this are outlined here. The more straightforward interpretation is that the 1350 cm^{-1} C=C stretching mode in which the excess energy is placed simply does not play a significant role in the ring-opening motion. Therefore, the rate at which the excited molecules escape over the barrier along the reaction coordinate is unaffected.

Another interpretation is that the excess vibrational energy is very quickly dispersed throughout the molecule by way of intramolecular vibrational redistribution (IVR). Compared to a 297 nm (33700 cm^{-1}) pulse, which corresponds to the 0-0 transition and populates the lowest vibrational state in the excited electronic state, a 266 nm (37600 cm^{-1}) pulse provides an additional 3900 cm^{-1} of vibrational energy to the molecule. DHC ($C_{27}H_{44}O$) contains N = 72 atoms, resulting in a total of 210 (3N – 6) normal modes within the molecule. This means that after the redistribution of this excess

energy, there is an additional 19 cm^{-1} of energy per mode on average. This amount of extra energy is much less than the 167 cm^{-1} barrier along the reaction coordinate. As such, DHC should not experience a faster decay rate following 266 nm excitation.

In addition to the absence of change in the decay rate of the excited state absorption, there does not seem to be an effect on the relative amplitudes of the fast and slow components of this decay.

3.4 Conclusions

The data presented here was collected in an attempt to investigate the effect of excitation frequency on the ultrafast photoreaction dynamics in 7-dehydrocholesterol. Following UV excitation at 266, 272, 277, 284, and 297 nm, transient absorption difference spectra were collected and used to examine both the spectral and kinetic effects of excitation wavelength. These results were then compared to previous experiments on the ultrafast dynamics of DHC.

There appear to be slight differences in the excited state absorption of DHC depending on the excitation wavelength. The relationship between peak position and excitation wavelength was not monotonic. There is no apparent difference between excitation wavelengths in the excited state kinetics describing the ring-opening and decay from S_1 back to S_0. Kinetic fits to the data show similar time constants to those reported previously, and no distinct difference in the relative amplitudes of the fit components is observed. Within the signal-to-noise ratio of these measurements, the ring-opening dynamics of 7-dehydrocholesterol do not depend on excitation frequency. This is

attributed to either the lack of a significant role in ring-opening for the excited vibrational mode or to very fast IVR following excitation.

3.5 References

1. W. Fuss; T. Höfer; P. Hering; K. L. Kompa; S. Lochbrunner; T. Schikarski; W. E. Schmid. *J. Phys. Chem.,* **1996,** *100*, 921-927.

2. B. C. Arruda; B. Smith; K. G. Spears; R. J. Sension. *Faraday Discuss.,* **2013,** *163*, 159-171.

3. N. A. Anderson; J. J. Shiang; R. J. Sension. *J. Phys. Chem. A,* **1999,** *103*, 10730-10736.

4. K.-C. Tang; A. Rury; M. B. Orozco; J. Egendorf; K. G. Spears; R. J. Sension. *J. Chem. Phys.,* **2011,** *134*, 104503.

5. K.-C. Tang; R. J. Sension. *Faraday Discuss.,* **2011,** *153*, 117-129.

6. N. A. Anderson; R. J. Sension, Solvent Dependence of Excited State Lifetimes in 7-Dehydrocholesterol and Simple Polyenes. In *Liquid Dynamics*, American Chemical Society: 2002; Vol. 820, pp 148-158.

7. H. J. C. Jacobs; J. W. J. Gielen; E. Havinga. *Tetrahedron Lett.,* **1981,** *22*, 4013-4016.

8. W. G. Dauben; B. Disanayaka; D. J. H. Funhoff; B. E. Kohler; D. E. Schilke; B. L. Zhou. *J. Am. Chem. Soc.,* **1991,** *113*, 8367-8374.

9. W. Fuß; S. Lochbrunner. *J. Photochem. Photobiol. A,* **1997**, 159-164.

10. R. Schinke, *Photodissociation Dynamics: Spectroscopy and Fragmentation of Small Polyatomic Molecules*. Cambridge University Press: 1995.

Chapter 4

Coherent Control Using Chirped Ultraviolet Excitation Pulses

One of the goals of this dissertation is to use shaped UV laser pulses to control chemical reactions. In the case of stilbene, the specific goal is to modify the branching ratios of trans-stilbene and DHP formation upon weak field excitation of cis-stilbene with a shaped 266 nm pump pulse. For 7-dehydrocholesterol (DHC), the goal is to influence the efficiency of the electrocyclic ring-opening reaction using the same technique. The use of chirped laser pulses to control the outcome of chemical reactions has already been demonstrated in the literature.[1-6]

Coherent control on stilbene utilizing a slightly different approach than that proposed here has been attempted previously. Greenfield, McGrane, and Moore[7] attempted to control the cis-to-trans and cis-to-DHP branching ratios following excitation of cis-stilbene with shaped UV pump pulses. However, unlike the work described here, they utilized multiphoton transitions in the strong field limit and determined that exciting these transitions was necessary in order to modify the reaction yields.

The chirp of a laser pulse has already been shown to have an effect on the relative amplitude of the two components of the biexponential excited state decay in DHC.[8] An excitation pulse with positive chirp reduces the amplitude of the slower of the two

components, thus decreasing the effective lifetime of the excited state. Tapavicza et al.[9] proposed that the fast component of decay is associated with a more reactive motion toward ring-open product than the slow component, which may lead to formation of more product. Based on this proposal and the dependence of the ring-opening dynamics on chirp, it is reasonable to hypothesize that the chirped laser pulse may also have an effect on the quantum yield of photoproduct. The work described here investigated this possibility.

4.1 Experimental details

4.1.1 Pulse shaping technique

In order to perform coherent control experiments, it is necessary to modulate the light pulses that interact with the system in question. An ultrafast pulse shaper can be described using two parameters: optical design and programmability. The pulse shaper optical arrangement can either be in the transverse configuration, where the individual frequency components of the pulse are separated spatially before modulation, and the collinear configuration, where the pulse is shaped without spatial separation of the frequency components. The programmability of the pulse shaper describes whether modulations can be made through the use of a computer (programmable) or if there must be physical adjustments to the optical elements in the pulse shaper (static). One simple example of a pulse shaper is a diffraction grating stretcher or pulse compressor, which would be considered a transverse, static pulse shaper. There are multiple experimental designs that can utilized to effectively shape ultrafast pulses, including designs based on spatial light modulators,[10-11] deformable mirrors,[12] and acousto-optic deflectors.[13]

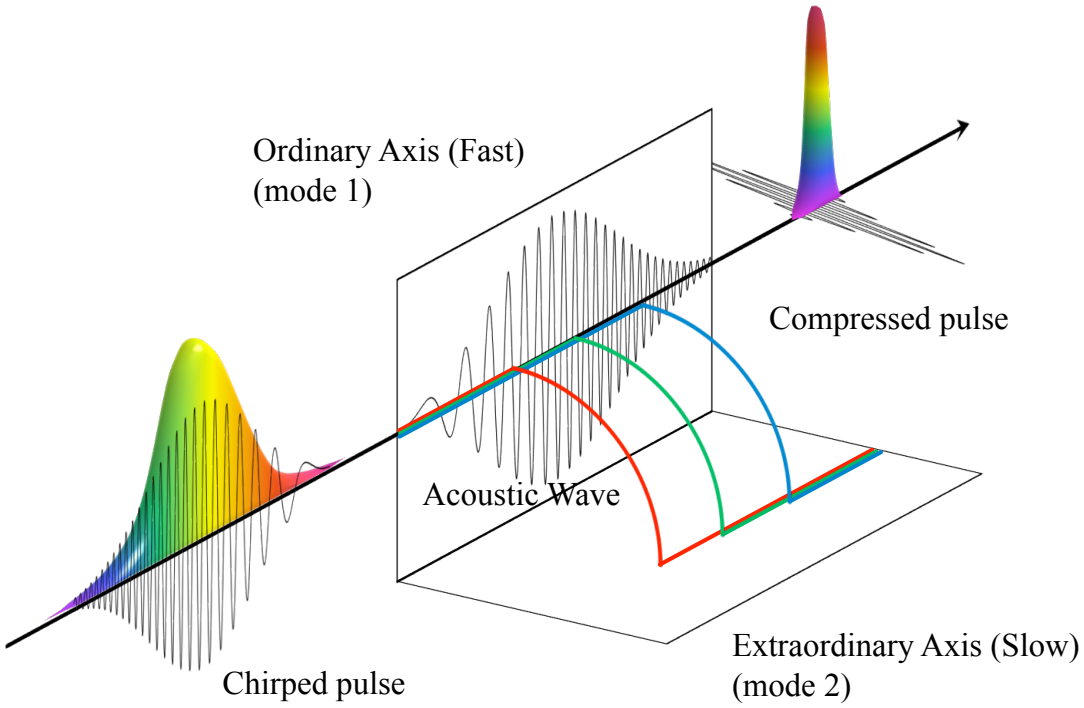

Figure 4.1 *Diagram of the Dazzler based on a figure by Verluise et al.*[14]

Transverse, programmable pulse modulators have been used previously in order to generate shaped ultrafast pulses for use in coherent control schemes.[6] These systems typically consist of a programmable liquid crystal spatial light modulator (LC SLM) placed in the fourier plane of a 4-f system. In addition, other studies[7] have employed the use of collinear, programmable pulse shapers known as acousto-optic programmable dispersive filters (AOPDF).[14-15] For all of the experiments described in this dissertation that utilize shaped UV laser pulses, an AOPDF was used for pulse modulation. The apparatus used was a Fastlite Dazzler with a potassium dihydrogen phosphate crystal (KDP), making it suitable for use with near-UV pulses. The Dazzler is an attractive option for pulse shaping due to its collinear design and ease of use.

The operation of the Dazzler, as described by Verluise et al.,[14] is based upon the interaction of the unshaped ultrafast laser pulse with an acoustic pulse inside of the Dazzler's KDP crystal. The acoustic pulse is generated by an RF signal that excites a transducer placed tangent to the crystal surface, and it reproduces spatially the temporal profile of the RF pulse. The RF signal is triggered such that temporal overlap between the generated acoustic pulse and the optical pulse is achieved. Due to the large difference between the speeds of sound and light in the crystal, the acoustic pulse can be considered to be essentially stationary as the optical pulse propagates through the crystal. The acousto-optic interaction allows two optical modes to be coupled, but only in the case where the phase matching condition is met.[16]

The KDP crystal is a negative uniaxial birefringent crystal, meaning it has polarization dependent refractive indices corresponding to a lower refractive index fast (ordinary) axis and a higher refractive index slow (extraordinary) axis. The coupled optical modes mentioned above have orthogonal polarizations. If the optical pulse propagating through the crystal is initially polarized along the fast axis, when the phase matching condition with the acoustic pulse is met some of the pulse energy will be coupled to another optical mode that has orthogonal polarization. This new mode propagates along the slow axis and is also diffracted, traveling along a slightly different angle through the crystal. Due to the requirement of the phase matching condition, the individual frequency components of the optical pulse will be diffracted at different positions in the crystal. This means that differing amounts of dispersion will be introduced to each frequency component due to the varying optical path lengths they experience.

This is where the advantage of the Dazzler is fully realized. The RF signal, and in turn the acoustic pulse, can be modulated such that particular frequency components in the optical pulse can be diffracted at specific positions. This allows for many different options when it comes to the shape of the output optical pulse, from simply correcting for the dispersion present in the input pulse to generating two output pulses. The Dazzler has numerous adjustable parameters that can be utilized to generate the desired pulse shape, including the center wavelength of the pulse and the intensity of the RF pulse. However, the most important of these are the phase parameters. These correspond to the group delay, group delay dispersion, third-order dispersion, and fourth-order dispersion (terms 2-5 in equation 1.2a).

Unfortunately, the Dazzler's efficiency in shaping the UV pulses used in the experiments described here is low. This is due to two factors. First, although the Dazzler utilizes the KDP crystal with near-UV pulses in mind, the transmittance of the crystal is problematic for pulses deeper in the UV (such as the 266 nm pulses used for these experiments). The transmission efficiency of an unmodulated 266 nm pulse is only ~10%. In addition, the efficiency of diffraction of the individual optical frequencies at the maximum RF pulse intensity is at best ~15-20%. This means that the 266 nm UV pulses originally generated at ~14 μJ will only produce shaped pulses with maximum pulse energy of ~280 nJ.

For most experiments, pulses in this energy range are actually ideal, as pulses with much greater energy can introduce nonlinear optical effects in the sample. However, another facet of the experimental process, the characterization of the shaped pulses, is affected when forced to use pulses with such low energies. It has been

demonstrated that pulse width measurements of UV laser pulses with pulse energies as low as 10 nJ are possible by utilizing a two-photon absorption autocorrelation technique.[17] While this method is feasible for wavelengths down to 220 nm, it does not provide any information regarding the complex phase of the pulse since it utilizes a square-law dependence. A technique for phase characterization of UV laser pulses has also been demonstrated, but this requires pulse energies of ~10-50 μJ.[18] This is a significant problem when modulating more than one phase parameter with the Dazzler, as it is not possible to know the actual phase of the modulated output pulse. Nevertheless, it is possible to perform an experiment while modulating a single parameter without the necessity of full pulse characterization. The experiments described in this dissertation modulate only the second order phase parameter (linear chirp) of the laser pulse.

4.1.2 Transient absorption apparatus

Descriptions of the Ti:sapphire oscillator and the amplifier systems used to generate the intense, ultrafast pulses centered near 800 nm can be found in chapter 2. Following amplification and compression, the pulses were split into pump and probe arms. The UV pump pulse for control experiments using shaped pulses is generated by third harmonic generation (~266 nm). These pulses are then shaped as described above before they are focused into the experimental sample using a UV coated off-axis parabolic mirror. For all chirps the pump energy was between 200-250 nJ. Energies in this regime should not cause any multiphoton effects in the data (with the possible exception of two-photon absorption of the pump and probe pulses by the solvent near t=0 ps).

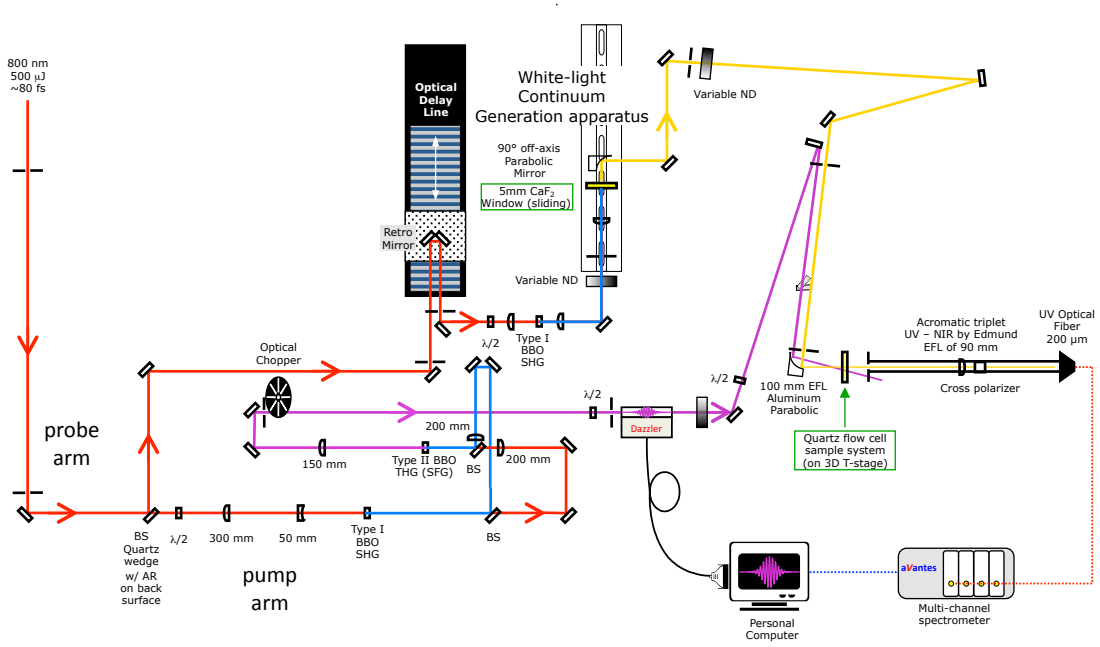

Figure 4.2 *Diagram of the apparatus used for these experiments. Original diagram by Kuo-Chun Tang. Modifications have been made to reflect changes to current design of experimental apparatus.*

The probe pulse for these experiments consists of a broadband, white light continuum generated by frequency doubling the fundamental laser pulses in a Type I BBO crystal (~400 nm), filtering out the residual fundamental light, and then focusing the frequency doubled light into a 5 mm CaF_2 window. The CaF_2 window is kept in motion at all times in order to prevent optical damage. The white light is collimated using a UV coated, off-axis parabolic mirror and is later focused into the sample using the same off-axis parabolic mirror that focuses the pump beam. After exiting the sample, the probe beam is focused into a 200 μm UV-Vis coated optical fiber from Avantes. This fiber couples the beam into an Avantes Multichannel spectrometer (2048 pixel, DUV coating 174-1100 nm, 10 nm slit width). In order to prevent saturation of the spectrometer by the large

amount of leftover 400 nm light in the probe beam, two 1.0 mm path length quartz cells filled with $NiSO_4$ (which absorbs strongly at this wavelength) are placed in the beam path. One of the cells is located before the sample position, while the other is placed after the sample but before the spectrometer. The concentration of the $NiSO_4$ is adjusted such that the first cell prevents the leftover 400 from causing any nonlinear optical effects in the sample, and the second cell filters enough of the remaining 400 to prevent saturation but not result in a large hole in the middle of the white light spectrum. The white light spectrum extended from ~270-600 nm, but only yielded reliable data between 300-520 nm for the cis-stilbene measurements due to the amount of noise on the edges of the spectrum. In addition, the region between 375-425 nm was quite noisy in all measurements due to the leftover 400 nm pump used to produce the white light continuum.

The pump beam is alternated on and off using either a Thorlabs MC1000A Optical Chopper or a New Focus 3501 Optical Chopper depending on the data set. In both cases, the chopping frequency is set to the sixth subharmonic of the 1 kHz repetition rate of the fundamental amplifier output (166.6 Hz, 3 on, 3 off). The pump-probe delay was adjusted through the use of a Newport ILS150PP Micro Step Drive Stepper Linear Stage driven by a Newport ESP300 Motion Controller. All samples were flowed continuously through a quartz flow cell with a peristaltic pump in order to prevent photodegradation of the sample.

4.2 Results and discussion

4.2.1 Cis-stilbene

For these experiments, the linear chirp of the 266 nm pump pulse after pulse shaping by the Dazzler is between -8000 and 8000 fs^2. The chirp of the pulse was not varied sequentially from the minimum to the maximum value or vice versa. Instead, a random order was chosen in order to avoid a trend due to laser drifts being falsely attributed to the chirp of the pump pulse. Data sets for both the transform limited pulse and a pulse with a chirp of -1000 fs^2 were collected twice in order to test the reliability of the measurements. There were no differences between the collected data in both sets of measurements. These scans were then averaged together for analysis. The transient absorption spectra were collected between -2 – 200 ps with varying time steps. All measurements were performed for cis-stilbene in 1-butanol.

Figure 4.3 shows a set of typical cis-stilbene transient absorption spectra following excitation at 266 nm. At early times, an excited state absorption corresponding to the cis-stilbene excited state minimum in S_1 is expected to appear near 630 nm,[19] but this signal is not visible due to the lack of intensity in that region of the continuum. The positive peak near 340 nm corresponds to the perpendicular phantom state where the dihedral angle about the double bond is 90 degrees.[19] This peak grows in within the first 500 fs as the initially excited state begins to decay to the phantom state. The phantom state then decays on a ca. 1.5 picosecond time scale (see inset of Figure 4.3).

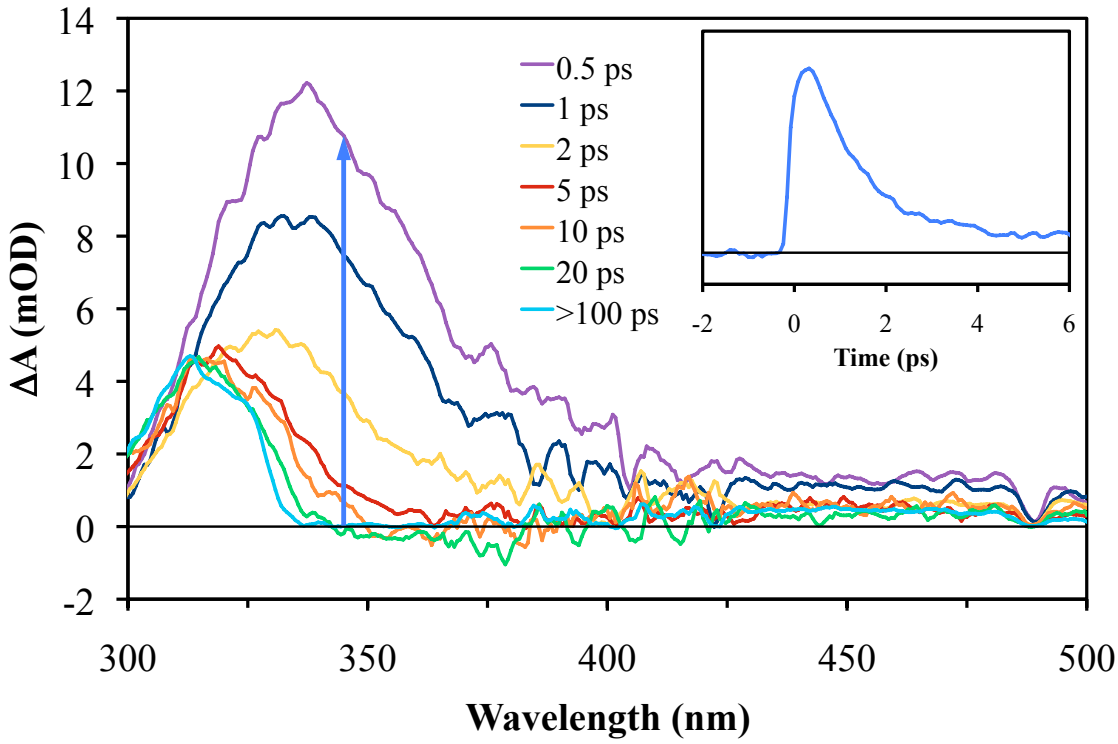

Figure 4.3 *Transient absorption spectra of cis-stilbene at various time delays following excitation with a transform limited pulse. (Inset) Kinetic trace of transient spectrum integrated between 340-350 nm (center wavelength highlighted by blue arrow).*

Because this research is concerned with the branching ratios of the products following excitation of cis-stilbene, it is important to focus on the late time aspects of the transient absorption spectra, long after the excited cis-stilbene molecules have returned to the ground state. All late time spectra presented here are an average of the transient spectra between 100 and 200 ps after excitation. At these time delays, there are a few noteworthy signals present within the region of interest. On the blue edge of the white light spectrum appears a large, positive signal that peaks around 310 nm. This peak corresponds to formation of the ground state absorption of the trans-stilbene photoproduct. There is also a ground state bleach of cis-stilbene that is not visible due to the overlap of the cis-stilbene absorption spectrum with the more strongly absorbing

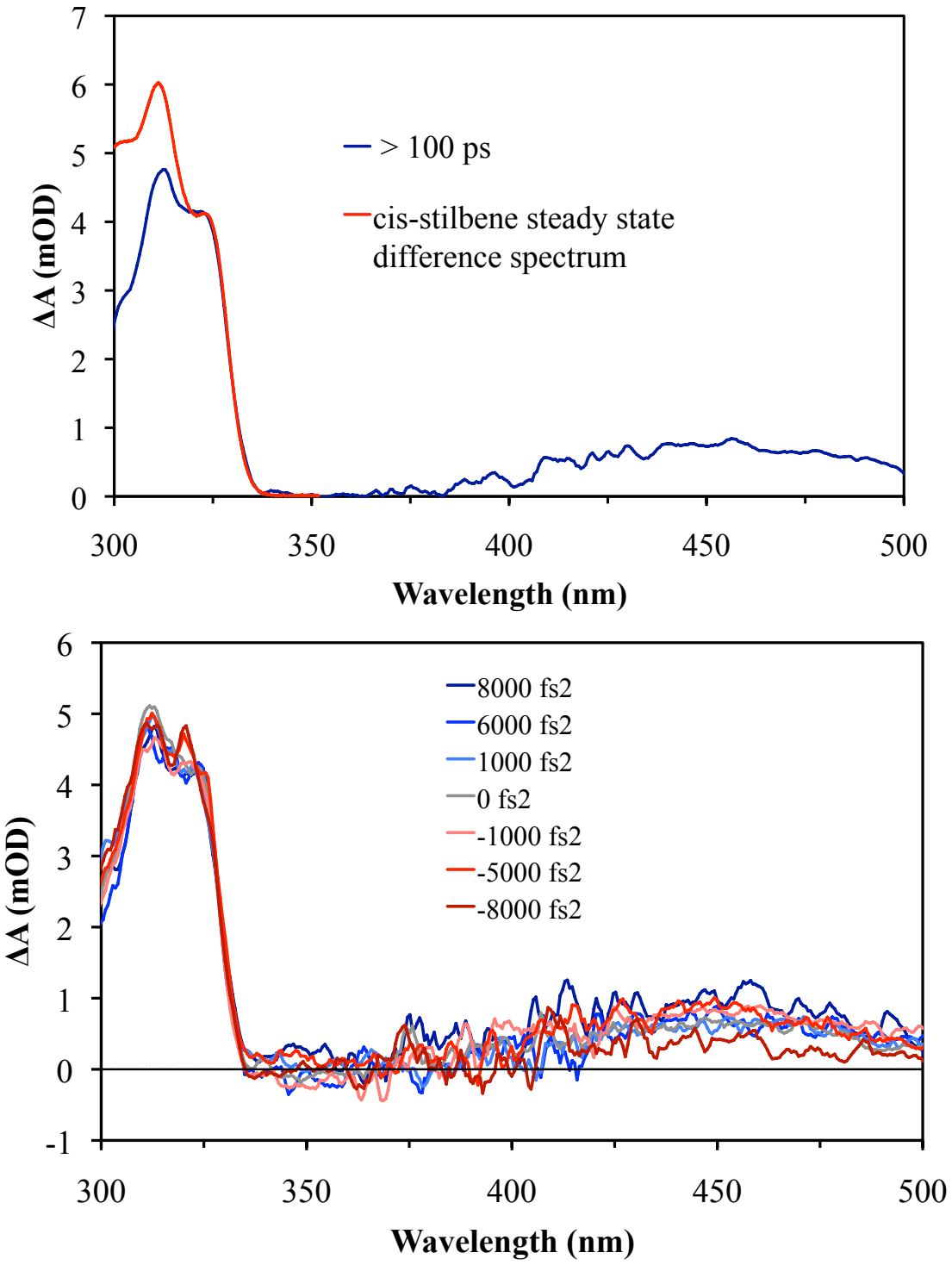

Figure 4.4 *(Top) Transient absorption spectrum of cis-stilbene averaged at times longer than 100 ps plotted with the steady state difference spectrum of cis-stilbene following irradiation with a mercury arc lamp for 30 s. Both spectra were collected in 1-butanol. (Bottom) Cis-stilbene transient absorption spectra for various values of linear chirp (100-200 ps). Spectra are scaled to the size of the trans-stilbene signal.*

trans-stilbene spectrum. Another much smaller signal is visible in the region between 400-500 nm that peaks near 450 nm. This signal corresponds to the ground state absorption of DHP photoproduct. By comparing the relative sizes of these two peaks, one can determine whether the product branching ratios are dependent on the chirp of the excitation pulse.

When plotted together and scaled by the height of the trans-stilbene photoproduct peak, the transient spectra of different chirps show small differences in the size of the DHP peak, which can be seen in Figure 4.4. However, whether this is characteristic of a chirp dependence must be more closely investigated, as the noise in the data is quite high. All scans with positive chirp and all scans with negative chirp were averaged together, and the resulting spectra can be seen in the upper portion of Figure 4.5. When analyzed in this fashion, there appears to be no difference in the relative contributions of the trans-stilbene and DHP signals to the difference spectra between positive and negative chirps.

In addition to averaging all scans with linear chirp of similar sign, the relative size of the trans-stilbene and DHP photoproduct signals were compared for each scan individually. This was performed by integrating over each peak in the difference spectrum (310-335 nm for trans-stilbene and 420-500 nm for DHP) and calculating the trans-stilbene:DHP peak area ratio. The results can be seen the lower portion of Figure 4.5. A linear least squares fit to the data (excluding the point at -8000 fs^2) confirms that the chirp of the laser pulse has no major effect on the ratio of the trans-stilbene and DHP signals, and thus, no effect on the quantum yields of photoproducts.

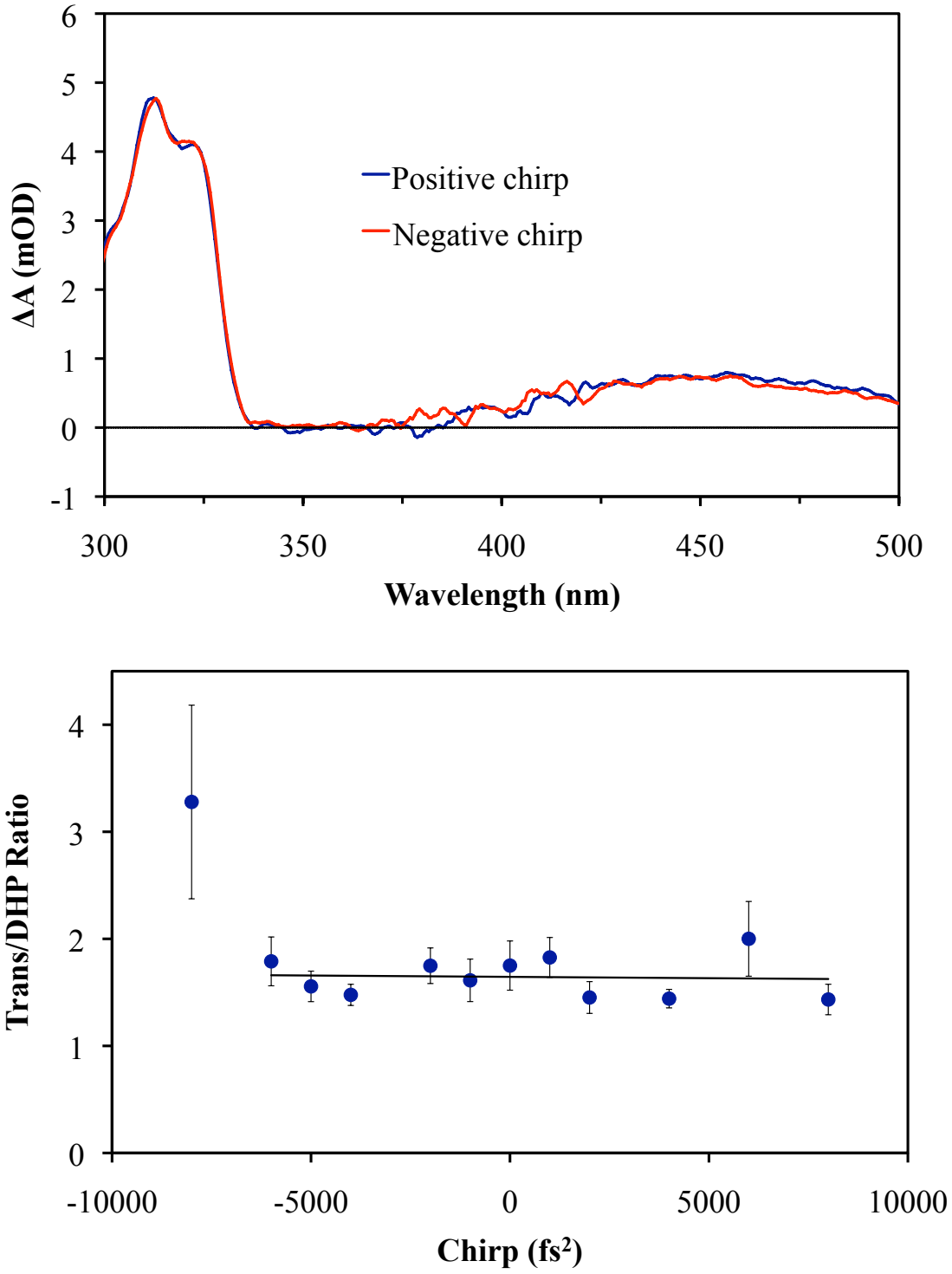

Figure 4.5 *(Top) Comparison of long time transient absorption spectra for positive and negative chirp. (Bottom) Plot of trans-stilbene/DHP peak area ratios as a function of chirp of the excitation pulse. The least squares fit to the data excludes the -8000 fs^2 point.*

4.2.2 7-Dehydrocholesterol

For these experiments, the linear chirp of the 266 nm pump pulse was varied between -8000 and 10000 fs^2. Like the cis-stilbene measurements, the chirp was not varied sequentially in order to prevent systematic errors in the data due to drifts in the instrumentation being mistaken for a chirp effect. Transient absorption spectra were collected between -1.5–100 ps, and all scans were performed in 2-butanol.

Typical transient absorption difference spectra for DHC can be seen in Figure 4.6. The broad, visible excited state absorption in these data does not extend as far into the red as the spectra shown in chapters 3 and 5 due to the much lower intensity in this region of the white light for these experiments. However, since the probe continuum was generated using 400 nm pulses, it extends further into the UV, allowing for the observation of the DHC ground state bleach and an UV excited state absorption peak. As this ESA peak (the blue side of which overlaps with the DHC ground state bleach) decays on the same time scale as the visible ESA, it has been assigned to the excited state ring-opening process.[20] There is also a slower decay component in this region (~5-8 ps) that is attributed to the isomerization of the gZg-Previtamin D_3 (Pre) photoproduct to tZg-Pre.[20] The spectrum of Pre overlaps with the ground state bleach of DHC, and a very small absorption corresponding to the red tail of this spectrum can be seen just to the red of the bleach following the decay of the ESA in Figure 4.6.

Like the cis-stilbene data, it is necessary to analyze the DHC spectra at long time delays are in order to investigate whether chirp has an effect on the quantum yield of ring-opening. Since the recovery of the ground state bleach is an indication of the efficiency of the photoreaction, this region is given focus. Unfortunately, spectral

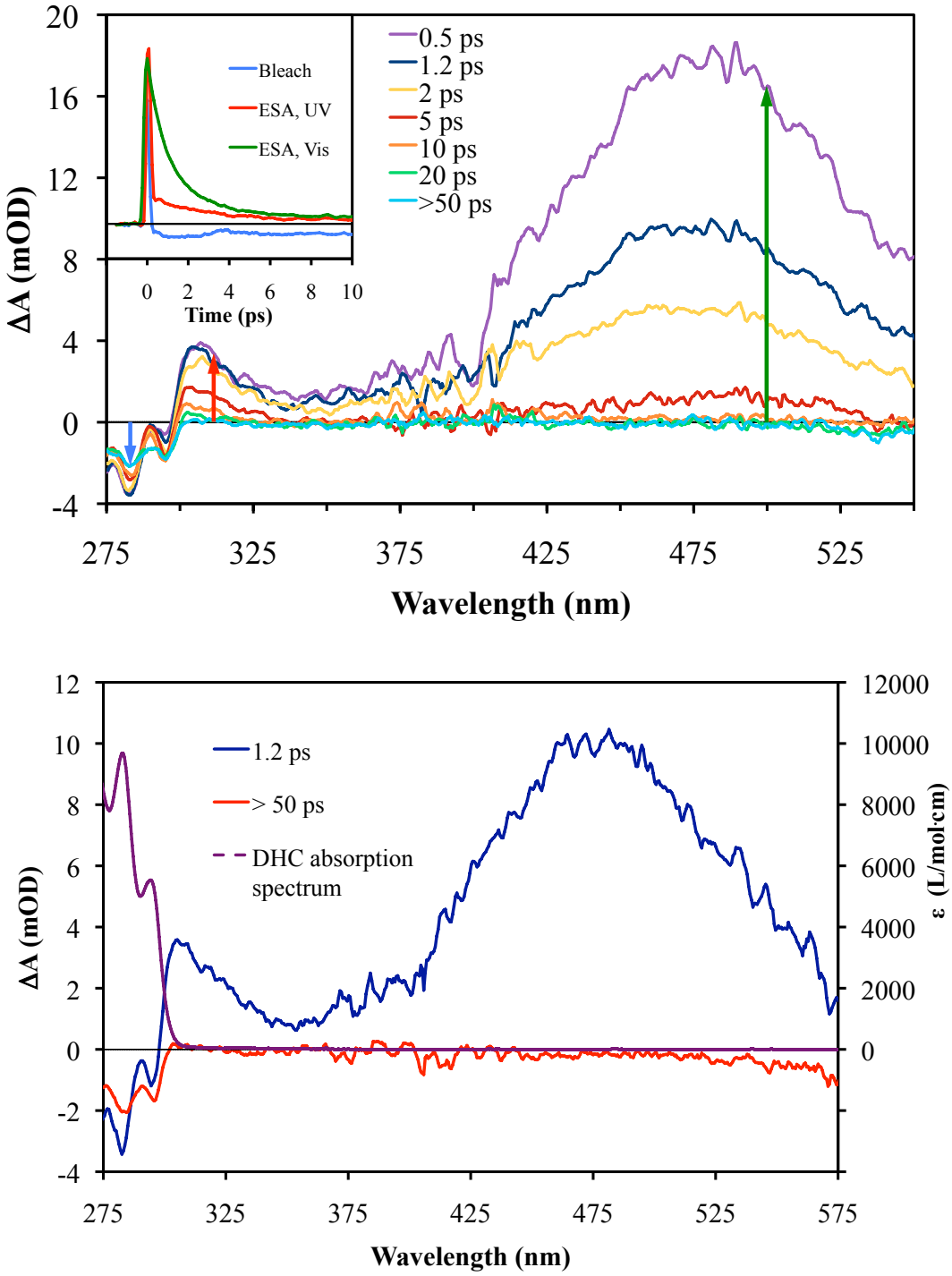

Figure 4.6 *(Top) Transient absorption spectra of DHC at various time delays following excitation with a transform limited pulse. (Inset) Kinetic traces at a few selected regions of interest (center wavelengths highlighted by colored arrows). (Bottom) Transient absorption spectra compared to DHC steady state absorption spectrum.*

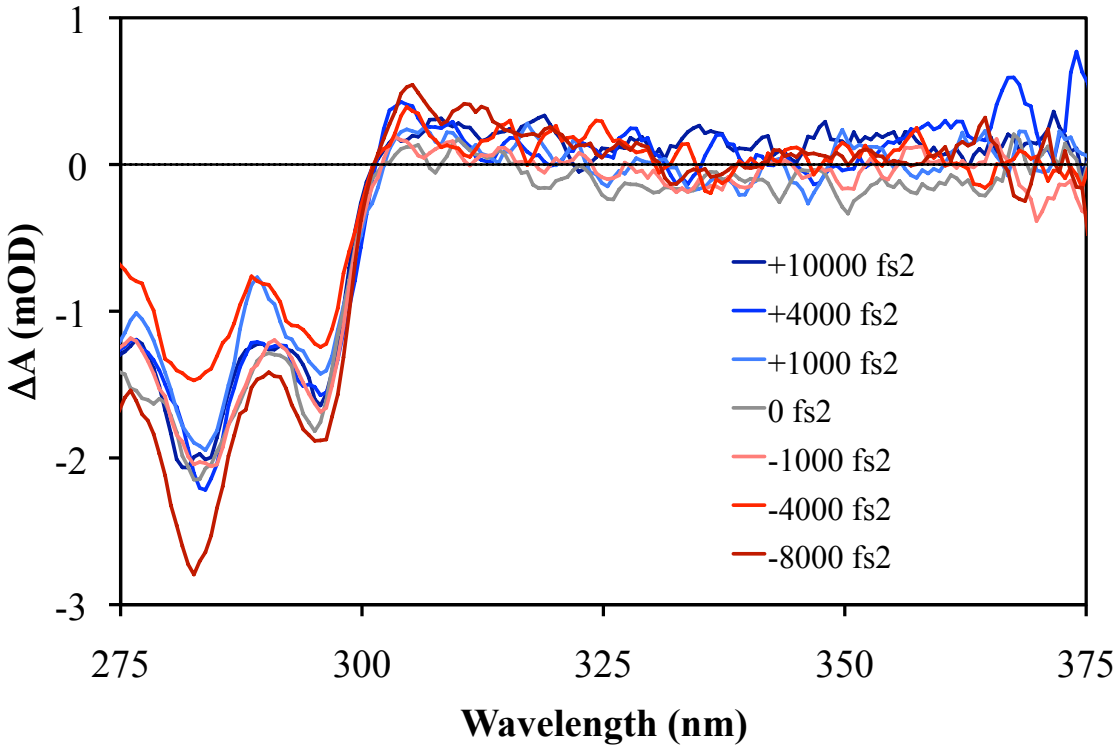

Figure 4.7 *DHC transient absorption spectra averaged between 50–100 ps.*

analysis in this region is not simple due to the overlap of the UV excited state DHC spectrum and ground state Pre spectrum with the ground state DHC spectrum. This is evident by the change in shape of the bleach signal as the Pre peak grows in. Figure 4.7 compares spectra averaged from 50-100 ps for the various chirped pulses used for excitation. As a whole there appear to be no major differences in the ground state bleach at these time delays that are dependent on the chirp of the excitation pulse. Two data sets that do show a larger and smaller signal than the others in this region are -8000 and -4000 fs^2, respectively.

In order to better compare the effect of positive and negative chirp on photoproduct formation, all spectra with chirp of similar sign were averaged together. These averaged spectra are shown in Figure 4.8. It is worthy to note that the chirp

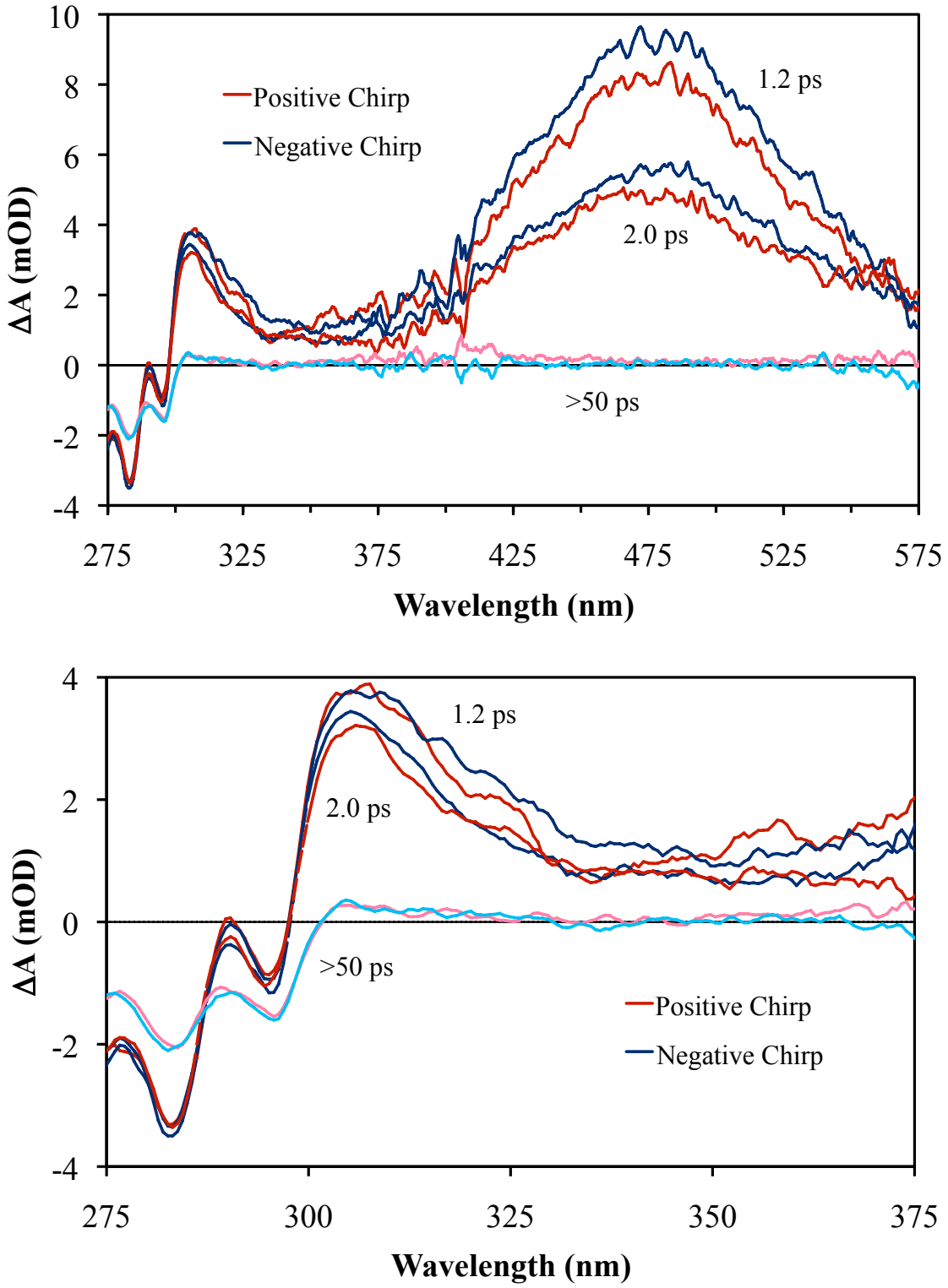

Figure 4.8 *Comparison of transient absorption spectra for positive and negative chirp. The lower panel shows a zoomed view of the spectra in the upper panel.*

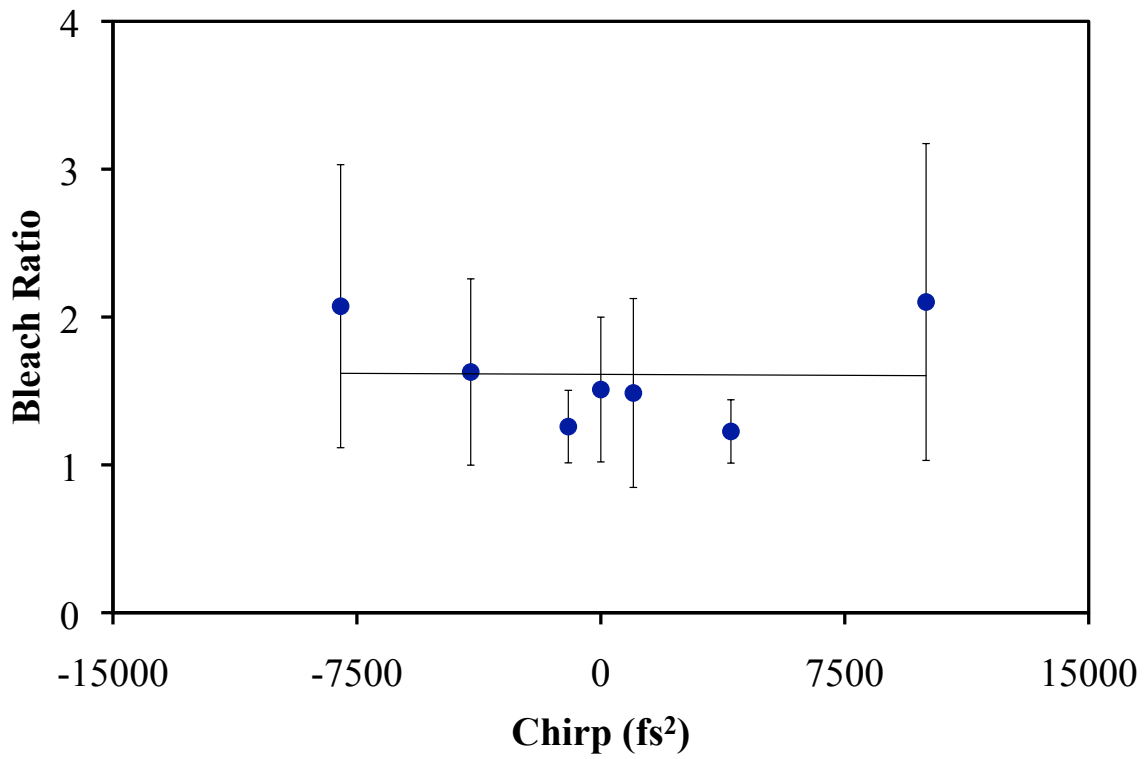

Figure 4.9 *Plot of the ratio of the integrated ground state bleach signal at early and late time delays.*

dependence of the relative amplitudes of the biexponential decay components reported by Tang and Sension[8] is observed in these data. These spectra show that pulses with positive chirp generate excited populations that experience a shorter effective lifetime on the excited state, which is consistent with a decrease in the amplitude of the slower decay component. While the chirp has an obvious effect on the kinetics, it does not appear that there is any difference in the size of the ground state bleach signals at time delays greater than 50 ps. In addition, each data set was examined individually by taking the ratio of the areas beneath the ground state bleach from 275–295 nm at 1 ps and >50 ps time delays (Figure 4.9). A linear least squares fit to the resulting data shows that the chirp of the excitation pulse has no effect on the relative sizes of this peak at early and late times.

4.3 Conclusions

In this chapter, the influence of the chirp of the excitation pulse on the photoisomerization of cis-stilbene and DHC was investigated. A dependence of the relative amplitudes of the two decay components of the DHC excited state on chirp was observed, as was reported previously.[8] Determination of photoproduct ratios was made by investigation of the long time spectra with varying amounts of linear chirp. Contrary to the hypothesis that the control of the ratio of the two decay components may result in an increase or decrease of photoproduct, DHC ring-opening efficiency showed no dependence on chirp. In addition, no significant differences in the relative amounts of DHP and trans-stilbene were observed for cis-stilbene.

4.4 References

1. G. Cerullo; C. J. Bardeen; Q. Wang; C. V. Shank. *Chem. Phys. Lett.,* **1996,** *262*, 362-368.

2. C. J. Bardeen; J. W. Che; K. R. Wilson; V. V. Yakovlev; P. J. Cong; B. Kohler; J. L. Krause; M. Messina. *J. Phys. Chem. A,* **1997,** *101*, 3815-3822.

3. C. J. Bardeen; V. V. Yakovlev; K. R. Wilson; S. D. Carpenter; P. M. Weber; W. S. Warren. *Chem. Phys. Lett.,* **1997,** *280*, 151-158.

4. C. J. Bardeen; V. V. Yakovlev; J. A. Squier; K. R. Wilson. *J. Am. Chem. Soc.,* **1998,** *120*, 13023-13027.

5. I. Pastirk; E. J. Brown; Q. Zhang; M. Dantus. *J. Chem. Phys.,* **1998,** *108*, 4375-4378.

6. E. C. Carroll; A. C. Florean; P. H. Bucksbaum; K. G. Spears; R. J. Sension. *Chem. Phys.,* **2008,** *350*, 75-86.

7. M. Greenfield; S. D. McGrane; D. S. Moore. *J. Phys. Chem. A,* **2009,** *113*, 2333-2339.

8. K.-C. Tang; R. J. Sension. *Faraday Discuss.,* **2011,** *153*, 117-129.

9. E. Tapavicza; A. M. Meyer; F. Furche. *Phys. Chem. Chem. Phys.,* **2011,** *13*, 20986-20998.

10. A. M. Weiner; D. E. Leaird; J. S. Patel; J. R. Wullert. *IEEE J. Quant. Electron.,* **1992,** *28*, 908-920.

11. A. Efimov; M. D. Moores; N. M. Beach; J. L. Krause; D. H. Reitze. *Opt. Lett.,* **1998,** *23*, 1915-1917.

12. E. Zeek; K. Maginnis; S. Backus; U. Russek; M. Murnane; G. Mourou; H. Kapteyn; G. Vdovin. *Opt. Lett.,* **1999,** *24*, 493-495.

13. M. A. Dugan; J. X. Tull; W. S. Warren. *J. Opt. Soc. Am. B: Opt. Phys.,* **1997,** *14*, 2348-2358.

14. F. Verluise; V. Laude; Z. Cheng; C. Spielmann; P. Tournois. *Opt. Lett.,* **2000,** *25*, 575-577.

15. P. Tournois. *Opt. Comm.,* **1997,** *140*, 245-249.

16. A. Yariv; P. Yeh, *Optical Waves in Crystals*. Wiley: New York, 1984.

17. J. I. Dadap; G. B. Focht; D. H. Reitze; M. C. Downer. *Opt. Lett.,* **1991,** *16*, 499-501.

18. D. J. Kane; A. J. Taylor; R. Trebino; K. W. DeLong. *Opt. Lett.,* **1994,** *19*, 1061-1063.

19. S. A. Kovalenko; A. L. Dobryakov; I. Ioffe; N. P. Ernsting. *Chem. Phys. Lett.,* **2010,** *493*, 255-258.

20. B. C. Arruda; J. Peng; B. Smith; K. G. Spears; R. J. Sension. *J. Phys. Chem. B,* **2013,** *117*, 4696-4704.

Chapter 5

Pump-Repump Control Experiments

The experiments described up to this point have been concerned with only the lowest electronic excited states of the molecules studied. In this chapter, a series of experiments on 7-dehydrocholesterol and cis and trans-stilbene using a UV pump pulse followed by a visible repump pulse and a broadband, white light probe are described. The UV pulse places the molecule in the same excited state as described in previous chapters and the visible pulse is tuned to be resonant with the subsequent excited state absorption bands present in these molecules. The white light probe allows for monitoring of the intensity of the visible excited state absorption, and for some experiments, the recovery of the ground state bleach. The time delay between the two pump pulses can be tuned in order to perturb the excited molecules at various times throughout the excited state decay. The goal of this work is to investigate whether or not this scheme has any effect on the quantum yield of the ring-opening reaction in DHC or the cis-trans isomerization or ring-closing reaction in stilbene.

Variations on the pump-repump scheme originally proposed by Rice, Tannor, and Kosloff[1] have been shown to provide an increase quantum yield for a multitude of photoreactions. Many experiments have used a single, long pulse in order to excite molecules with the leading edge of the pulse and re-excite them to a higher electronic

state with the trailing edge of the pulse.[2-8] Other studies have utilized two femtosecond pulses with an adjustable time delay between them to create the same effect.[9-11] In either case, the underlying premise behind the experiments is that exciting molecules to states higher than S_1 may provide access to a separate decay pathway that bypasses S_1 completely during relaxation, resulting in a different branching ratio of reactants to products or a different branching ration between products.

Some aspects of the photochemistry of cis-stilbene following excitation to states above the lowest electronic excited state (1^1B) have already been explored.[12] In their study, Bao, Minitti, and Weber used 6 eV (207 nm) pulses to excite gas phase cis-stilbene to the 7^1B state. They determined that following excitation to this state, the molecules rapidly decayed down the excited state manifold and preferentially formed 4a,4b-dihydrophenanthrene (DHP). It is possible that the states accessed by the repump pulse in the experiments described here could demonstrate similar relaxation dynamics. The ability to tune the delay between pump and repump may also provide the means to alter the processes that occur in these higher states. If the structure of the repumped molecules immediately following re-excitation is important to the reactive pathway, then allowing the initially pumped population to evolve on the 1^1B surface for a shorter or longer amount of time could affect the dynamics of the re-excited population.

Takeuchi et al. performed a three-pulse experiment on cis-stilbene in solution similar to our experiment described in this chapter.[13] In their work, they used the two-pulse pumping sequence to study the structural evolution of the S_1 during photoisomerization. While the first pump pulse was relatively long (150 fs) and was used to generate a population in the S_1 state, the second excitation pulse, which was tuned to

be resonant with the visible excited state absorption in cis-stilbene, was very short (11 fs). This enabled generation of an impulsive Raman signal and creation of a nuclear wave packet on the S_1 (1^1B) state. With this information they were able to monitor the structural evolution of the S_1 state during photoisomerization, but they were unconcerned with populating the S_n state and determining its effect on the photoisomerization quantum yields to trans-stilbene and DHP.

Like cis-stilbene, much less focus has been given to the states that lie above the lowest excited state (1^1B_u) in trans-stilbene, but some studies using both single and two-photon absorption have been performed. Bao and Weber excited trans-stilbene to the S_5 state (3^1B_u) with 5.93 eV pulses (209 nm) and studied the torsional motions of the phenyl groups before the decay of the molecule back to a lower surface.[14] Houk et al. studied the two-photon excitation to multiple ^1A_g states with transition energies of 5.1 and 6.4 eV.[15] The pump-repump experiments described here use pulses at 266 nm and ~590 nm (combined energy of ~6.8 eV) to explore the higher energy states of trans-stilbene.

While the isomerization of trans-stilbene to cis-stilbene is well known and has been studied extensively, the direct photocyclization of trans-stilbene to DHP has been given much less consideration. Due to the requirement that the excited molecule undergo two separate photochemical processes, this reaction is highly unlikely to occur. However, Jiang et al. have shown theoretically that direct trans-to-DHP photocyclization following excitation by a femtosecond pulse is indeed possible through an excited cis intermediate and should be observable.[16] It is possible that exciting above the S_1 state may allow excited trans-stilbene easier access to this excited state configuration, thus improving the quantum yield of cyclization to DHP directly from trans-stilbene.

5.1 Experimental details

5.1.1 Apparatus for pump-repump experiment

The apparatus used for the pump-repump experiment was the same as that used for the tunable pump experiments, but with a few changes. Pump pulses were generated from the third harmonic of the Ti:Sapphire laser as described in section 2.2.2. Visible NOPA pulses were used without further modification as repump pulses. These pulses could be tuned between 530-620 nm. Typical pump pulse energies were ~270 nJ and repump energies were ~300 nJ. The white light continuum for the probe was generated by focusing either 800 nm fundamental pulses or 400 nm second harmonic pulses into a moving CaF_2 plate, depending on the desired probe region.

The pump and repump beams were initially set to be collinear with one another as they entered the sample by passing the NOPA beam through the back of a UV dielectric mirror. Both beams were focused into the sample with the same 175 mm FL lens (resulting in a larger spot size at the sample for the repump beam). A noncollinear configuration was also used for some experiments to ensure that the pump and repump beams were focused at the same position. In this configuration, the two beams were focused with two separate lenses (pump lens = 175 mm FL; repump lens = 200 mm FL).

A single optical chopper (New Focus 3501) was used in the collinear configuration while two different choppers were used in the noncollinear configuration (Digirad C-980 and New Focus 3501). The optical chopping frequency was set to 100 Hz (5 pulses on, 5 off) for the DHC experiments and 125 Hz (4 on, 4 off) for the cis and trans-stilbene experiments. The repump pulses were delayed with respect to the pump pulses through the use of a Klinger stage with 0.1 μm step resolution driven by a

Newport MM3000 stage controller. Samples were flowed continuously to prevent photodegradation using the wire-guided flow apparatus. All measurements were made in 2-butanol (except for one measurement on cis-stilbene made in cyclohexane), and sample concentrations were ~0.8 mM for DHC, ~1.5 mM for cis-stilbene, and ~0.75 mM for trans-stilbene.

The selection of pump-repump polarization orientation is important, as the ability of any pulse to induce a particular optical transition is dependent on the alignment between the electric field of the light and the transition dipole moment. The angle between the polarizations of these two pulses should be chosen based on the angle between the transition dipole moments of the $S_1 \leftarrow S_0$ and $S_n \leftarrow S_1$ transitions. The polarization anisotropy can be measured and used to calculate the average angle between the two transition dipole moments:[17]

$$r = \frac{I_{par} - I_{perp}}{I_{par} + 2I_{perp}} = \frac{2}{5}\langle P_2(\cos\theta)\rangle = \frac{1}{5}(3\cos^2\theta - 1) \tag{5.1}$$

where I_{par} and I_{perp} are the signals for the parallel and perpendicular orientations of the two pulses used to induce the two transitions in question and $P_2(\cos\theta)$ is the second Legendre Polynomial of the cosine of the angle between the two transition dipole moments. The anisotropy of the DHC excited state absorption in 2-butanol has been measured as 0.2-0.3, corresponding to angles of 23-33° between transition dipoles.[18] Rotational reorientation of the excited molecules occurs on a time scale much slower than the excited state decay. The anisotropy of the excited state absorption of cis-stilbene in hexane and hexadecane was measured to be 0.38,[19] and the anisotropy of trans-stilbene is measured to be about the same,[20] corresponding to an angle of 10° or less between transition dipoles. For trans-stilbene, the anisotropy decay time is 15 ps in hexane and 80

ps in hexadecane,[21] while in cis-stilbene it is slightly faster in both cases (but still much slower than the decay of the ESA).[22] As the viscosity of 2-butanol falls between that of hexane and hexadecane, the anisotropy decay time is expected to be between 15-80 ps.

The rotation of a 266 nm half-wave plate controlled the polarization of the pump relative to the repump and probe beams. For all experiments, pump and repump pulses were set with parallel polarization. Based on the angles between transition dipoles described above, it is reasonable to believe that this configuration should allow for re-excitation of the pumped molecules by the repump pulse, especially since the repump delay in most experiments is very short relative to the anisotropy decay times mentioned above. The probe pulse polarization was set at magic angle to the pump and repump pulses in order to minimize contributions to the signal due to rotational diffusion at longer times.

5.1.2 Data collection technique

In order to examine the differences in the evolution of the system being studied due to the pump and repump beams using this technique, it is useful to produce a double difference spectrum (ΔΔA) in addition to the simple transient absorption difference spectrum (ΔA):

$$\Delta\Delta A = \Delta A_{\text{Both}} - \Delta A_{\text{Pump}} - \Delta A_{\text{Repump}} \tag{5.2}$$

This equation requires one to sample all four of the possible pulse sequences for the experiment: pump-repump-probe, pump-probe, repump-probe, and probe only. This is usually achieved by using different optical choppers for the pump and repump beams, one of which is chopping at twice the frequency as the other to allow for all four pulse

sequences. Unfortunately, due to the design of the apparatus used for data collection syncing the two choppers and collecting the data in this manner is not trivial. Instead of chopping at two different frequencies, in these experiments the pump and repump are chopped at the same frequency and may be physically blocked to produce the desired pulse sequence (The probe only case is present in every difference spectrum). Although data collection speeds are slower, the advantage of collecting the data in this manner is the ability to look at the difference spectra for each sampled pulse sequence (i.e. with or without the repump pulse).

Fortunately, for these experiments it is not necessary to collect the repump-probe case. Since the repump pulses are anywhere between 545-620 nm, they exhibit no resonance with any one photon transitions in 7-dehydrocholesterol, cis-stilbene, or trans-stilbene. The only signal that is produced in this case is a solvent spike near t_0. This allows one to effectively reduce equation (5.2) to:

$$\Delta\Delta A = \Delta A_{\text{Both}} - \Delta A_{\text{Pump}} \tag{5.3}$$

which requires only two pulse sequences to be collected: pump-repump-probe and pump-probe.

5.2 Results and discussion

5.2.1 7-Dehydrocholesterol

Pump-repump experiments on DHC used repump pulses centered at 545 nm. The data described here used a set delay of 0.6 ps between pump and repump pulses. Kinetic traces of both the repump and pump only scans averaged between 400-650 nm, ignoring the region between 530-560 nm to avoid the artifact from the repump scatter are

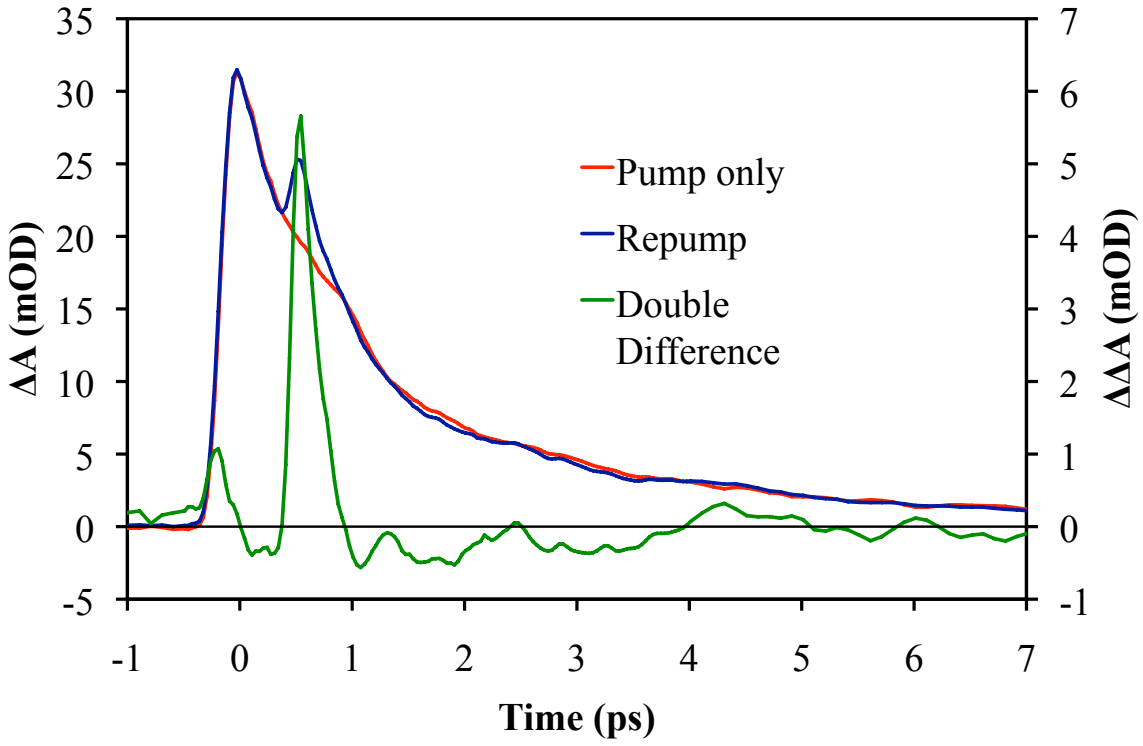

Figure 5.1 *Pump and repump kinetics for DHC in 2-butanol with repump delay set at 0.6 ps.*

displayed in Figure 5.1. For comparison to the pump only data, repump data were scaled so that the peak signal intensity at t_0 was the same for both sets of data. Following the arrival of the repump pulse, there is a short-lived increase in the total intensity of the visible absorption, followed by a very small net decrease in the intensity of the ESA. There is no significant change in the shape of the spectrum following the repump pulse as illustrated in Figure 5.2.

Since the repump pulse was tuned to be resonant with the $S_n \leftarrow S_1$ excited state absorption (specifically a region on the red side of the peak), one could expect that a depletion of the excited state population would be observed. Although the effect is small, the decrease in signal intensity across the excited state absorption suggests that this is the

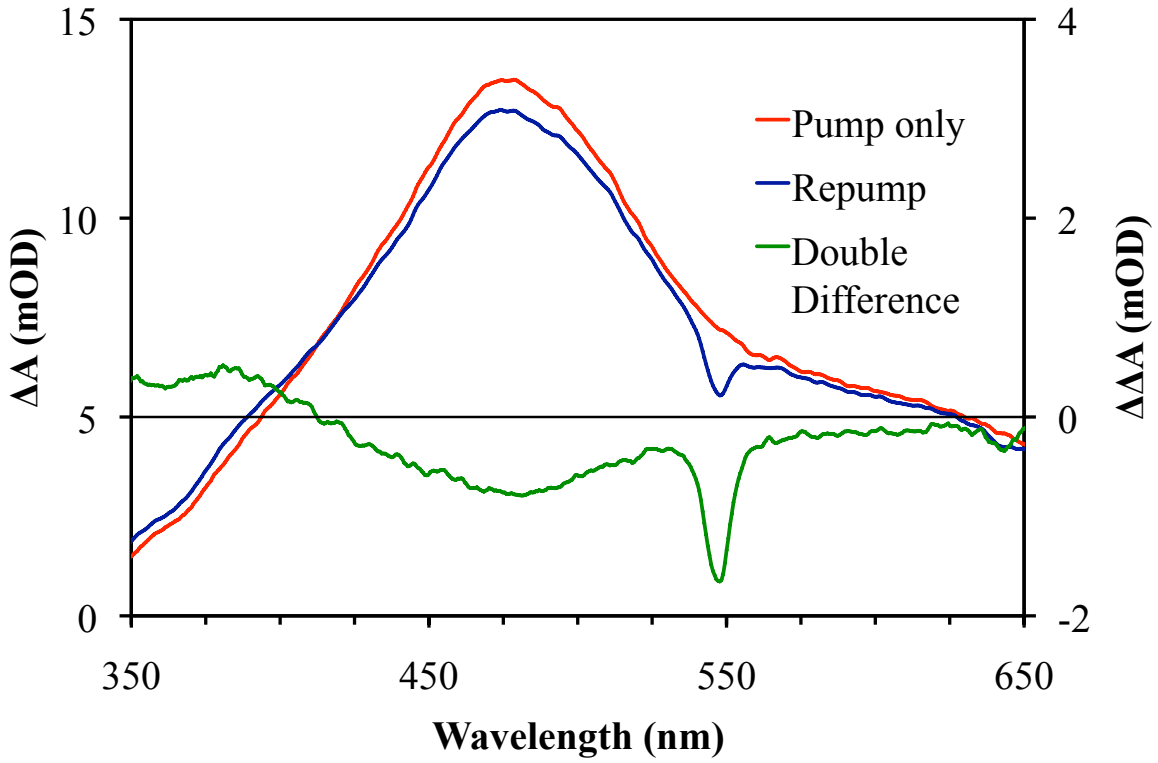

Figure 5.2 *Pump, repump, and double difference spectra for DHC in 2-butanol with repump delay at 0.6 ps. The dip in the repump spectrum at 545 nm is due to scattering of the repump pulse into the spectrometer.*

case. It is possible that following re-excitation much of the population in the S_n state decays quickly back to the S_1 state. Since this population would be vibrationally excited following the decay back to the S_1 state, one could expect to observe a broadened excited state absorption. Figure 5.2 shows that the repump spectrum is slightly broader than the pump only spectrum. If this process is in fact what is observed, then it appears that the vibrationally excited S_1 state following re-excitation decays back to the ground state in the same manner as the S_1 state in the case with no repump pulse.

Since the white light continuum did not extend deep into the UV it is not possible to determine if the repump pulse had any effect on the recovery of the ground state bleach, and thus, the quantum yield of ring-opening. Nevertheless, due to the very small

depletion of the excited state it is unlikely that an effect on the quantum yield would be detectable even if it were present.

5.2.2 Cis-stilbene

All measurements on cis-stilbene used repump pulses tuned to 625 nm with the delay between pump and repump pulses set to 0.5 ps. Pump-repump scans were scaled in the same manner as in the DHC analysis in order for comparison to pump-only scans. The upper panel of Figure 5.3 shows typical transient spectra probed by 800 nm white light continuum following UV excitation. The $S_n \leftarrow S_1$ (1^1B) excited state absorption from the initially excited cis-stilbene (c*) can be seen at ~630 nm immediately following 266 nm excitation. This state decays on a ~1.2 ps time scale. As this state decays, the phantom state ESA (p*) signal grows in at 340 nm within 1 ps, at which point both signals decay together. At very long time delays, the broad ground state absorption spectrum of DHP can be seen between 400-500 nm, along with a very small peak corresponding to the red edge of the trans-stilbene ground state absorption that is visible at the blue edge of the continuum. Unfortunately, the quality of much of the cis-stilbene data suffers due to the presence of trans-stilbene impurity in the sample (the trans-stilbene ESA peak can be seen at 580 nm in the upper panel of Figure 5.3 and is discussed in detail in the next section).

The lower panel of Figure 5.3 shows typical cis-stilbene transient spectra probed by 400 nm white light continuum. Here the phantom state ESA and the trans-stilbene photoproduct spectra can be seen in much more detail. Also visible in this figure is the ground state bleach of cis-stilbene between ~270-290 nm, overlapping with the p* ESA

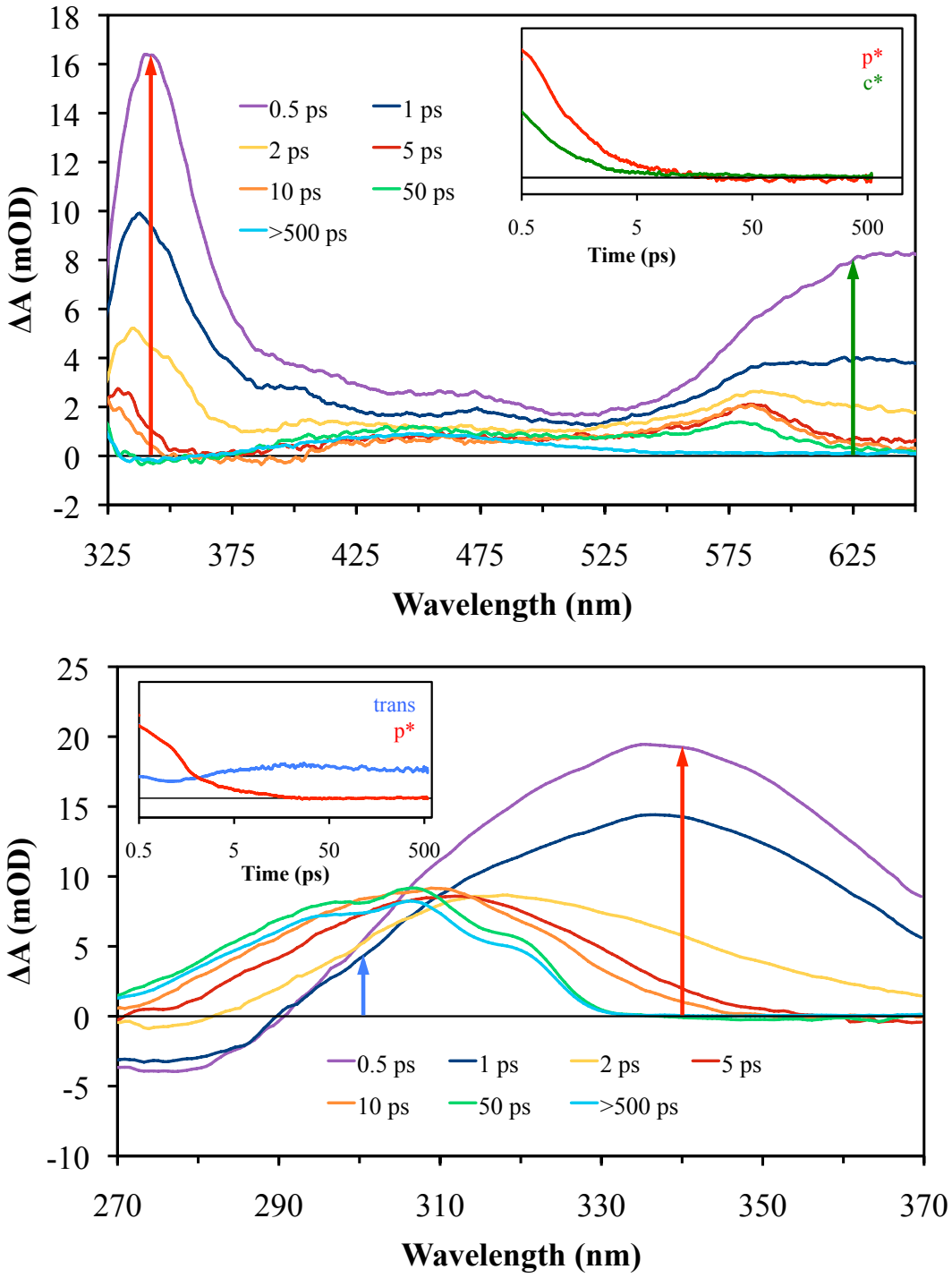

Figure 5.3 *(Top) Transient absorption spectra for cis-stilbene collected with 800 nm white light continuum. Trans-stilbene impurity can be seen at 580 nm. (Bottom) Similar spectra collected with 400 nm white light continuum. The arrows in both plots correspond to the wavelength selected for the kinetic traces shown in the insets, with the green arrow in the upper panel also representing the center wavelength of the repump pulse.*

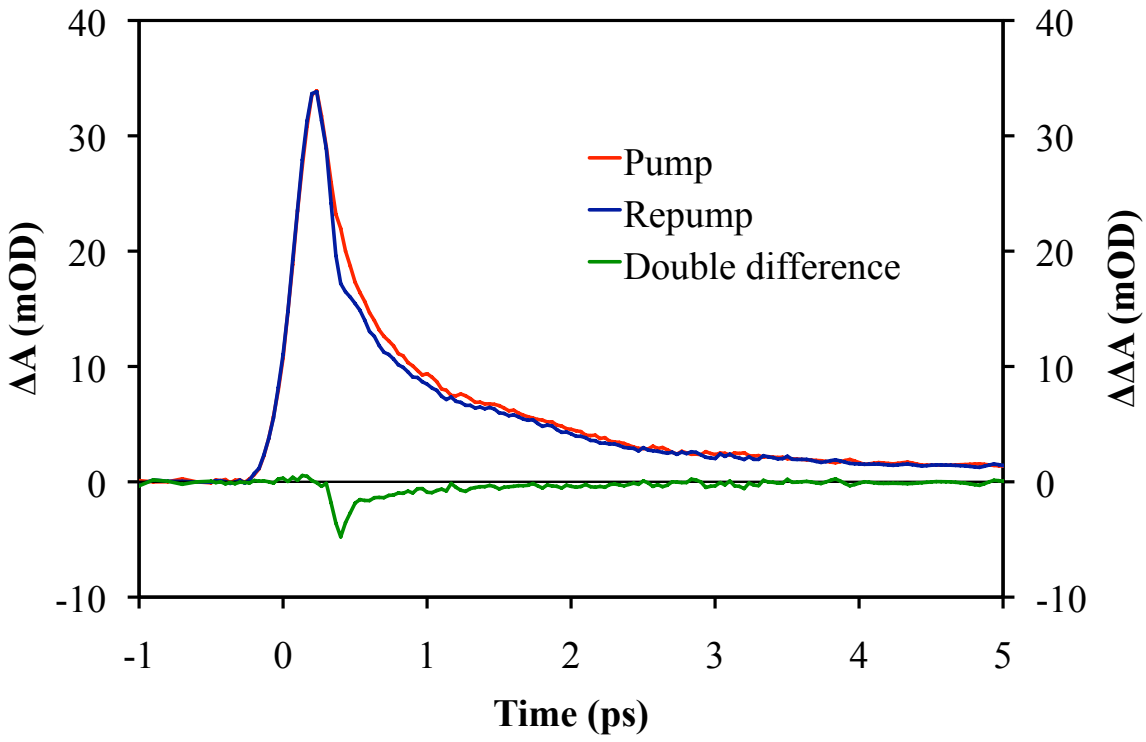

Figure 5.4 *Lineouts of cis-stilbene transient absorption spectra for both pump and repump cases, along with the double difference lineout. Residual signal at long times is due to trans-stilbene impurity in the sample.*

and trans-stilbene photoproduct spectra. In addition, there is a small contribution to the signal in this region from trans-stilbene ground state bleach due to the impurity in the sample. This is fairly small relative to the other signals, however, and is not clearly visible.

Comparison of the kinetics between pump-only and pump-repump data at the peak of the cis-stilbene ESA at 630 nm can be seen in Figure 5.4. A small, but unmistakable, depletion of the ESA similar to that measured by Takeuchi et al.[13] can be seen upon the arrival of the repump pulse at 0.5 ps. It should be noted that the ESA signal of trans-stilbene does extend into this region, although the intensity of this signal is very low. It is possible that this depletion is due to absorption of the repump by excited

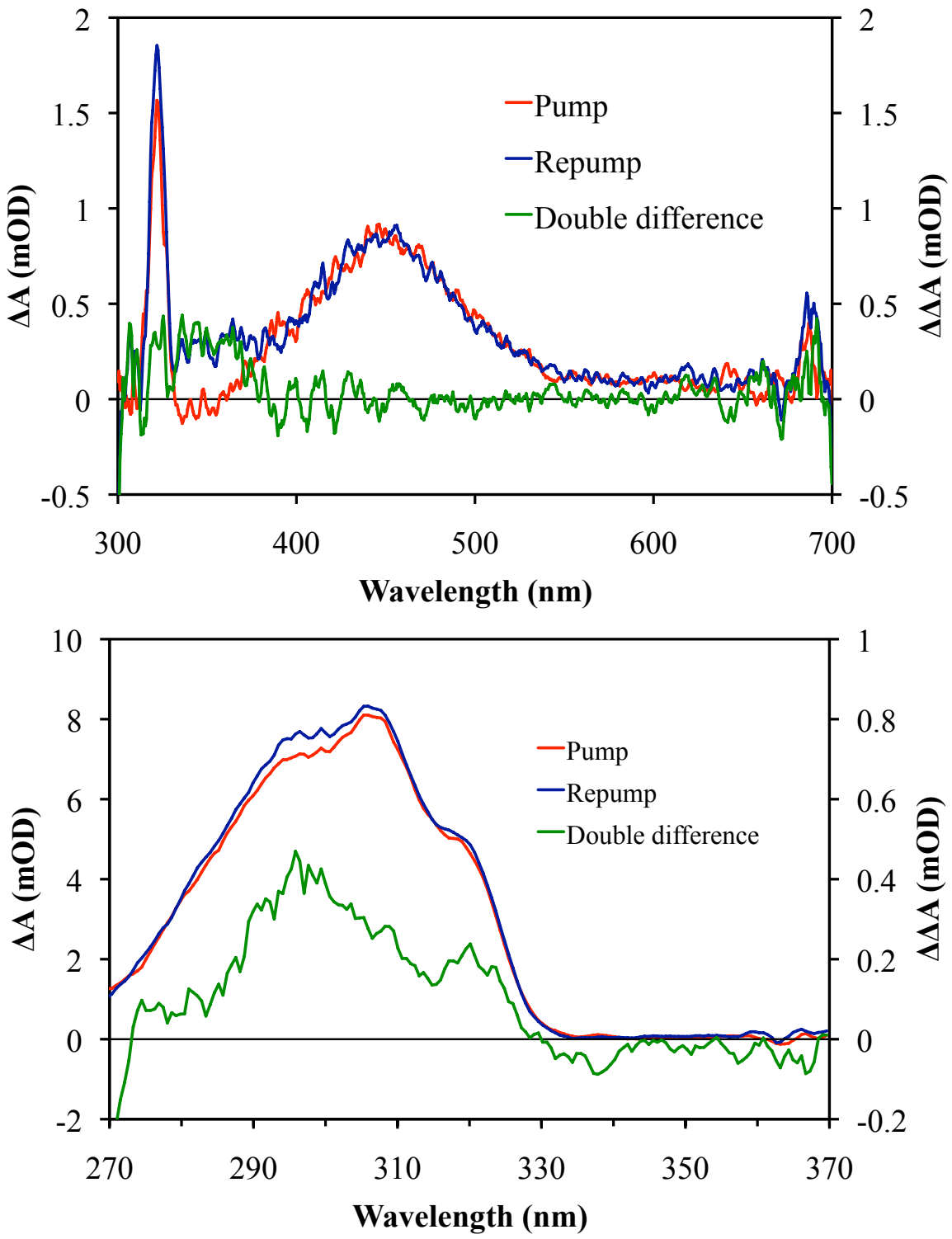

Figure 5.5 *(Top) DHP photoproduct spectra for pump and repump cases along with the double difference spectrum. (Bottom) Trans-stilbene photoproduct spectra for pump and repump cases along with the double difference spectrum.*

trans-stilbene (t*) rather than c*. However, the very fast decay of the double difference kinetic trace is on the order of the decay rate of c* (~1.2 ps), which supports the conclusion that this depletion is indeed due to the absorption of repump by cis-stilbene.

In order to determine whether the repump pulse has any effect on the formation of DHP or trans-stilbene from cis-stilbene, the transient absorption difference and double difference spectra were averaged at time delays greater than 500 ps. These averaged spectra can be seen in Figure 5.5. It should be noted that the two sets of spectra shown are necessarily from two different sets of data, as the spectral range covered is not possible within a single experiment. The c* signal was not visible in the spectra collected in the UV, and therefore, it was not possible to determine the extent of the c* population depletion in these experiments. In spite of this, it should be possible to indirectly monitor a depletion of the c* state by comparing the growth and decay of the p* ESA in pump and repump cases. While there do appear to be slight differences between the p* kinetics in the two cases, the stage-related systematic error originally mentioned in chapter 3 prevents one from making a definitive statement about them.

The averaged double difference spectrum within the region in which DHP appears conclusively shows that there is no difference in DHP production between the pump-only and pump-repump measurements. On the other hand, the double difference spectrum displayed in the lower panel of Figure 5.5 shows a difference in the production of trans-stilbene. While this difference is small, the shape of the double difference spectrum matches that of the trans-stilbene ground state spectrum quite well, suggesting that the presence of a repump pulse can indeed modify the quantum yield of this photoreaction.

That the sign of this signal is positive illustrates that there is a net increase in the formation of trans-stilbene photoproduct following re-excitation.

5.2.3 Trans-stilbene – visible probe

All measurements on trans-stilbene used repump pulses tuned between 590-595 nm. The repump delay time was set to 0, 2.5, 3.0, or 40 ps, depending on the data set. Repump data was scaled in the same manner as the DHC and cis-stilbene measurements.

Transient absorption difference spectra collected using 800 nm white light continuum for both the pump and repump (3 ps delay) are found in Figure 5.6. The most prominent signal in these spectra is the strong, broad excited state absorption that peaks near 580 nm. The decay of this peak is biexponential. One component is a 50 ± 2 ps decay corresponding to the escape of excited trans-stilbene (t*) over an activation barrier as it twists toward the phantom state (p*) configuration. The second component is due to vibrational cooling of the t* population. Since the UV pulse has much more energy per photon than what is required to drive the 0-0 transition in trans-stilbene (see steady state spectrum in chapter 1), the excited trans-stilbene has a large amount of excess vibrational energy. The 0-0 transition appears at 321 nm, meaning that a 266 pulse will impart an extra 6400 cm^{-1} of vibrational energy to the excited trans-stilbene. The vibrational cooling effect in trans-stilbene due to this excess energy has been studied previously.[23-25] This cooling process sees the ESA undergo a blue shift and narrowing of the peak width, and occurs on the order of 5.5 ± 1 ps. Another smaller signal visible in these data is the stimulated emission from t* back to ground state trans-stilbene. Since this process is

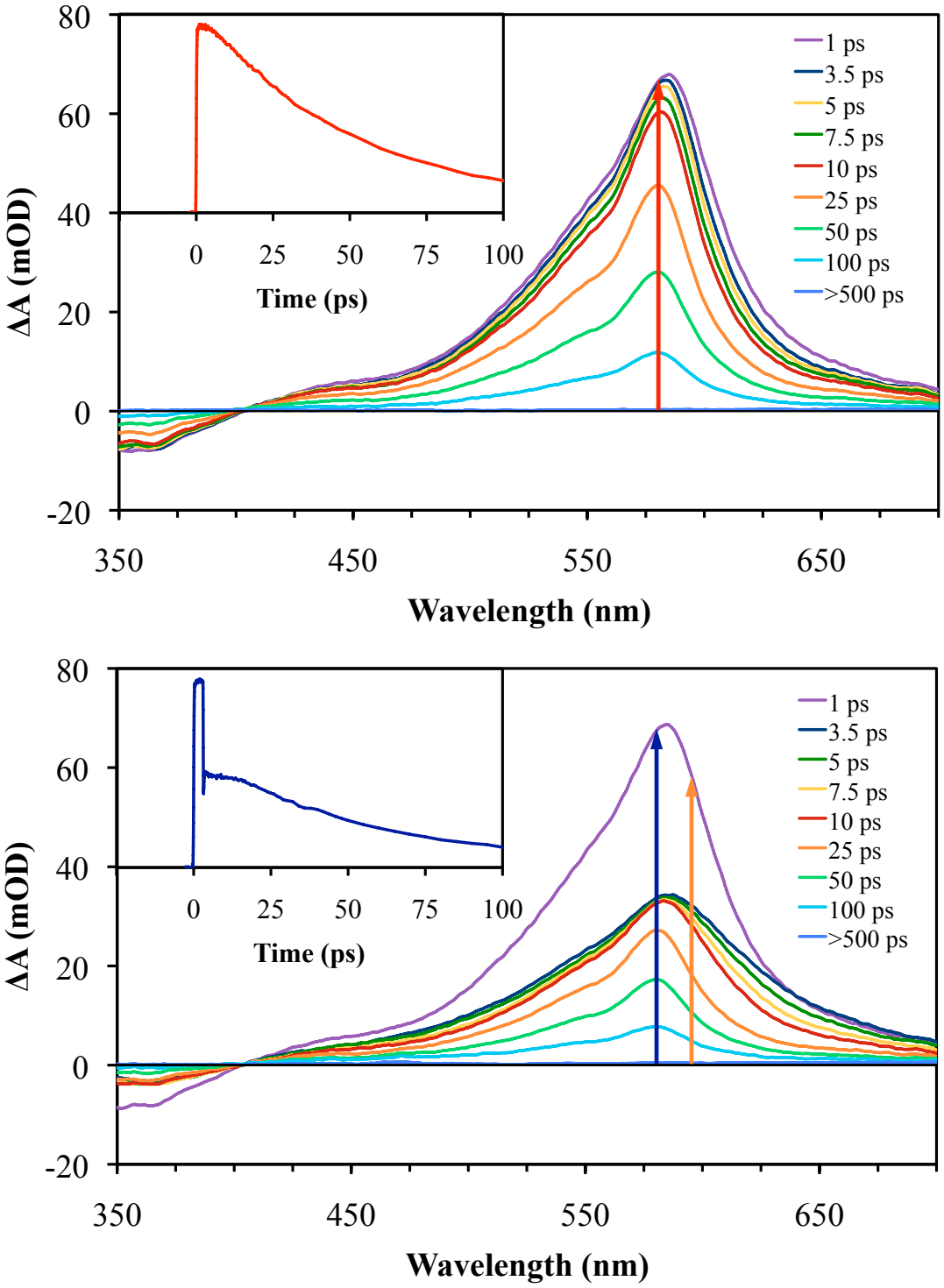

Figure 5.6 *(Top) Typical transient absorption spectra of trans-stilbene through time following 266 nm excitation. (Bottom) TA spectra of trans-stilbene at the same time delays as the top panel with the arrival of a repump pulse at 3 ps. Red and blue arrows correspond to the wavelengths of the kinetic traces shown in the insets. The orange arrow corresponds to the center wavelength of the repump pulse.*

from the same state as the $S_n \leftarrow S_1$ (1_1B_u) excited state absorption, the decay rates of these two signals are the same.

In comparing the pump (upper panel) to the repump (lower panel) data in Figure 5.6, the most striking difference between the two is the depletion of the excited state absorption signal intensity by nearly half. This is due to excitation of t* population to the S_n state upon the arrival of the repump pulse. A small fraction of this re-excited population (t**) undergoes internal conversion to the S_1 state on a sub-picosecond timescale. Similar internal conversion from the S_2 state back to the S_1 state after single photon excitaiton (226 nm) was observed on a <100 fs time scale by Kovalenko et al.[26] This newly formed t* population has a much higher amount of vibrational energy than the initial t* population following UV excitation, as evidenced by the much broader excited state absorption peak following repumping (see Figure 5.7).

The model used to fit these data is a sum of n weighted exponentials:

$$S(t) = s_0 + \sum_i^n A_i e^{-k_i t} \tag{5.1}$$

where s_0 is a baseline offset, A_i and k_i are the amplitude and rate constants of the i^{th} component, respectively. Taking the difference between the two different fitting models for the pump-only and pump-repump data will generate a new model for the double difference data that contains all of the fitting components of the original two models (in addition to a modified baseline offset and a change in amplitude of components found in both sets of data). Overall, the results of both the repump and double difference fits seemed to be consistent with each other and with the pump data. Each had a slow decay of t* population and faster decay due to vibrational cooling in addition to a very fast third term corresponding to the growth of the signal ESA after the signal depletion due to

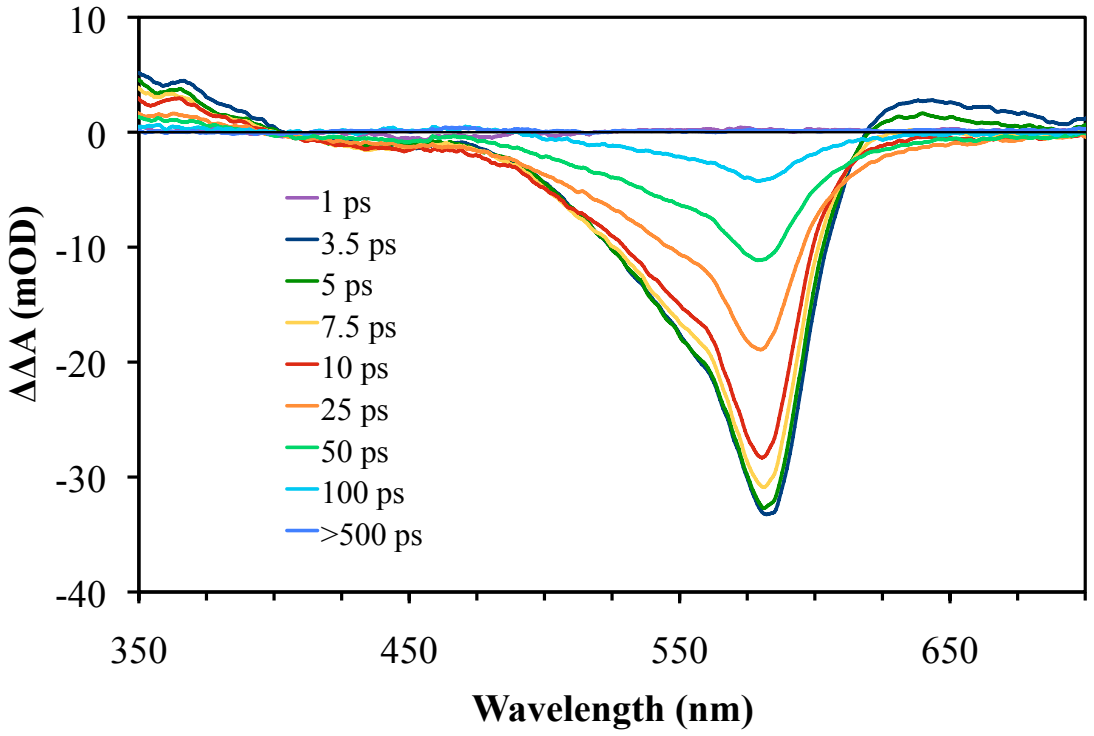

Figure 5.7 *Double difference transient absorption spectra of trans-stilbene. The repump delay is 3 ps. Note that there is a large overall decrease in signal intensity after 3 ps, but the red edge sees an increase due to the vibrational energy in the repumped population.*

internal conversion of t** to t*.

In order to investigate whether repumping trans-stilbene allows for the direct photocyclization to DHP, the pump, repump, and double difference spectra were averaged over many points at long time delays. The resulting spectra are shown in Figure 5.8. Based on this data, it does not appear that any DHP is formed in either the pump-only or pump-repump measurements.

All of the data discussed above concerned the case with repump delay set at 3 ps. Similar measurements were also made with repump delay set to 0 ps and 40 ps. In all cases, the results are consistent with those found for the 3 ps repump delay. There is no

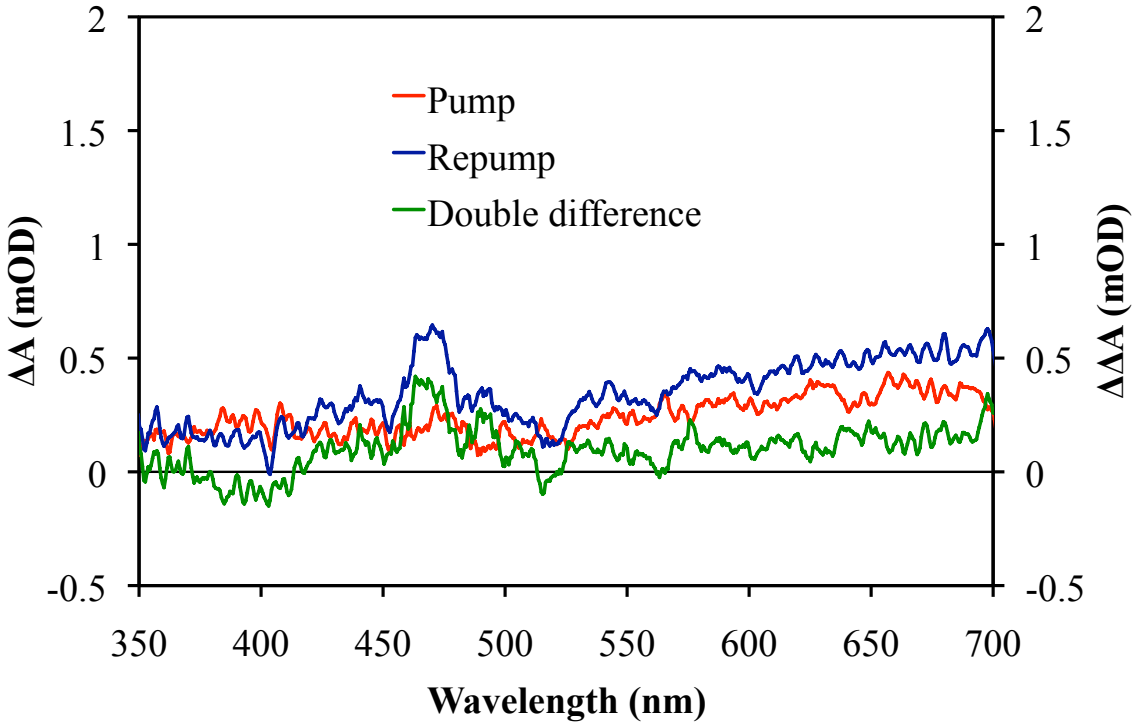

Figure 5.8 *Pump, repump, and double difference spectra within the region the DHP ground state absorption is located. Conclusive formation of DHP is not seen either the pump or repump data.*

obvious dependence of the kinetics of the t* visible excited state absorption on the repump delay time. In addition, no DHP was formed in any of the experiments conducted here.

5.2.4 Trans-stilbene – UV probe

Experiments analogous to those described in the previous section were performed using 400 nm white light continuum. Typical transient absorption spectra for these measurements can be seen in Figure 5.9. The stimulated emission peak seen at the very blue edge of the white light continuum in the visible probe experiments appears on the red edge of the UV continuum used to probe the sample in these experiments. As in the

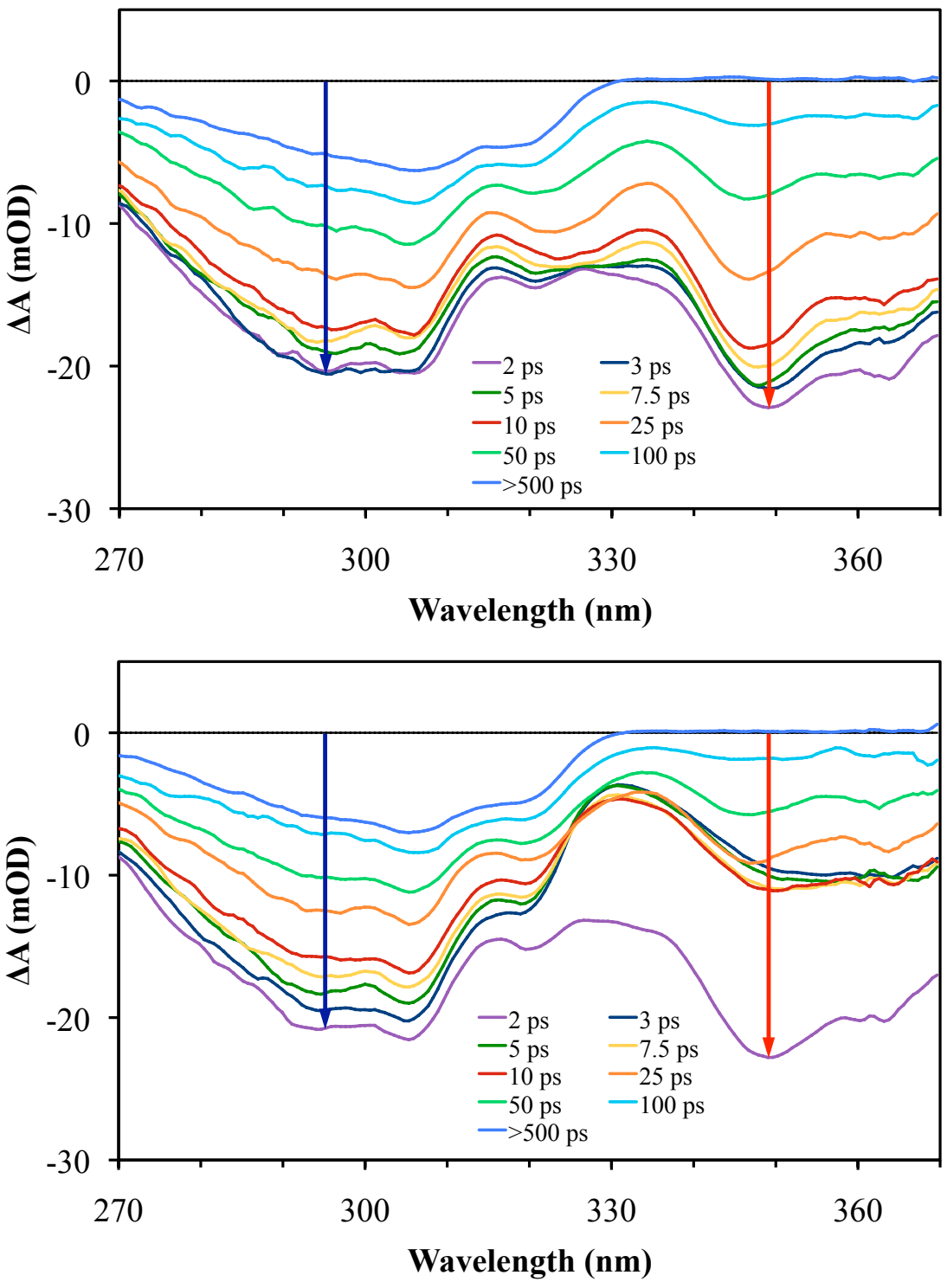

Figure 5.9 *Transient absorption spectra at various delay times for pump only (top) and repump (bottom) data sets with repump delay set to 2.5 ps. Colored arrows represent wavelengths chosen for the kinetic traces shown in Figures 5.10 and 5.11.*

previous experiments, the kinetics of this signal exhibits a slow decay of the S_1 state on the order of 50 ps with a vibrational cooling component on the order of 5-6 ps. As the excited population cools, the vibronic bands in the emission spectrum become sharper, as expected.

The ground state bleach of trans-stilbene dominates on the blue edge of the spectrum in Figure 5.9. This signal overlaps with the stimulated emission signal since both signals involve the S_0 and S_1 states and are separated only by the Stokes shift of the emission spectrum. Since the decay of the phantom state, which leads directly to the recovery of ground state trans-stilbene (and cis-stilbene), occurs on a ~1 ps time scale, the time scale of recovery of the ground state bleach is limited by the slow decay of the t* state to the p* state. Thus, this signal decays on the same time scale as the stimulated emission.

Eventually, the stimulated emission decays to zero as the t* population returns to the ground state either as trans reactant or cis photoproduct. The ground state bleach decays to a constant value, the size of which is dependent on the quantum yield of isomerization. As molecules react to form cis-stilbene, they will no longer contribute to the trans-stilbene steady state absorption spectrum, which means that larger isomerization quantum yields result in larger residual ground state bleach signals.

Upon the arrival of the repump pulse 2.5 ps after the pump pulse a depletion of the stimulated emission peak due to depopulation of the S_1 state is clear. Some of this signal grows back in as the t** population decays back to the S_1 state just as in the visible probe measurements. Because the ground state bleach arises due to a lack of trans-stilbene ground state population, the depletion of the t* population by the repump pulse

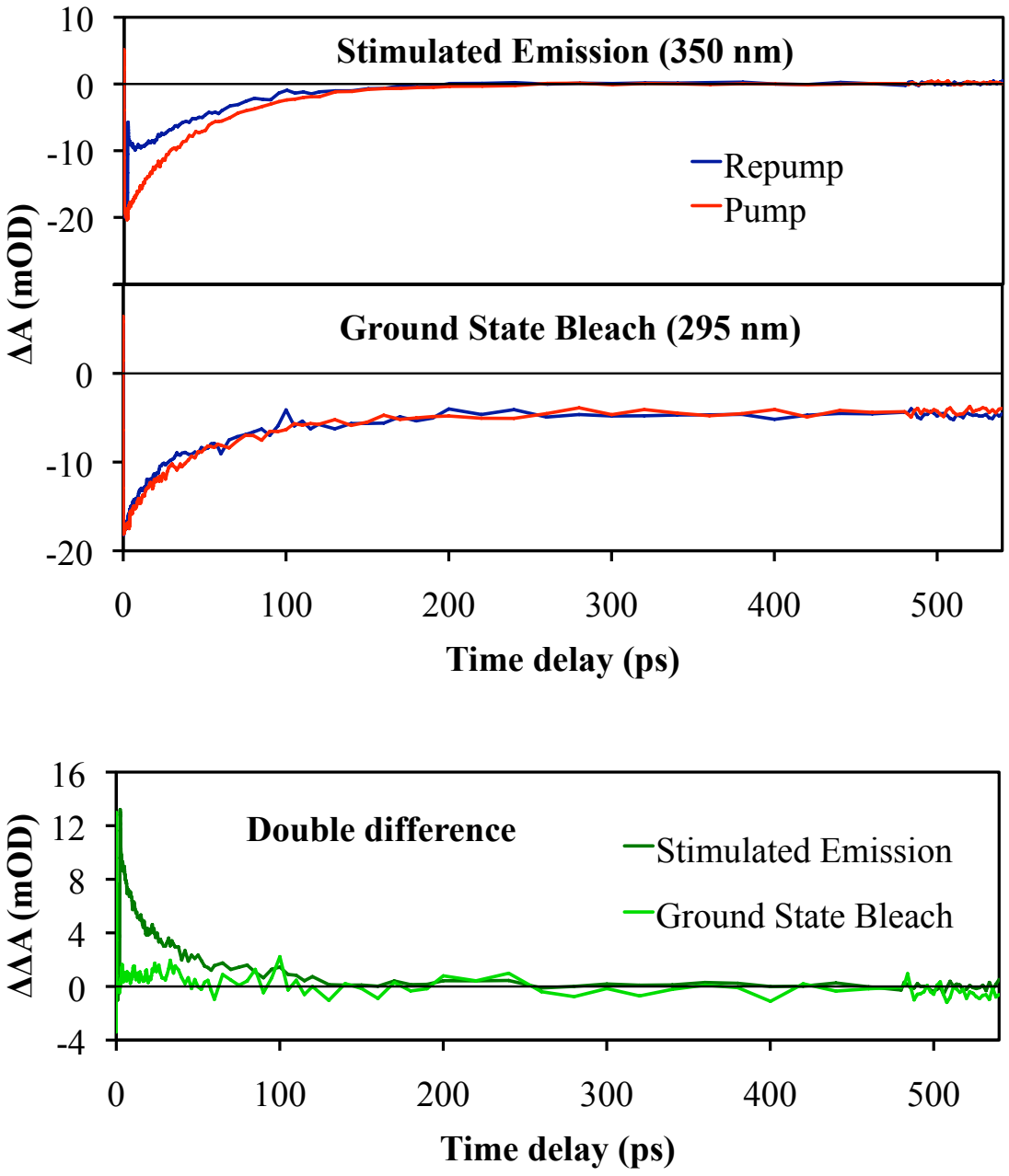

Figure 5.10 *(Top) Kinetic traces of stimulated emission and ground state bleach signals following 266 nm excitation at 0 ps and 590 nm re-excitation at 2.5 ps for both pump-only and pump-repump scans. (Bottom) Double difference lineouts of the stimulated emission and ground state bleach signals shown in the top panel.*

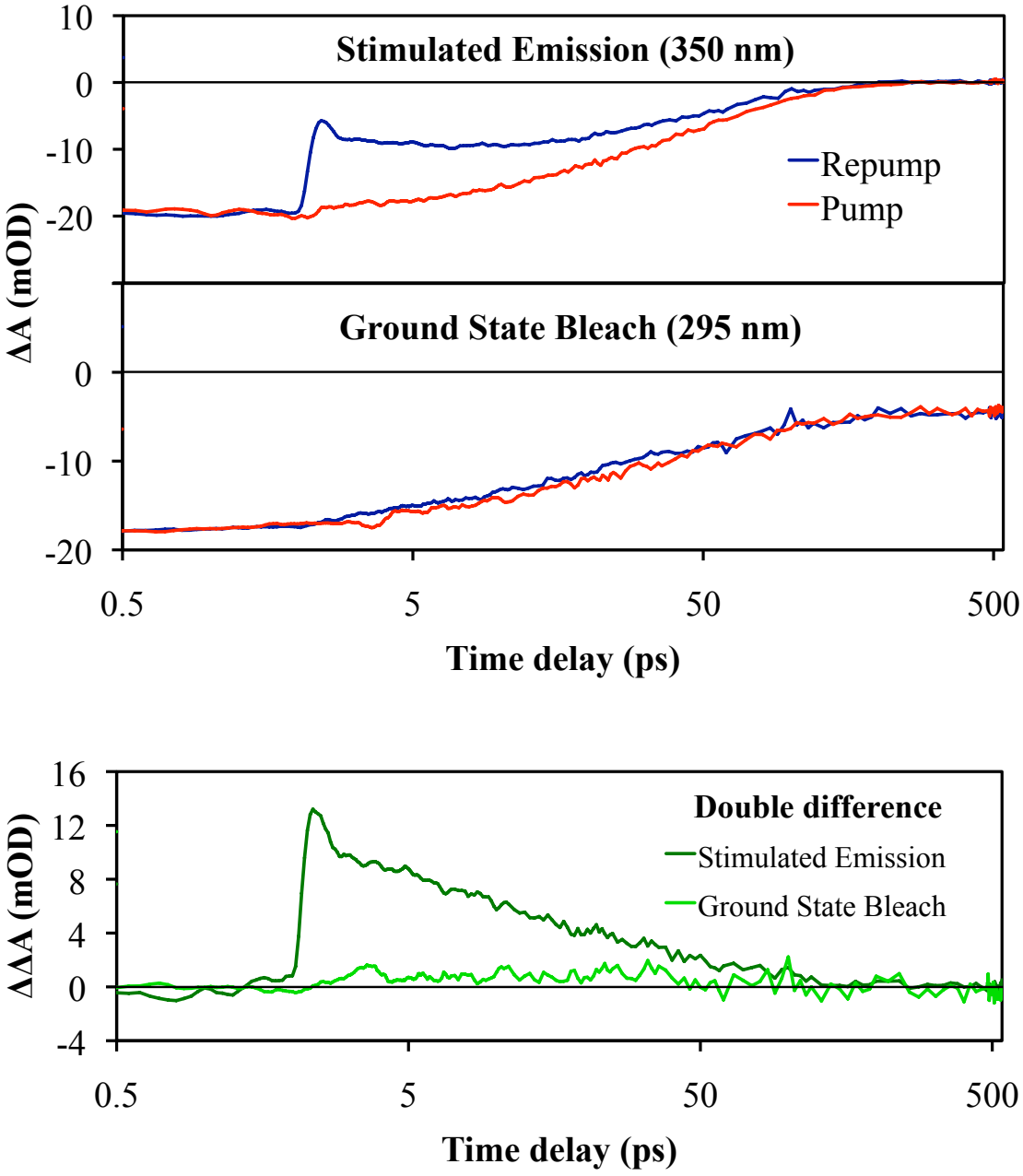

Figure 5.11 *(Top) Kinetic traces of stimulated emission and ground state bleach signals following 266 nm excitation at 0 ps and 590 nm re-excitation at 2.5 ps for both pump-only and pump-repump scans on a logarithmic scale. (Bottom) Double difference lineouts of the stimulated emission and ground state bleach signals shown in the top panel.*

has no immediate effect on the size of this signal. This can be seen in the kinetics plotted in Figures 5.10 and 5.11. The decay of the stimulated emission following a repump pulse is the same as in the pump-only measurement.

In contrast, the kinetics of the ground state bleach recovery show a small but clear difference between the pump and repump data. When a repump pulse is present this signal appears to recover slightly faster. Two possible explanations for this decrease in signal intensity exist. One explanation is that some of the t** population on the S_n state is indeed able to undergo a faster internal conversion back to ground state trans-stilbene through some series of states following a pathway that bypasses the S_1 state. A second explanation is that the state to which the molecules are excited following repumping (or some other state the molecules reach after decaying out of this state) may absorb in this region, decreasing the intensity of the bleach signal. The question remains whether or not the decay pathway accessed in either of these situations leads the excited state population exclusively to ground state trans-stilbene or if it involves some configuration where a branching to either cis or trans-stilbene is possible. The ground state bleach at long times can answer this question.

Figure 5.12 shows pump-only, pump-repump, and double difference spectra averaged for time delays from 480-500 ps. The shape of the double difference spectrum displayed here matches that of the trans-stilbene ground state bleach. This, along with the negative sign of the spectrum, clearly illustrates that the presence of a repump pulse reduces the number of molecules that return to trans-stilbene in the ground state. This result coincides with an increase in the quantum yield of either cis-stilbene or DHP. Since the experiments with visible probe show no evidence that DHP is formed upon

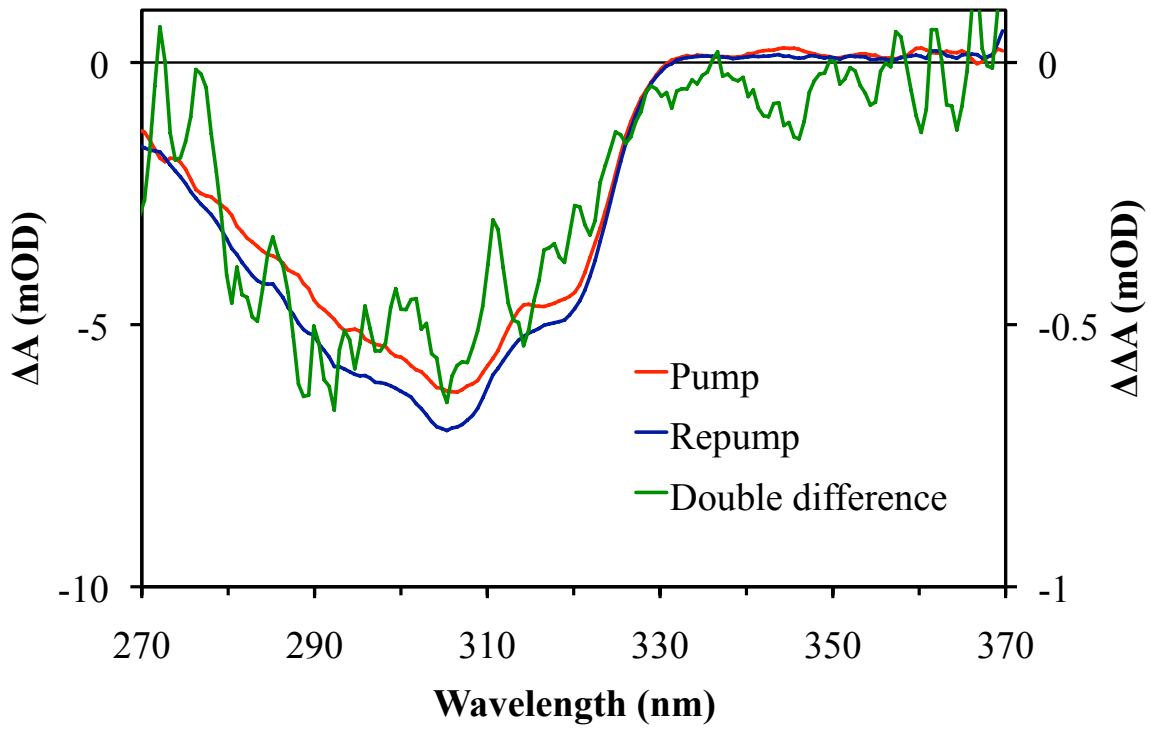

Figure 5.12 *Long time transient absorption spectra of trans-stilbene ground state bleach.*

repumping, this suggests that the quantum yield of trans-to-cis isomerization is increased under these conditions.

5.3 Conclusions

While pump-repump measurements on DHC initially show some observable depletion of the S_1 state following re-excitation, this difference quickly disappears as the excited molecules decay from S_n to S_1. Following the recovery of the excited state absorption signal, there is no difference between the pump-only and pump-repump cases. It appears that the repump pulse has little effect on the ring-opening dynamics of DHC.

Repumping the cis-stilbene excited state before conversion to the phantom state shows a higher amount of excited state depletion than the DHC measurements, but the kinetics between pump and repump data sets show no distinct differences. The amount of DHP formed by ring-closure of the excited cis-stilbene population is not affected by the presence or absence of repump pulses. Conversely, analysis of the trans-stilbene photoproduct spectrum shows that repumping the c* state slightly improves the quantum yield of cis-to-trans isomerization.

Trans-stilbene exhibits a very large depletion of the excited state population following re-excitation. Experiments conducted with a visible probe suggest that there is no disparity in the decay kinetics between pump and repump data sets. In addition, no formation of direct photocyclization of trans-stilbene to DHP photoproduct is observed. Neither of these results appears to be affected by the time delay of the repump pulses. Pump-repump experiments on trans-stilbene using a UV probe were also conducted. These measurements show that the kinetics of the ground state bleach recovery are indeed modified by repump pulses. Following re-excitation, the ground state bleach experiences a slightly faster decay. It is concluded that this excitation of t* population to the S_n state presents a new decay pathway for internal conversion back to the ground state that bypasses the S_1 state. In addition, spectral analysis at late times reveals that the quantum yield of trans-to-cis isomerization is positively influenced by the presence of a secondary excitation pulse.

The ability of a repump pulse to modify the product yields of the cis-to-trans and trans-to-cis isomerization of stilbene sets the stage for future measurements on stilbene based molecular motors. A repump pulse may provide a means to enhance the yield of

isomerization and overcome the rate-limiting ground state barriers encountered following single photon excitation in these systems.[27] The circumvention of this slow thermal step is crucial to improving the efficiency of these molecular machines.

5.4 References

1. S. A. Rice; D. J. Tannor; R. Kosloff. *J. Chem. Soc., Faraday Trans. 2,* **1986,** *82*, 2423-2444.

2. Y. Ishibashi; M. Murakami; H. Miyasaka; S. Kobatake; M. Irie; Y. Yokoyama. *J. Phys. Chem. C,* **2007,** *111*, 2730-2737.

3. Y. Ishibashi; K. Okuno; C. Ota; T. Umesato; T. Katayama; M. Murakami; S. Kobatake; M. Irie; H. Miyasaka. *Photochem. Photobiol. Sci.,* **2010,** *9*, 172-180.

4. Y. Ishibashi; K. Tani; H. Miyasaka; S. Kobatake; M. Irie. *Chem. Phys. Lett.,* **2007,** *437*, 243-247.

5. H. Miyasaka; M. Murakami; A. Itaya; D. Guillaumont; S. Nakamura; M. Irie. *J. Am. Chem. Soc.,* **2001,** *123*, 753-754.

6. H. Miyasaka; M. Murakami; T. Okada; Y. Nagata; A. Itaya; S. Kobatake; M. Irie. *Chem. Phys. Lett.,* **2003,** *371*, 40-48.

7. M. Murakami; H. Miyasaka; T. Okada; S. Kobatake; M. Irie. *J. Am. Chem. Soc.,* **2004,** *126*, 14764-14772.

8. K. Tani; Y. Ishibashi; H. Miyasaka; S. Kobatake; M. Irie. *J. Phys. Chem. C,* **2008,** *112*, 11150-11157.

9. T. Brust; S. Draxler; J. Eicher; W. J. Lees; K. Rueck-Braun; W. Zinth; M. Braun. *Chem. Phys. Lett.,* **2010,** *489*, 175-180.

10. C. L. Ward; C. G. Elles. *J. Phys. Chem. Lett.,* **2012,** *3*, 2995-3000.

11. C. L. Ward; C. G. Elles. *J. Phys. Chem. A,* **2014,** *118*, 10011-10019.

12. J. Bao; M. P. Minitti; P. M. Weber. *J. Phys. Chem. A,* **2011,** *115*, 1508-1515.

13. S. Takeuchi; S. Ruhman; T. Tsuneda; M. Chiba; T. Taketsugu; T. Tahara. *Science,* **2008,** *322*, 1073-1077.

14. J. Bao; P. M. Weber. *J. Phys. Chem. Lett.,* **2010,** *1*, 224-227.

15. A. L. Houk; I. L. Zheldakov; T. A. Tommey; C. G. Elles. *J. Phys. Chem. B,* **2014**.

16. C.-W. Jiang; R.-H. Xie; F.-L. Li; R. E. Allen. *Chem. Phys. Lett.,* **2010,** *487*, 177-182.

17. G. R. Fleming, *Chemical Applications of Ultrafast Spectroscopy*. Oxford University Press: New York, 1986.

18. K.-C. Tang; A. Rury; M. B. Orozco; J. Egendorf; K. G. Spears; R. J. Sension. *J. Chem. Phys.,* **2011,** *134*, 104503.

19. S. Abrash; S. Repinec; R. M. Hochstrasser. *J. Chem. Phys.,* **1990,** *93*, 1041-1053.

20. J. S. Baskin; L. Banares; S. Pedersen; A. H. Zewail. *J. Phys. Chem.,* **1996,** *100*, 11920-11933.

21. M. Lee; A. J. Bain; P. J. McCarthy; C. H. Han; J. N. Haseltine; A. B. Smith; R. M. Hochstrasser. *J. Chem. Phys.,* **1986,** *85*, 4341-4347.

22. S. T. Repinec; R. J. Sension; S. A. Abrash; R. M. Hochstrasser, Molecular Alignment in the Photoisomerization of Stilbene. In *Ultrafast Phenomena VII*, Harris, C.; Ippen, E.; Mourou, G.; Zewail, A., Eds. Springer Berlin Heidelberg: 1990; Vol. 53, pp 495-497.

23. S. A. Kovalenko; A. L. Dobryakov. *Chem. Phys. Lett.,* **2013,** *570*, 56-60.

24. S. A. Kovalenko; A. L. Dobryakov; E. Pollak; N. P. Ernsting. *J. Chem. Phys.,* **2013,** *139*.

25. K. Iwata; H.-o. Hamaguchi. *Chem. Phys. Lett.,* **1992,** *196*, 462-468.

26. S. A. Kovalenko; R. Schanz; H. Hennig; N. P. Ernsting. *J. Chem. Phys.,* **2001,** *115*, 3256-3273.

27. M. Klok; L. P. Janssen; W. R. Browne; B. L. Feringa. *Faraday Discuss.,* **2009,** *143*, 319-334.

Chapter 6

Conclusions and Outlook

The experiments presented here used an assortment of methods in the attempt to control the photoreactions of molecules that have long been considered paradigm systems for photochemistry (cis and trans-stilbene) and molecules with biological significance (7-dehydrocholesterol). Gaining a better understanding of the response to control stimuli by these molecular systems, which are the basis for many types of molecular switches and motors,[1-8] allows for future researchers to improve on these steps and drive the fields of optical control and molecular machines forward.

Experiments using a tunable excitation pulse were described in chapter 3. These measurements investigated the effect of excess vibrational energy on the ring-opening dynamics of DHC. While there was a dependence of the peak wavelength of the DHC excited state spectrum on pump wavelength, there was no monotonic trend observed. Fits to the kinetics of the integrated spectrum yielded rate constants for excited state decay that match those reported previously for 266 nm excitation.[9] These measurements show that there is no observable dependence of the excited state decay on excitation wavelength. Two possible explanations for the lack of a rate dependence on excitation wavelength are that the excited vibrational mode simply plays no significant

role in the ring-opening motion or that this excess vibrational energy is very quickly spread throughout the remaining modes through IVR.

Chapter 4 described attempts at coherent control on DHC and cis-stilbene using chirped laser pulses. These experiments conclusively showed that there is no dependence of the photoreaction quantum yields in either molecule on the chirp of the excitation pulse. Therefore, if weak field coherent control of reactions such as those in DHC and stilbene is possible, the key is to modulate more than a single parameter. Future experiments on the effects of Dazzler shaped laser pulses on the photochemistry of DHC or stilbene should utilize the Dazzler's ability to introduce third and fourth order dispersion to the exciting laser pulse. In addition, since the optimal pulse shape may not be intuitive, the use of a genetic algorithm to find the parameters describing this laser pulse is a must. These types of experiments have been purported to produce positive results.[10-14]

Although stilbene has been studied extensively, few studies focus on the electronic states above the reactive S_1 state that plays a dominant role in the cis-trans isomerization and ring-closing. Some studies have shown that states at higher energy can play a significant role in the reactions of excited stilbene.[15-16] It is only fitting that the reactivity of these states be exploited in order to obtain a desired photochemical outcome. The work described within chapter 5 used a sequential two-pulse pumping scheme in order to populate states much higher in energy than the lowest excited state in cis and trans-stilbene as well as DHC.

DHC showed very little depletion of the initially excited S_1 population after repumping. Because studies on DHC were performed using visible white light probe, no

assessment of the effect of repumping on the quantum yield of ring-opening could be made. Future, investigation of the influence of repumping should focus on the UV region of the difference spectrum to assess product yield as well as excited state dynamics.

Experiments on cis-stilbene demonstrated a larger depletion of the S_1 population than experiments on DHC. Although no effect on the formation of the ring-closure DHP product was observed, there was a notable increase in the cis-to-trans isomerization quantum yield. Of the three molecules investigated, trans-stilbene showed by far the largest depletion of excited state population by the repump pulse. While direct photocyclization of trans-stilbene to DHP was not detected, a distinct increase in the trans-to-cis isomerization quantum yield was observed.

The influence of the repump pulse on the cis-trans isomerization of stilbene shown in this work could be significant for subsequent work on stilbene based molecular motors, and opens the door to pursue a multitude of other experiments on these molecules. The easiest of these to execute is a measurement of the dependence of quantum yield on the delay of the repump with respect to the pump, since allowing excited molecules to decay before re-excitation may allow for coupling to states and configurations that improve the reactivity of the molecules. These measurements can be carried out simply by keeping the pump-probe delay fixed at very long times in order to see the photoproduct or ground state bleach spectra and using the mechanical stage to delay the repump pulses with respect to the other pulses. The construction of an arrangement where two stages are utilized in order to control the delay of either the repump or probe is currently in progress.

The next step in advancing the project is tuning the repump pulses to different positions relative to the peak of the excited state absorption. In all of the experiments here, the repump was tuned to the red side of this peak, except in the case of cis-stilbene where the repump was tuned to the peak maximum. The consequence of this is that repumped molecules are deposited into the S_n state with a low amount of vibrational energy. Increasing this excess energy by tuning to the blue side of the ESA peak could significantly affect the decay of the population out of the S_n state, changing the way the molecules undergo internal conversion through the excited state manifold on their way back to the ground state.

The last immediate step that should be taken to move this project forward is the repumping of the phantom state population following the excitation of cis-stilbene. (The phantom state is also involved in the decay of the trans-stilbene, but the very short lifetime in comparison to that of the initially excited trans-stilbene means that there is no appreciable build up of phantom state population.) Exciting the molecules while in this configuration could play a significant role in photoproduct formation, as the phantom state structure is key to the reactivity of the S_1 potential surface. In order to perform these measurements, the pump pulses must tuned to the phantom state absorption maximum (340 nm). This could be done by either doubling the NOPA pulses (680 nm), or harnessing the sum frequency generation of NOPA pulses (590 nm) combined with fundamental 800 pulses.

Overall, the research in this dissertation has shown that while single pulse control of the photochemistry in these small molecules remains elusive, other avenues may be available to produce the desired effect. Re-exciting the excited states of molecules to

very high energy states has been shown to have a clear effect on the quantum yield of the photoreactions studied. The control of molecular processes using light has long been regarded as a dream in the field of chemistry. In this age of femtosecond (and faster) chemistry, this dream has a chance to become reality, and the research described and proposed here is only one small step out of many toward the aspiration of true quantum control.

3.1 References

1. M. Irie. *Chem. Rev.,* **2000,** *100*, 1685-1716.
2. Y. Yokoyama. *Chem. Rev.,* **2000,** *100*, 1717-1739.
3. D. Geppert; L. Seyfarth; R. de Vivie-Riedle. *Appl. Phys. B,* **2004,** *79*, 987-992.
4. W. R. Browne; B. L. Feringa. *Nat. Nanotechnol.,* **2006,** *1*, 25-35.
5. J. Conyard; K. Addison; I. A. Heisler; A. Cnossen; W. R. Browne; B. L. Feringa; S. R. Meech. *Nat Chem,* **2012,** *4*, 547-551.
6. N. Koumura; E. M. Geertsema; M. B. van Gelder; A. Meetsma; B. L. Feringa. *J. Am. Chem. Soc.,* **2002,** *124*, 5037-5051.
7. N. Koumura; R. W. J. Zijlstra; R. A. van Delden; N. Harada; B. L. Feringa. *Nature,* **1999,** *401*, 152-155.
8. R. A. van Delden; M. K. J. ter Wiel; M. M. Pollard; J. Vicario; N. Koumura; B. L. Feringa. *Nature,* **2005,** *437*, 1337-1340.
9. K.-C. Tang; A. Rury; M. B. Orozco; J. Egendorf; K. G. Spears; R. J. Sension. *J. Chem. Phys.,* **2011,** *134*, 104503.
10. M. Kotur; T. Weinacht; B. J. Pearson; S. Matsika. *J. Chem. Phys.,* **2009,** *130*.
11. E. C. Carroll; J. L. White; A. C. Florean; P. H. Bucksbaum; R. J. Sension. *J. Phys. Chem. A,* **2008,** *112*, 6811-6822.
12. C. J. Bardeen; V. V. Yakovlev; K. R. Wilson; S. D. Carpenter; P. M. Weber; W. S. Warren. *Chem. Phys. Lett.,* **1997,** *280*, 151-158.

13. M. Greenfield; S. D. McGrane; D. S. Moore. *J. Phys. Chem. A,* **2009,** *113*, 2333-2339.

14. G. Vogt; G. Krampert; P. Niklaus; P. Nuemberger; G. Gerber. *Phys. Rev. Lett.,* **2005,** *94*, 068305.

15. J. Bao; P. M. Weber. *J. Phys. Chem. Lett.,* **2010,** *1*, 224-227.

16. J. Bao; M. P. Minitti; P. M. Weber. *J. Phys. Chem. A,* **2011,** *115*, 1508-1515.